CRYSTAL GROWTH OF DEVICE QUALITY GAAS IN SPACE

MASSACHUSETTS INST. OF TECH., CAMBRIDGE

JUL 1984

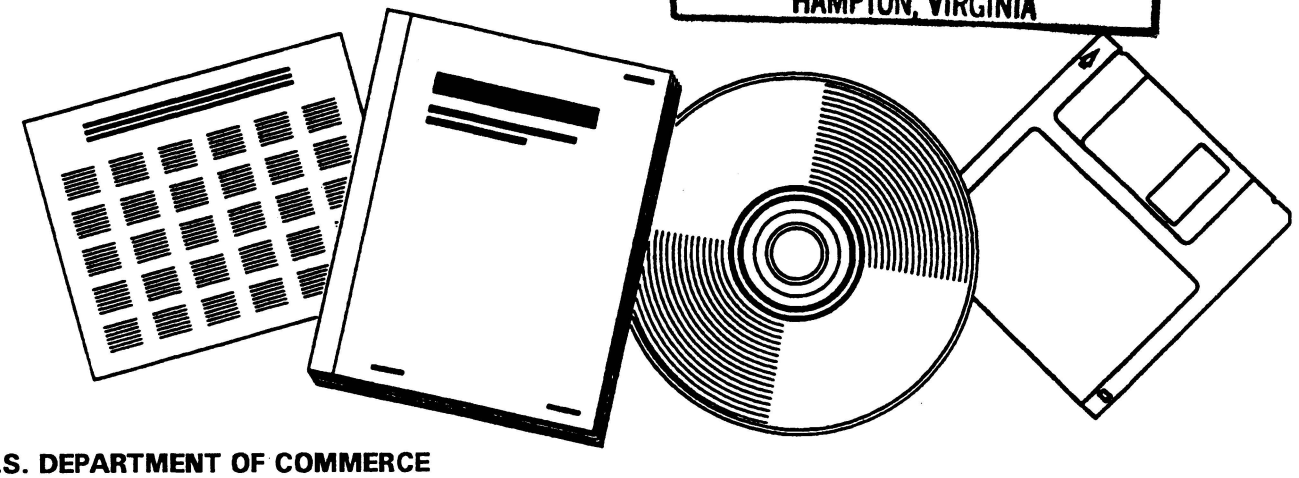

U.S. DEPARTMENT OF COMMERCE
National Technical Information Service

Bookmark this site today!

The Department of Commerce

Online International Trade Center Bookstore

Managed by the National Technical Information Service

The Department of Commerce International Trade Center Bookstore brings together a world-class collection of publications from government and non-profit organizations. This collection is now available through a new online bookstore.

Tap into information from these leading research institutions:

- The Brookings Institution
- Center for Strategic and International Studies
- Export-Import Bank of the United States
- Library of Congress
- World Bank
- United Nations
- Organization for Economic Cooperation and Development
- Battelle

New features and collections added regularly!

Visit the web site at http://tradecenter.ntis.gov/

U.S. DEPARTMENT OF COMMERCE
Technology Administration
National Technical Information Service
Springfield, VA 22161 (703) 605-6000

An essential online tool providing one-stop access to the very best international trade information available anywhere.

SEARCH & ORDER ONLINE FROM THIS GROWING COLLECTION: Search the complete ITC Bookstore by keyword or narrow your search to a specific collection.

A WIDE RANGE OF SUBJECTS: International trade related subjects in the Bookstore include agriculture and food, behavior and society, business and economics, communication, computers, energy, environmental pollution and control, health care, military sciences, and transportation.

BROWSE BY REGION: Review titles that focus on issues as they relate to seven world regions. Narrow your focus by combining this feature with keyword searching.

BROWSE BY INDUSTRY SECTORS: Select from more than 20 industry sectors and their sub-sectors. Combine this feature with a keyword search for a more precise list of titles.

EASY ACCESS TO OTHER TRADE RELATED INFORMATION: Use the site to easily locate other trade related sites, to find international trade bestsellers, and to search for industry standards.

To: NATIONAL AERONAUTICS AND SPACE ADMINISTRATION
WASHINGTON, D. C. 20546

ANNUAL REPORT

Crystal Growth of Device Quality GaAs in Space

(NSG 7331)

Peri. April 1, 1983 to March 31, 1984

Submitted by:

Professor Harry C. Gatos and Dr. Jacek Lagowski
Department of Materials Science and Engineering
Massachusetts Institute of Technology
Cambridge, Massachusetts 02139

July 1984

TABLE OF CONTENTS

CRYSTAL GROWTH OF DEVICE QUALITY GaAs IN SPACE

I. SUMMARY

Recent developments in GaAs device technology have clearly established the unique role of GaAs in high speed devices, integrated circuits, and optoelectronic systems for commercial and governmental applications. At the same time, it has become apparent that further advancements and the transition to the next generation of electronic devices hinges on new quantum steps in three interrelated areas: crystal growth, device processing and device-related properties and phenomena. Our GaAs research evolves about these key thrust areas. The overall program combines: (1) studies of crystal growth on novel approaches to engineering of semiconductor material (i.e., GaAs and related compounds); (2) investigation and correlation of materials properties and electronic characteristics on a macro- and microscale; (3) investigation of electronic properties and phenomena controlling device applications and device performance.

It is becoming rapidly very clear, primarily on the basis of our work, but also on the basis of that of the others, that each melt-grown GaAs electronic quality cannot exceed a modest level which is theoretically dictated by the unavoidable inclusion of Ga and As vacancies.

Our effort is aimed at the essential ground-based program which would insure successful experimentation with and eventually processing of GaAs in a near-zero gravity environment. We further believe that this program addresses in a unique way materials engineering aspects which bear directly on the future exploitation of the potential of GaAs and related materials in device and systems applications. We will summarize below the last two-year developments of our program. An overall summary of the major developments in the course of this investigation is given in Table I.

Our recent discovery that stoichiometry is a fundamental factor affecting structural and electronic properties of melt-grown GaAs has made a major impact

TABLE I

PROGRESS TO DATE - SUMMARY OF MAJOR DEVELOPMENTS

(Shaded areas indicate the most important achievements in the last two years)

	Development	Comments	Publications
LPEE-Liquid Phase Electroepitaxy	1. Growth Kinetics Model 2. Dopant Segregation Model 3. Model of Multicomponent Systems 4. Interface Stability Model	Theoretical model was developed which explains experimental LPEE characteristics. The model is based on a mass transport process with two driving forces: solute electromigration and the Peltier Effect.	1-10
	5. In-situ Monitoring of Growth	Successful in-situ monitoring of the growth velocity was realized for the first time in LPE using the contactless LPEE configuration.	
	6. Growth of Bulk Crystals	LPEE process was successfully extended to a growth of bulk crystals of the thickness of the order of 1 mm.	
	7. Growth in Space Environment	LPEE process was selected in 1983 in order to realize the growth of GaAs in Space. Further R&D effort in this area is realized under a sponsorship of Microgravity Research Associates.	1 2 1
MELT GROWTH	1. Construction of Advanced GaAs Melt-Growth System	Advanced system has been designed & constructed for horizontal and/or vertical growth of GaAs. The system provides unique feasibility for controlling and monitoring growth parameters.	11, 12
	2. Growth of n-type Dislocation-Free GaAs	Utilizing precise control of As pressure above the melt we have achieved reproducible growth of dislocation-free GaAs in a horizontal Bridgman configuration.	12, 13
	3. Growth of Electron Trap-Free GaAs	Growth conditions were discovered which lead to melt-grown GaAs of superior structural & electronic properties. For the first time electron trap-free bulk GaAs was achieved.	14, 15
	4. Identification of the Role of Oxygen in Melt Growth of GaAs	Oxygen has been identified as a constituent of growth system which affects electronic and stuctual properties of GaAs.	16, 17

PROGRESS TO DATE - SUMMARY OF MAJOR DEVELOPMENTS

(Shaded areas indicate the most important achievements in the last two years)

	Development	Comments	Publications
MELT GROWTH (cont.)	5. Role of Stoichiometry	Stoichiometry was identified as a fundamental factor controlling structural & electronic properties of GaAs.	12-20
PROPERTIES AND PHENOMENA	1. Relationships between Electronic Properties & Melt-Growth Conditions on Micro-Scale	Microprofiles of electron & ionized impurity concentrations in melt-grown GaAs were obtained for the first time.	11-19, 21
	2. Stoichiometry controlled segregation;	It was shown that impurity segregation in melt-grown GaAs is governed by amphoteric doping and deviation from stoichiometry.	11, 21
	3. Interaction between Epitaxial Layer & Substrate	It was demonstrated that outdiffusion of recombination centers from the substrate into LEP layers during growth process takes place. Growth conditions were formulated to minimize outdiffusion	22
	4. Growth-Property Relationships in Epitaxial Growth	It was found that growth rate variations have significant effect on the formation of recombination centers in GaAs.	23, 24
	5. Stoichiometry controlled deep levels	A direct relationship was established between As atom fraction in the melt and the concentration of electron traps in GaAs.	15
	6. Stoichiometry controlled dislocation density	It was found that an optimum stoichiometry defined by arsenic source temperature 617-618°C corresponds to a minimum dislocation density	20
	7. Oxygen related midgap level	We have unambiguously identified the oxygen related deep level ELO at 0.825 eV below the conduction band.	16
	8. Origin and properties of Major Electron Trap in GaAs	0.82 eV electron trap in GaAs has been identified as native defect complex involving the antisite As_{Ga}	15, 25-28

TABLE I

PROGRESS TO DATE - SUMMARY OF MAJOR DEVELOPMENTS

(Shaded areas indicate the most important achievements in the last two years)

	Development	Comments	Publications
PROPERTIES AND PHENOMENA (cont.)	9. Passivation of Deep Levels by Hydrogen	It was found that a concentration of the major deep level in GaAs can be effectively controlled by atomic hydrogen introduced by a standard plasma treatment.	29
	10. Optoelectronic Properties of InP	Cathodoluminescence studies of InP were completed	30
	11. Interface States	Surface states on GaAs-anodic oxide interface were determined with modified DLTS	31
	12. GaAs-Anodic Oxide Interface	A gigantic photoionization effect on GaAs-oxide interfaces was discovered. Utilizing this phenomenon it was shown, for the first time, that both deep & shallow interface states originate from Ga and As vacancies.	32-37
CHARACTERIZATION	1. Characterization methods based on electron mobility and free carrier absorption	Quantitative methods were developed for determination of compensation ratio in GaAs and InP	38-44
	2. IR Scanning Absorption	Quantitative method was developed for microprofiling of carrier concentration & compensation ratio through free carrier absorption	21
	3. Derivative Surface Photovoltage and Photocapacitance Spectroscopies	New Approach was developed for determination of deep levels, band structure and shallow impurites	45-47
	4. Characterization of Semi-Insulating GaAs	A rigorous procedure was developed for the determination of ionized impurity concentration from transport measurements in SI material	48
	5. SEM-Cathodoluminescence	Advanced variable temperature system was set up for cathodoluminescence microprofiling of defects, impurities & carrier concentration	30

PROGRESS TO DATE - SUMMARY OF MAJOR DEVELOPMENTS

(Shaded areas indicate the most important achievements in the last two years)

	Development	Comments	Publications
CHARACTERIZATION (cont.)	6. SEM-Electron Beam-Induced Current	Variable temperature system was set up for instantaneous profiling of diffusion length	
	7. Laser Scanning Photovoltage	Photovoltage microprofiling was developed for studying homogeneity of semi-insulating GaAs	
INTERACTION WITH INDUSTRIAL ORGANIZATIONS	1. Workshops, 1977 1981	Workshops were held with representatives of leading industrial & educational institutions devoted to the assessment of present status, major problems & future prospects for GaAs growth & applications	49
	2. Literature Survey, 1977 1982	The literature survey on GaAs was updated identifying the leading organization & most important trends in GaAs research and development	
	3. Exposure of the Program to Scientific Community	The present program and its major developments were exposed to the scientific community through a series of seminars given in industrial organizations (RCA, Texas Instruments, Hewlett-Packard, Hughes Int'l., Xerox, Eastman Kodak, Fujitsu Laboratories, NTT, etc.), presentations at scientific meetings and/or direct contacts with individual scientists	19, 49, 50
	4. Working Contacts	Contacts were established with industrial organizations in the area of GaAs characterization, growth & device applications. Material supplied by industrial organizations has been characterized on many occasions	
		Interaction with Microgravity Research Associates was established and aimed at the growth of GaAs in a space environment.	

on GaAs research and development programs in industry and universities. We have established, for example, that deviations from stoichiometry control dislocation density, concentration of point defects, related deep levels, and the amphoteric behavior of impurities. This discovery has also led to the identification of the causes of irreproducible growth and of the lack of precise control of the electronic properties of bulk GaAs. We have shown for the first time that these processes are linked directly to stoichiometry-induced defects and their interactions during the post-solidification cooling.

Every industrial and academic facility is incorporating our stoichiometry finding into its GaAs crystal growth program.

We have significantly advanced our understanding of the role of oxygen in melt-grown GaAs and especially of achieving semi-insulating material. We have shown that oxygen reduces the concentration of shallow silicon donors, and it also is involved in the creation of the midgap level. Our microscopic model of the major deep donor level EL2 (i.e., arsenic on gallium site plus arsenic vacancy) enabled for the first time the consistent explanation of the unique electronic properties of the EL2 and its sensitivity to the growth conditions. The above results bear directly on processes leading to semi-insulating behavior of GaAs, and thus are of fundamental importance in the pursuit of significantly improved quality GaAs for high-speed IC applications.

In electroepitaxial growth we have completed the development of a unified theoretical treatment which explains quantitatively the unique growth kinetics, the segregation behavior, and the morphological stability. We have demonstrated the feasibility of electroepitaxial growth of bulk crystals. Further work on electroepitaxy will be devoted to adaptation and optimization of the LPEE growth in space. The support of this part of the investigation has been undertaken by Microgravity Research Associates (MRA) in accord with the MRA-NASA joint endeavor.

We have completed the study of electrical and photo-electrical properties of GaAs-anodic oxide interfaces. Our interface-state model involving discrete deep and shallow levels (originating from oxidation-induced defects) made it possible to consistently explain hysteresis and anomalous frequency responses of GaAs MOS structures. We have successfully initiated a theoretical study of electron mobility limits of GaAs ultra-high-speed devices (specifically the HEMT-High Electron Mobility Transistor). Thus, we have developed a mobility model suitable for the treatment of transport properties of a two-dimensional gas confined in a triangular quantum well.

Our electronic characterization facility was extensively utilized to assess the quality of bulk and epitaxial GaAs and to study the relationships of electronic properties and growth parameters. Characterization techniques based on analysis of free carrier mobility were extended to semi-insulating (SI) GaAs and also to p-type material, i.e., to cases particularly important for IC applications.

Our study of melt growth will be extended to the assessment of relationships between growth conditions and structural and electronic properties of GaAs. Particular emphasis will be placed on the growth of improved quality semi-insulating material. We believe that it is of paramount importance to identify and eventually control stoichiometry-induced defect interactions which limit the structural and electronic quality of SI GaAs in a macro- and microscale. These interactions and related microscopic homogeneity are considered particularly important for the transition to the next generation of GaAs integrated circuits.

Our electronic characterization facility is being combined with impurity and structural analysis for optimizing the establishment of growth-property relationships, assessing electronic properties and studying their role in device applications. This characterization facility is being updated according

to recently emerged needs and developments. Techniques for microscale characterization and for high resolution two-dimensional mapping (based on scanning IR absorption and various SEM modes) are being refined through our most recent theoretical and experimental studies and computerized data processing.

Our discoveries of stoichiometry-induced defects and their paramount role in controlling all essential structural and electronic properties of GaAs has brought about significant implications for space processing of semiconducting compounds which have not been previously recognized. For example, classical segregation kinetics, applicable to processing of elemental semiconductors in space, are not applicable to GaAs processing. These implications are being studied in conjunction with a search for a melt-growth configuration compatible with space environment. We are convinced that our program is essential for arriving at new approaches which will ensure successful experimentation with and processing of GaAs and other semiconductor compounds under zero gravity conditions. We also believe that this program will continue to impact the overall national program on GaAs growth and applications through the advancement of knowledge and development of new growth and processing techniques, and extensive electronic characterization.

II. PROGRESS TO DATE

II.1. Introduction

Since the initiation of this investigation we have succeeded in the development of unique crystal growth approaches, new effective techniques for a macro- and microscale characterization of key electronic properties and in the discovery of new phenomena and processes relevant to GaAs device applications. Growth-property relationships established for the first time have led us to defining stoichiometry as a fundamental factor controlling structural and electronic properties of GaAs and to the growth of bulk GaAs of improved quality (dislocation-free and electron trap-free material). Table I summarizes the major achievements. Detailed discussion is given in our publications and our annual reports. In the "Progress to Date" section of this proposal a brief outline of our most significant developments during the last three years will be presented, so that last year's findings can be viewed in better perspective.

II.2. Crystal Growth

In our crystal growth studies we have thus far concentrated on two approaches: liquid phase electroepitaxy and Bridgman-type growth from the melt. The original selection of these techniques was made on the basis of their compatibility with space environment and also because they lend themselves to the control of the growth process and thus to the study of growth-property relationships.

We have completed the fundamental study on electroepitaxy. Results of this study provide the basis for the development of an LPEE apparatus for the growth of bulk crystals in space. Related ground-based research will be carried out by our Electronic Materials Group at MIT under the sponsorship of Microgravity Research Associates.

During the last three years we have grown about 100 GaAs crystals utilizing our unique Bridgman-type apparatus especially designed and constructed for the investigation of relationships between crystal growth parameters and electronic and structural properties. The results of these studies turned out to be of major significance, as they have led, for the first time, to the establishment of growth-property relationships of fundamental importance for obtaining undoped dislocation-free GaAs and electron trap-free shallow donor doped GaAs. These relationships made it possible to resolve the origin of the dominating deep levels and elucidate the role of oxygen in obtaining undoped semi-insulating GaAs.

II.2.a. Growth-Property Relationships—Critical Role of Stoichiometry

In our growth experiments the stoichiometry was varied by varying the arsenic source temperature, T_{As}, which in turn controls the arsenic pressure over the melt and thus the melt composition. A typical range of T_{As}, 610-628°C, corresponded to melt composition (determined by arsenic-to-gallium ratio) changes from 0.52 to 0.485.

Dislocation Density. We have found that the dislocation density is a very sensitive function of T_{As}. Typical results are shown in Fig. 1-2. They demonstrate that dislocation etch pit density (revealed by etching in a molten KOH) exhibits minimum concentration for $T_{As} \approx 617°C$. In a number of crystal growth experiments we have confirmed the importance of these optimum stoichiometry conditions. Thus, undoped crystals routinely grown under these optimum conditions exhibited dislocation density below 500. Doping at the level of $10^{17} cm^{-3}$ with shallow donors suppressed dislocation density to values below 100 cm^{-2}, i.e., to values referred to as corresponding to "dislocation free" material. Doping with shallow acceptors at a concentration above $10^{17} cm^{-3}$ was found to enhance the formation of dislocations, as shown in Fig. 3.

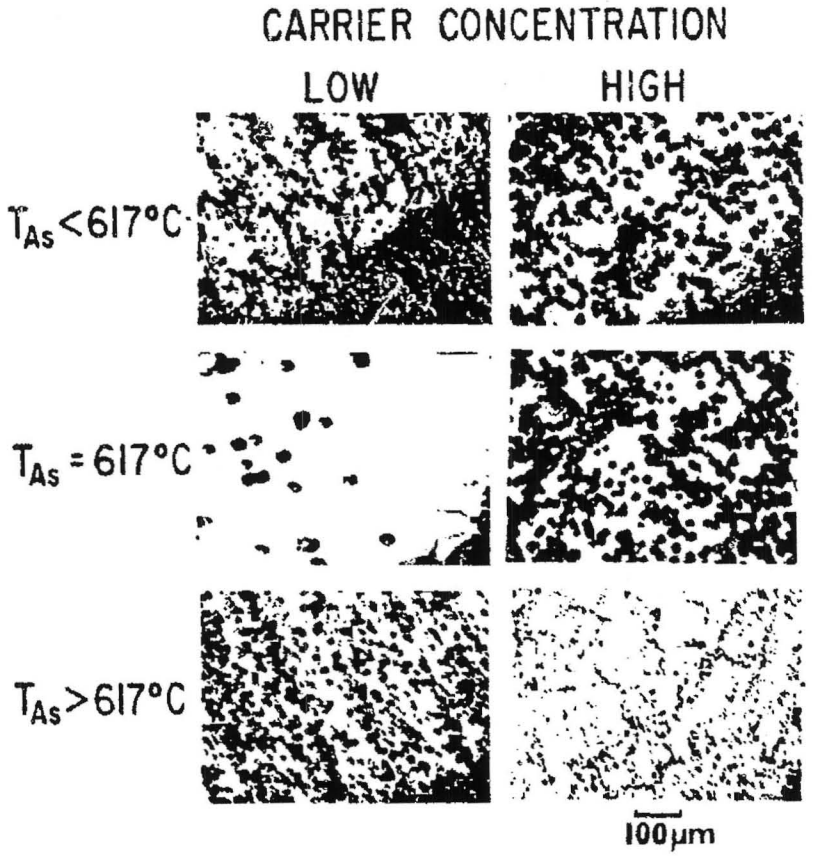

Figure 1. Dislocation in segments of GaAs p-type crystals grown under different As source temperature for low and high hole concentration, respectively.

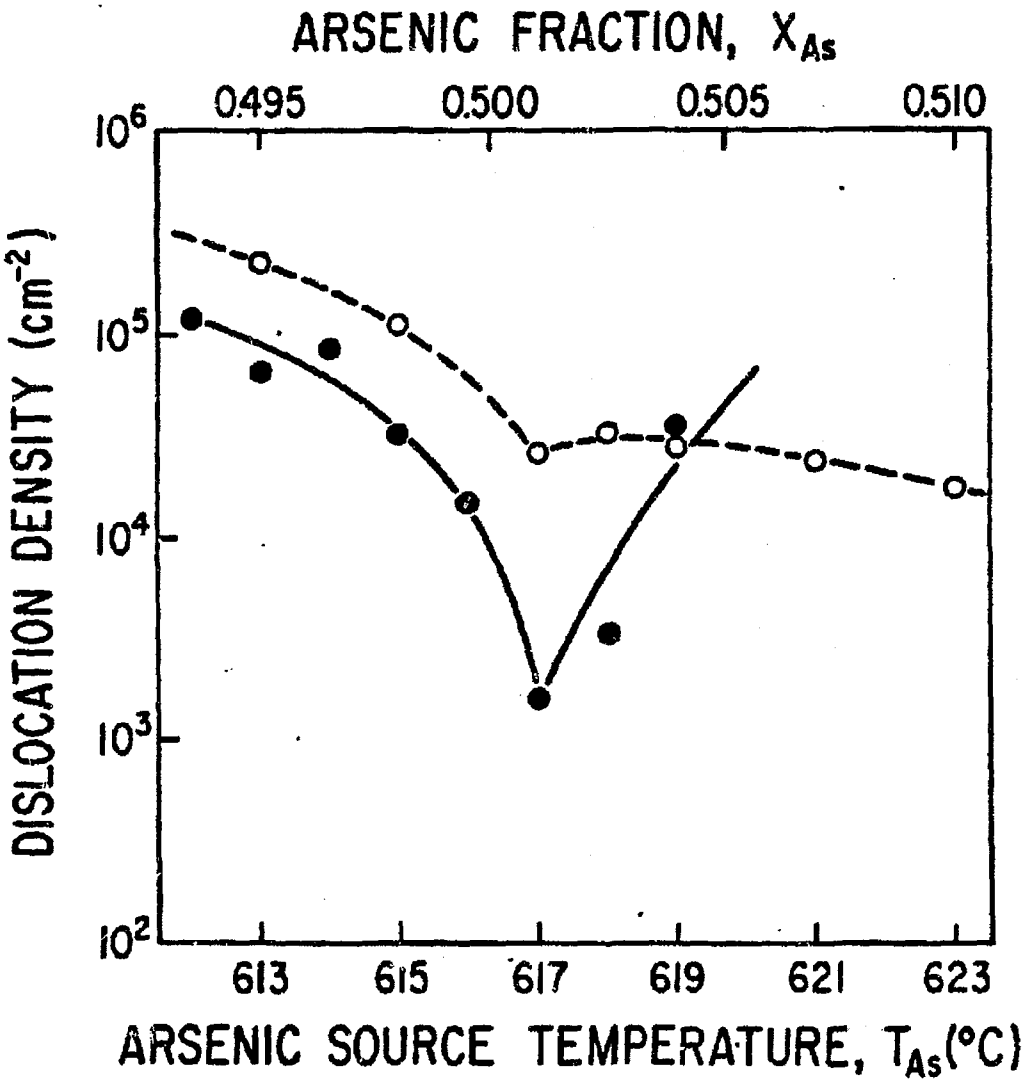

Figure 2.

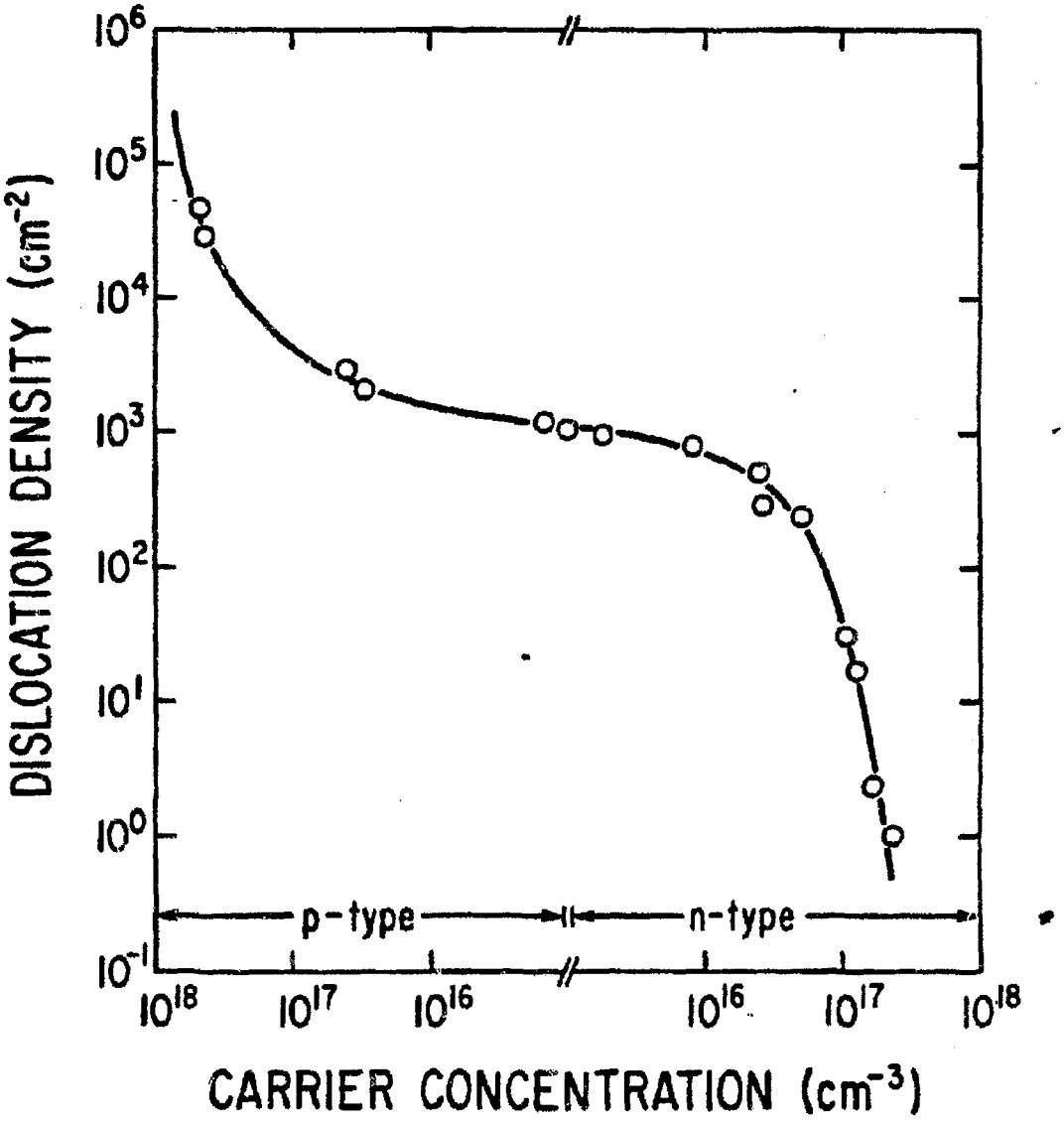

Figure 3.

Dislocations are commonly known to play a detrimental role in GaAs integrated circuits. Accordingly, the establishment of growth conditions yielding minimum dislocation density can be considered as a significant step toward the growth of improved device quality GaAs bulk crystals. We also believe that this finding will become of critical importance in future stages of crystal growth developments as other factors contributing to dislocation formation during post-solidification (e.g., thermal stress during cooling) are addressed in conjunction with large diameter crystals.

Impurity Segregation. The optimum arsenic source temperature 617°C was also found to yield the lowest compensation ratio and the highest electron mobility value of n-type GaAs crystals. Thus, these results showed that deviation from stoichiometry is a contributing factor to the amphoteric behavior of shallow impurities in melt-grown GaAs crystals. In earlier studies we have observed unique spacial variations which could not be explained on the basis of classic segregation kinetics controlled by the microscopic growth rate. Representative results are shown in Fig. 4a where the carrier concentration undergoes significant variations, whereas the concentration of the

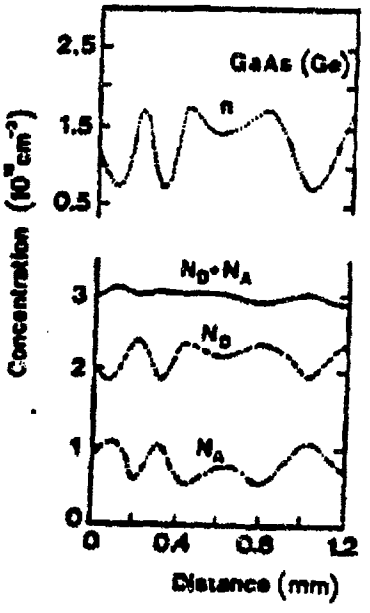

Figure 4a. Electron concentration and ionized impurity microprofiles of Ge-doped melt-grown GaAs obtained with scanning IR absorption spectroscopy. Note different behavior of N_D and N_A.

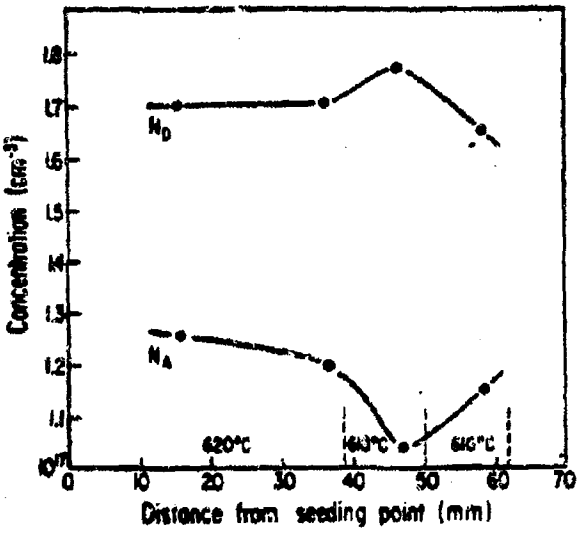

Figure 4b. Stoichiometry-induced changes in incorporation of donors and acceptors. Note similarity to Fig. 2a.

dopant impurity (N_D+N_A) remains essentially constant. As seen in Fig. 4b, similar behavior is caused by changes in arsenic pressure.

Deep Levels. The arsenic pressure was also found to control the concentration of a major deep level, EL2. Typical dependence of the EL2 concentration on T_{As} obtained for unintentionally doped GaAs is presented in Fig. 5. It is seen that the concentration of the EL2 decreases in going from arsenic-rich to gallium-rich growth conditions. This finding proves that arsenic-rich conditions are most desired for the growth of undoped semi-insulating GaAs which requires a high concentration of EL2. Such behavior has been indeed observed in a recent study of Liquid-Encapsulated Czochralski growth of semi-insulating GaAs.

II.2.b. Post-Solidification Processes; Role of Impurities

The stoichiometry effects discussed above are caused by native defects generated during the solidification process. Upon post-solidification cooling of the crystal these defects interact and form other defects and defect complexes which determine the final properties of the as-grown crystal and also its behavior during subsequent heat treatment involved in device processing. In our study we have employed intentional doping in order to distinguish between solidification effects and the post-solidification phenomena (during cooling of the crystal). It is a general feature of the post-solidification defect interactions in GaAs that they are affected by shallow donors or acceptors, irrespective of the lattice-site the dopant occupies. Furthermore, the threshold dopant concentration determines the critical temperature range at which the post-solidification interactions take place.

Our finding that the EL2 level as well as dislocations are annihilated by shallow donors provides unique evidence of the above behavior. The effects

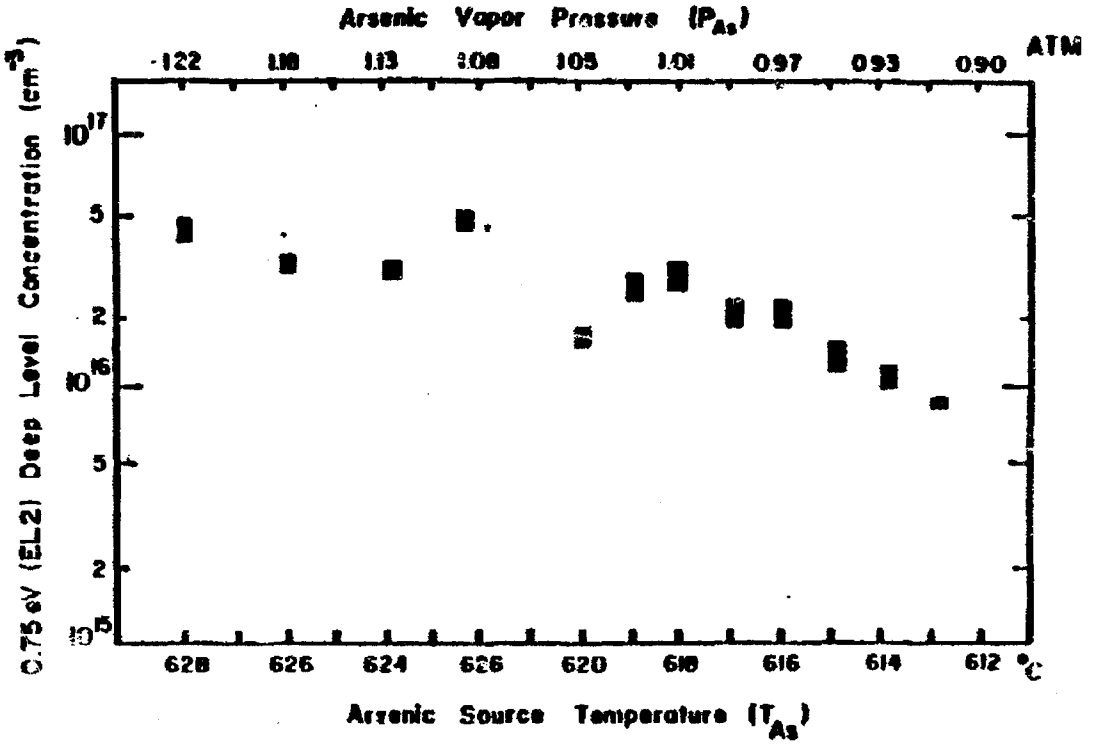

Fig. 5. Concentration of the 0.75 eV deep level (EL2) vs. the arsenic source temperature (T_{As})

of doping on the EL2 level were adequately explained by our microscopic model of this center identifying the EL2 with a complex consisting of an antisite defect (arsenic on a gallium site) and an arsenic vacancy, $As_{Ga}V_{As}$. This complex (shown in Fig. 6) is formed during the migration of a gallium vacancy V_{Ga} to a neighboring arsenic site. The pertinent reaction of charge defects is $V_{Ga}^{-}+As_{As}^{+}\rightleftharpoons As_{Ga}^{++}+V_{As}^{+}+4e$; thus the concentration of the EL2 center $[As_{Ga}V_{As}]$ is proportional to n^{-4} where n is the electron concentration at elevated temperature. By increasing n above the intrinsic concentration, the EL2 level is effectively suppressed and annihilated as pointed out above. From the threshold value of electron concentration, it is concluded that the formation of the 0.82 eV deep level takes place at temperatures below about 1050 K, i.e., during the post-growth cooling in the case of melt-grown GaAs.

II.2.c. The Role of Oxygen in Melt Growth of GaAs

Semi-insulating GaAs (i.e., the material used in advanced IC applications) is grown with Ga or As oxides added to the melt or with boric acid used as a liquid encapsulant. Our study has been devoted to the establishment of the role of oxygen in the growth of SI material, and especially to the verification of (i) Si gettering by oxygen and (ii) the effect of oxygen on deep levels.

Gettering of Si. Our experimental results on the Si concentration in GaAs as a function of the amount of Ga_2O_3 added to the charge material is given in Fig. 7 for two source materials containing large (source A) and small amounts (source B) of silicon. It is seen that for source B the concentration of Si in the crystals is about 200 times higher than the Si concentration in the source. The contamination with Si results from the chemical interaction of gallium in the melt with the quartz boat:

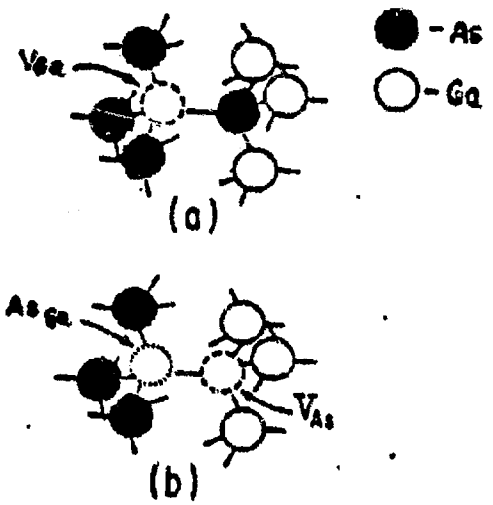

Figure 6. Formation of the EL2 complex; (a) gallium vacancy, (b) $As_{Ga}V_{As}$ complex formed as a result of V_{Ga} migration to As site.

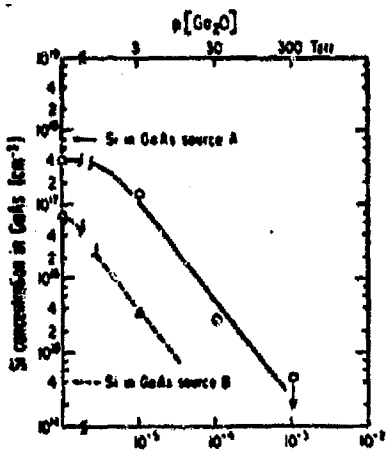

7a

Weight fraction of added Ga_2O_3: $[\frac{Ga_2O_3}{GaAs}]$

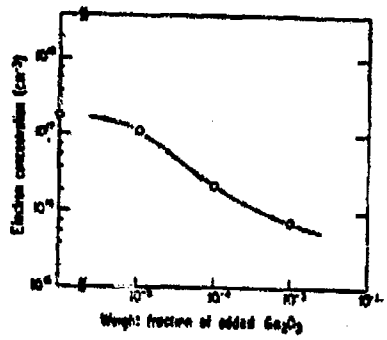

7b

$$4\,Ga_{(\text{in melt})} + SiO_2 \rightleftarrows 2\,Ga_2O_{(\text{vapor})} + Si_{(\text{in melt})} \qquad (1)$$

According to this reaction, the Si concentration in the melt is controlled by the vapor pressure of Ga_2O. The addition of any oxygen compound which upon interaction with GaAs forms Ga_2O, increases the Ga_2O pressure, and thus reduces the silicon contamination. Consequently, the reduction of the Si concentration by Ga_2O_3 in the case of the source A, must be interpreted as purification of the melt, via reaction (1) proceeding from right to left.

SIMS analysis showed that oxygen is not incorporatedinto GaAs at concentrations exceeding a few times $10^{16}cm^{-3}$. Thus, it appears that all of the oxygen participates in the formation of the volatile Ga_2O, which suppresses Si contamination from the quartz, and even removes Si from the melt.

Oxygen-Related Deep Level. Employing Bridgman-grown crystals with controlled oxygen doping we have successfully identified an oxygen-related deep level, ELO. The activation energy (825 ± 5 meV) of ELO is almost the same as that of the dominant midgap level, EL2 (815 ± 2 meV). This fact impedes the identification of ELO by standard DLTS. However, we found that the electron capture cross section of ELO is about four times greater than that of EL2. This characteristic served as the basis for the separation and quantitative investigation of ELO employing detailed capacitance transient measurements in conjunction with reference measurements on crystals grown without oxygen doping and containing only EL2. Emission rate thermal activation plot T^2e^{-1} vs. $10^3/T$ for EL2 and for the oxygen-related level, ELO, is presented in Fig. 8.

Our experimental data for EL2 span over about 7 orders of magnitude, i.e., a much greater range than any previous study. Least square analysis yielded, for EL2, an activation energy of 815 ± 2 meV and an electron cross section $\sigma_{na} = (1.2 \pm 0.1) \times 10^{-13}cm^2$. We consider these values more accurate

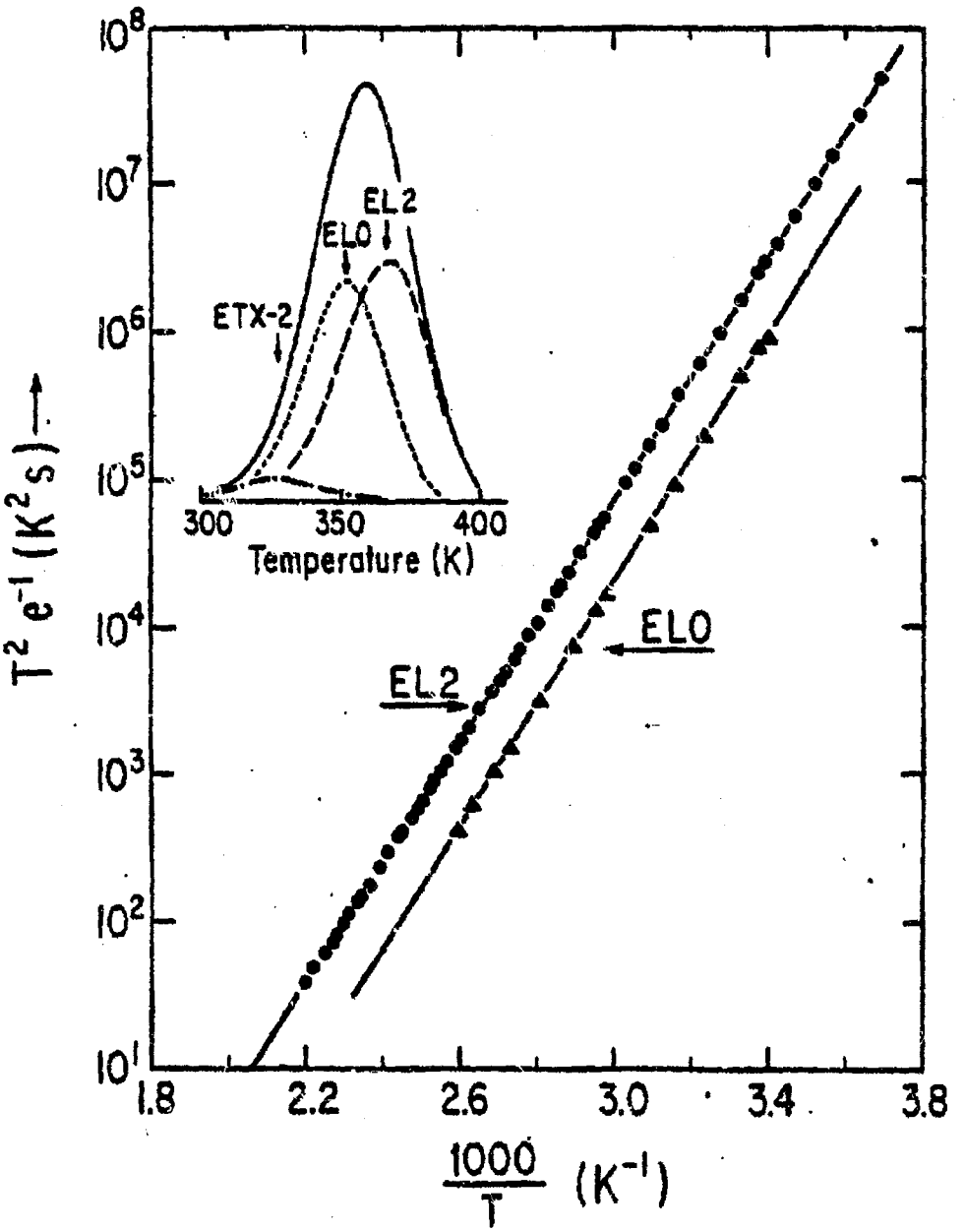

Fig. 8.

than any previously published. Emission rate data for ELO obtained with the transient separation method are presented here for the first time. The activation energy is 825 $\pm$ 5 meV and the capture cross section $\sigma_{na} = (4.8 \pm 0.6) \times 10^{-13} cm^2$. It is seen that the energies of ELO and EL2 are virtually the same. However, the capture cross section of ELO is four times greater than that of EL2 which offers the only means for distinguishing between these levels in transient capacitance measurements.

Emission rate as a function of temperature data was used to deconvolute the DLTS peak of oxygen-doped GaAs. As shown in the insert of Fig. 8, the major components are: EL2 and ELO. The rate window t_1/t_2 = 10 ms/100 ms was intentionally selected to reproduce the experimental conditions of the recent deep level study in LEC GaAs.[54] A comparison with these results indicates that ELO is identical to the dominant midgap level in LEC material labelled as ETX-1. (A third minor level also seen in the deconvoluted DLTS peak of Fig. 8 corresponds to the ETX-2 level LEC GaAs.) The presence of ELO in LEC GaAs is not surprising, since boric oxide used as the encapsulant of the GaAs melt serves also as a source of oxygen.

II.3. Properties and Phenomena

New Shallow Donor Associated with EL2. From a systematic analysis of Hall effect measurements on a large number of melt-grown GaAs crystals with different concentrations of the major deep trap (EL2) we have identified a new shallow donor level (20-30 meV below the conduction band). As shown in Fig. 9, this shallow donor leads to a specific temperature dependence of the electron concentration which was used for the determination of the donor energy.

The presence of the shallow donor state has important consequences for a compensation mechanism in semi-insulating GaAs.

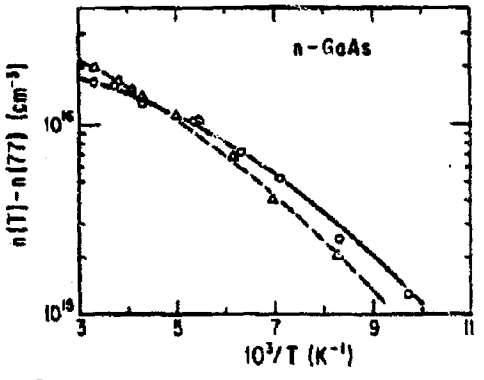

Fig. 9. Dependence of the electron concentration (freezeout), $n(T) - n(77)$ on temperature in GaAs containing EL2. (○) $n(300) = 1.25 \times 10^{17}$ cm^{-3}, $N_{EL2} = 2.2 \times 10^{16}$ cm^{-3}; (△) $n(300) = 1.98 \times 10^{17}$, $N_{EL2} = 3.0 \times 10^{16}$ cm^{-3}. Curves are theoretically calculated from Eqs. (2) and (3)—see text.

Intracenter Transitions in the EL2. We have identified intracenter transitions in the major deep level EL2 in GaAs for the first time by superimposing photocurrent measurements on those of optical absorption. These transitions were found to be responsible for the characteristic EL2 absorption band between 1.0 and 1.3 eV as shown in Fig. 10. At low temperatures (<60 K) intracenter absorption exhibits a fine structure (Fig. 11) involving the zero phonon line and replicas at energies close to those of transverse acoustic phonons (TA). This coupling with TA phonons is a strong indication that EL2 is an extrinsic self-trapping center.

Effects of Arsenic Pressure on the Surface Morphology of Heat-Treated GaAs. The effects of arsenic pressure, during high temperature heat treatment, on the surface morphology of GaAs crystals were investigated by controlling the arsenic pressure in a two-heat-zone apparatus. Heat treatments were carried out at 900°C and 700°C (a temperature range relevant to device applications) for 16 hours under arsenic pressure of 48-458 Torr and 4.2-539 Torr, respectively. It was found that for every temperature there is an optimum arsenic pressure under which the surface morphology exhibits no detectable changes during heat treatment. As shown in Fig. 12, below and above the optimum arsenic pressure pronounced changes of the surface morphology were observed. The optimum pressure must represent the condition of minimum deviation from stoichiometry.

Fundamental Limitations of HEMT Devices. We have extended our theoretical mobility treatment of GaAs to the analysis of an electron transport in high electron mobility transistors. Thus, we have modeled the HEMT structure employing a two-dimensional triangular quantum well confining an electron gas free to move parallel to the walls of the well. We have calculated scattering rates for all major scattering mechanisms, i.e., phonons, impurities and alloy

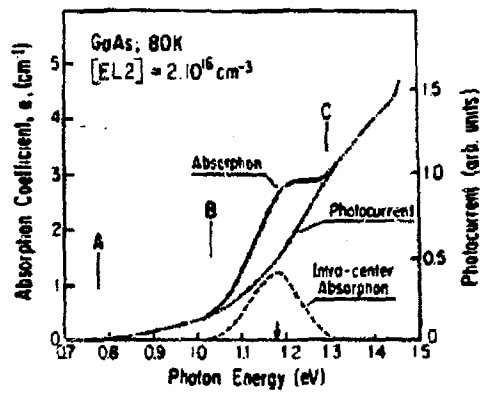

Fig. 10. Optical absorption and photocurrent spectra measured on the same sample of melt-grown GaAs with EL2 concentration of about 2×10^{16} cm^{-3}. The difference between the two spectra defines the intracenter absorption band which extends from 1.03 to 1.32 eV and is responsible for the characteristic shape of the EL2 absorption (shaded area).

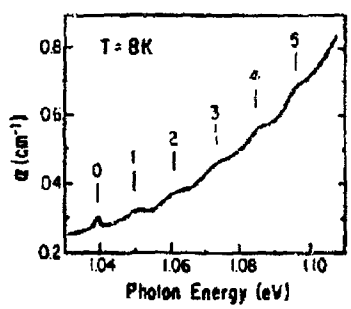

Fig. 11. Fine structure of the EL2 intracenter absorption which shows zero-phonon line at $h\nu = 1.0395$ eV and phonon replica at energy interval of 11 ± 1 meV.

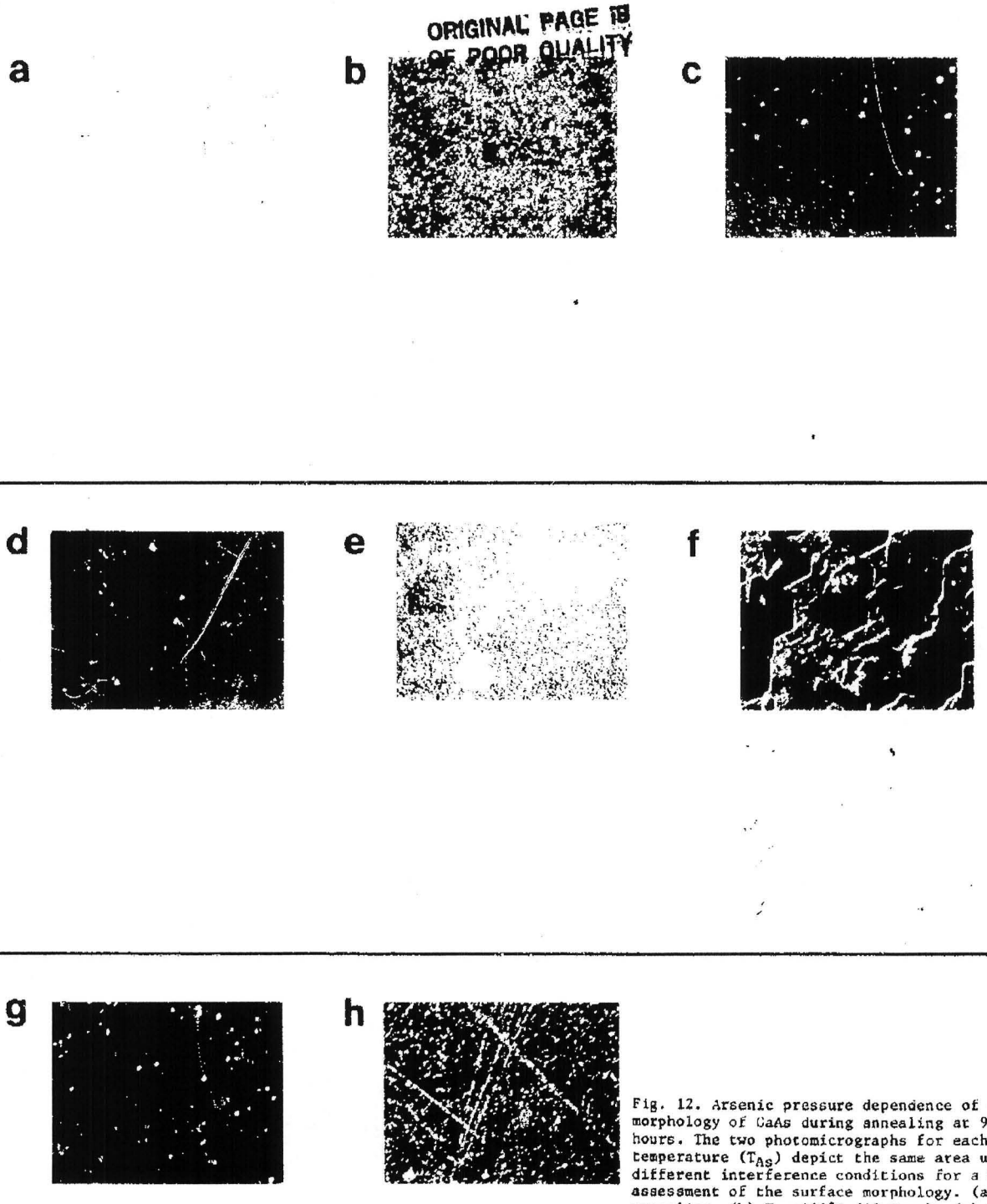

Fig. 12. Arsenic pressure dependence of the surface morphology of GaAs during annealing at 900°C for 16 hours. The two photomicrographs for each As source temperature (T_{As}) depict the same area under two different interference conditions for a better assessment of the surface morphology. (a) before annealing, (b) T_{As}=494°C (48 Torr), (c) T_{As}=510°C (71 Torr), (d) T_{As}=521°C (94 Torr), (e) T_{As}=530°C (116 Torr), (f) T_{As}=541°C (151 Torr), (g) T_{As}= 551°C (190 Torr), (h) T_{As}=570°C (288 Torr).

disorder. In ideal two-dimensional gas an absolute mobility limit is controlled by phonon and alloy scattering, and it reaches a value of about $5 \times 10^6 cm^2/Vs$ at 5 K which is about 25 times greater than the mobility ever reported for the highest purity GaAs. Calculated mobilities are shown in Fig. 13 as a function of the gas density. It is seen that our model accounts very well for experimental mobility characteristics.

GaAs-Oxide Interface. In the recently completed study of the electrical properties of GaAs-native oxide interface we have found two discrete states with energies 0.7 and 0.84 eV below the conduction band, i.e., very similar to surface states in real GaAs surfaces and on the surfaces with submonolayer metal coverages. We have discovered a new photodischarge process which involves the ejection of electrons from deep surface states following an energy transfer from photo-excited donor-acceptor pairs associated with a high density of states (about $10^{14} cm^{-2}$) in the interface region. Utilizing the new process, we were able to confirm the energetics and dynamic parameters of the deep levels, and also, for the first time, those of donor and acceptor interface levels, consistent with theoretical predictions.

Our interface photodischarge study of p-type GaAs MOS structures revealed the presence of deep interface states and shallow donors and acceptors which were also observed in n-type GaAs MOS through subbandgap photoionization transitions. For higher photon energies internal photoemission was observed, i.e., injection of electrons to the conduction band of the oxide from either the metal (Au) or from the GaAs valance band; the threshold energies were found to be 3.25 ± 0.1 eV and 3.7 ± 0.1 eV, respectively. The measured photoemission current exhibits a thermal activation energy of about 0.06 eV, which is consistent with a hopping mechanism of electron transport in the oxide.

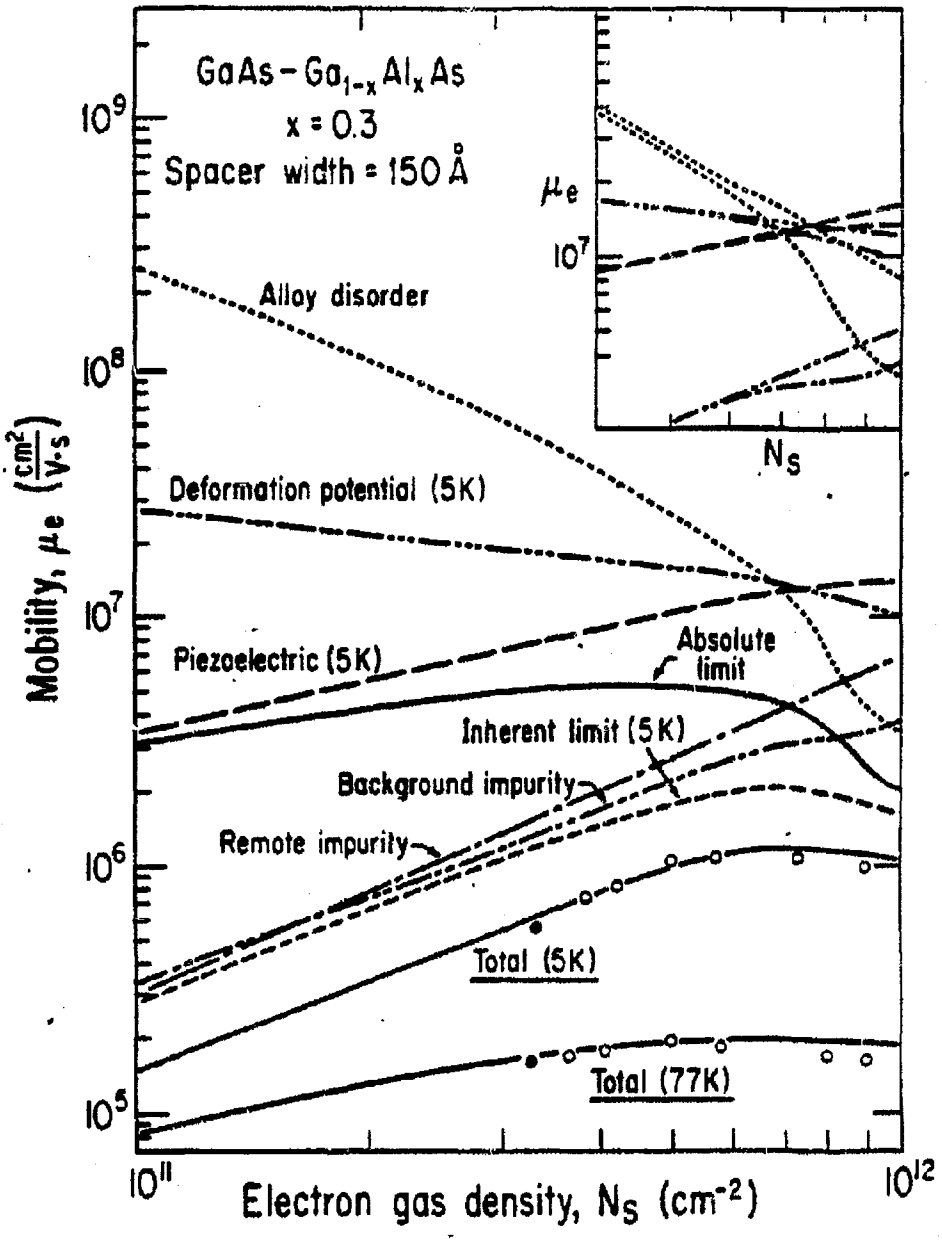

Fig. 13. Electron mobility of two-dimensional electron gas confined at GaAs-$Ga_{1-x}Al_xAs$ interfaces vs. gas density. Lines-theoretical; points-state of art mobility values (unpublished)

The energy band diagram of the GaAs-native oxide MOS structure determined from our internal photoemission study is shown in Fig. 14.

We have also utilized the photoionization discharge of GaAs-oxide interface in conjunction with capacitance measurements and thermal emission to establish the origin of C-V hysteresis and anomalous frequency dispersion inherent in GaAs-MOS structures. It was shown that, for n-type GaAs, discrete states at E_c-E_t play a major role. Due to the low rate of thermal emission the occupation of these states does not obey equilibrium characteristics (determined by Fermi level position at the surface) which leads at low temperatures to very large C-V hysteresis.

II.4. Characterization

Our electronic characterization facility was essentially completed in 1980. Since then it has been used for evaluation of grown crystals on a macro- and microscale, for the study of growth-property relationships and for quantitative investigation of device-related phenomena and properties of GaAs. Our characterization approaches are of course being continuously upgraded experimentally and theoretically in accord with the state-of-the-art knowledge. During the last year we have refined two approaches for electrical and optical characterization of semi-insulating GaAs.

Optical Evaluation of the EL2 Concentration in Semi-Insulating GaAs. We have developed a practical procedure for the evaluation of the Fermi energy in semi-insulating (SI) GaAs from electrical measurements. This procedure makes it possible to reliably extend the determination of the major deep level (EL2) concentration, by near-infrared absorption measurements, to SI GaAs. Employing this procedure, we showed (see Fig. 15) that the EL2 concentration in Czochralski-grown GaAs increases monotonically with increasing As/Ga ratio

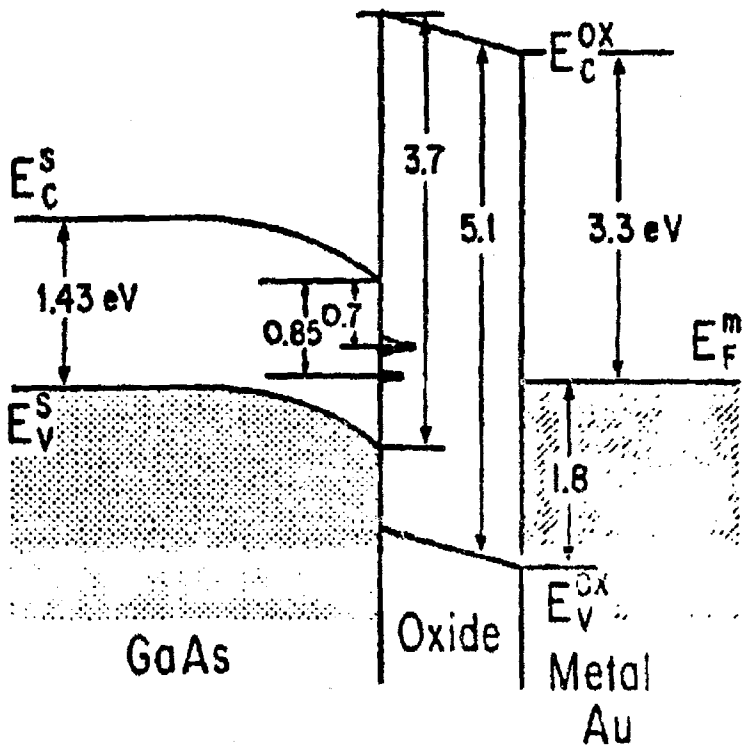

Figure 14. Energy band configuration of the GaAs-native oxide MOS structure.

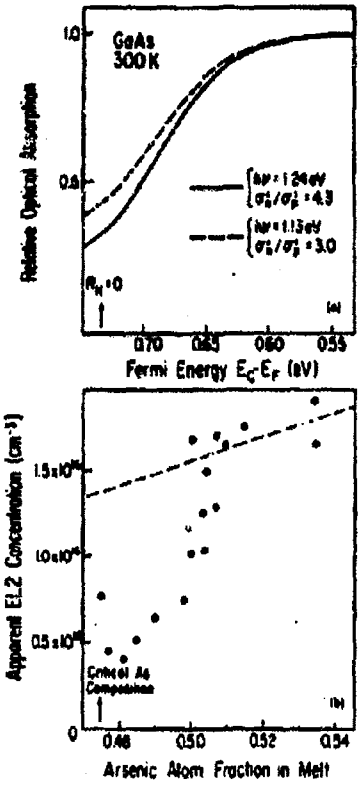

FIG15. (a) Calculated relative optical absorption (for two photon energies) due to the photoionization of a constant concentration of EL2 as a function of Fermi energy; $R_H = 0$ corresponds to vanishing Hall mobility. (b) Experimental results of optical absorption expressed as EL2 concentration as a function of arsenic atom fraction in melt after Ref. 2. Dashed line shows actual EL2 concentrations after experimental results are corrected for changes in the EL2 occupancy. Critical As composition corresponds to $R_H = 0$ in (a).

(throughout the conversion from SI n-type to semiconducting p-type crystals) rather than abruptly as previously proposed.

Free Carrier Mobility. Free carrier mobility values are commonly taken as an overall measure of perfection and purity. We have completed a rigorous theoretical and experimental study of carrier mobilities in GaAs which led to the development of a practical means for fast quantitative characterization of GaAs using computed values of mobility conveniently tabulated as a function of free carrier concentration and compensation ratio. More recently we have succeeded in developing a straightforward (but rigorous) procedure for the characterization of semi-insulating GaAs from Hall mobility values measured at slightly elevated temperatures. Thus, the mobility curves presented in Figs. 16a and 16b permit the determination of the total concentration of ionized impurities ($N_D^+ + N_A^-$) in semi-insulating GaAs.

PUBLICATIONS RESULTING FROM WORK SPONSORED BY NASA ON
"CRYSTAL GROWTH OF DEVICE QUALITY GaAs IN SPACE"

1. L. Jastrzebski, J. Lagowski, H.C. Gatos and A.F. Witt, "Model of Liquid Phase Electroepitaxial Growth: GaAs," presented at Fourth American Conf. on Crystal Growth, July 1978, Gaithersburg, Maryland.

2. L. Jastrzebski, J. Lagowski, H.C. Gatos and A.F. Witt, "Liquid-Phase Electroepitaxy: Growth Kinetics," J. Appl. Phys. 49, 5909 (1978).

3. L. Jastrzebski, J. Lagowski, H.C. Gatos and A.F. Witt, "Dopant Segregation in Liquid Phase Electroepitaxy; GaAs," presented at Fourth American Conf. on Crystal Growth, July 1978, Gaithersburg, Maryland.

4. J. Lagowski, L. Jastrzebski and H.C. Gatos, "Liquid PHase Electroepitaxy: Dopant Segregation," J. Appl. Phys. 51, 364 (1980).

5. T. Bryskiewicz, J. Lagowski and H.C. Gatos, "Electroepitaxy of Multicomponent Systems," J. Appl. Phys. 51, 988 (1980).

6. A. Okamoto, "Study of the Dynamic Behavior of Electroepitaxy: Growth Kinetics, Impurity Segregation and Surface Morphology," Ph.D. Thesis, M.I.T., 1982.

7. A. Okamoto, J. Lagowski and H.C. Gatos, "Enhancement of Interface Stability in Liquid Phase Electroepitaxy," J. Appl. Phys. 53, 1706 (1982).

8. Y. Imamura, L. Jastrzebski and H.C. Gatos, "Defect Structure and Electronic Characteristics of GaAs Layers Grown by Electroepitaxy and Thermal LPE," J. Electrochem. Soc. 126, 1381 (1979).

9. S. Isozumi, C. Herman, A. Okamoto, J. Lagowski and H.C. Gatos, "A New Approach to Liquid Phase Electroepitaxy," presented at 158 Annual Meeting of Electrochem. Soc., October 1980; J. Electrochem. Soc. 128, 2220 (1981).

10. A. Okamoto, S. Isozumi, J. Lagowski and H.C. Gatos, "In Situ Monitoring of GaAs LPEE Growth Rate," presented at 159 Annual Meeting of Electrochem. Soc., May 1981, Minneapolis: J. Electrochem. Soc. 129, 2095 (1982).

11. J. Parsey, Y. Nanishi, J. Lagowski and H.C. Gatos, "Bridgman-Type Apparatus for the Study of Growth-Property Relationships," J. Electrochem. Soc. 129, 388 (1982).

12. J.M. Parsey, Jr., "An Investigation of Growth-Property Relationships in Bulk GaAs Single Crystals," Ph.D. Thesis, M.I.T. 1982.

13. Y. Nanishi, J. Parsey, J. Lagowski and H.C. Gatos, "Dislocation-Free Undoped GaAs by Controlled Horizontal Bridgman Method," presented at 158 Meeting of Electrochem. Soc., October 1980, Hollywood, Fla.

14. J. Parsey, Y. Nanishi, J. Lagowski and H.C. Gatos, "Electron Trap-Free Low Dislocation Melt-Grown GaAs," J. Electrochem. Soc. 128, 936 (1981).

15. J. Lagowski, H.C. Gatos, J. Parsey, K. Wada, M. Kaminska and W. Walukiewicz, "Origin of the 0.82 eV Electron Trap in GaAs and Its Annihilation by Shallow Donors," Appl. Phys. Lett. 40, 342 (1982).

16. J. Lagowski, D. G. Lin, T. Aoyama and H. C. Gatos, "Identification of Oxygen-Related Midgap Level in GaAs," Appl. Phys. Lett. 44, 336 (1984)

17. M. Kaminska, J. Lagowski, J. Parsey and H. C. Gatos, "Oxygen-Induced Levels in GaAs," Inst. Phys. Conf. Ser. 63, 197 (1981).

18. H. C. Gatos, "Bulk Growth of III-V Compounds and Growth-Property Relationships," Summer School of EPS on III-V Compounds and Their Applications, Erice, Italy, 1981.

19. H.C. Gatos and J. Lagowski, "Challenges in III-V Semiconductor Compounds," Proc. of Symp. on "III-V Optoelectronics Epitaxy and Device Related Processes," ed. by V.G. Keramidas and S. Mahajan, The Electrochemical Society, Pennington, NJ, 1983. p. 1.

20. J.M. Parsey, Jr., J. Lagowski and H.C. Gatos, "The Effects of Melt Stoichiometry and Impurities on the Formation of Dislocations in Bulk GaAs," Proc. of Symp. on "III-V Optoelectronics Epitaxy and Device Related Processes," ed. by V.G. Keramidas and S. Mahajan, The Electrochemical Society, Pennington, NJ, 1983. p. 61.

21. L. Jastrzebski, J. Lagowski, W. Walukiewicz and H. C. Gatos, "Determination of Carrier Concentration and Compensation Microprofiles in GaAs," J. Appl. Phys. 51, 2301 (1980).

22. L. Jastrzebski, J. Lagowski and H. C. Gatos, "Outdiffusion of Recombination Centers from the Substrate into LPE Layers; GaAs," J. Electrochem. Soc. 126, 2231 (1979).

23. L. Jastrzebski, J. Lagowski and H. C. Gatos, "Effect of Growth Kinetics on Formation of Recombination Centers in GaAs," presented at 155th Annual Meeting of Electrochem. Soc., May 1979, Boston.

24. L. Jastrzebski, J. Lagowski and H. C. Gatos, "Formation of Recombination Centers in Epitaxial GaAs Due to Rapid Changes of the Growth Velocity," J. Electrochem. Soc. 128, 697 (1981).

25. J. Lagowski, M. Kaminska, J. M. Parsey, H. C. Gatos and W. Walukiewicz, "Microscopic Model of the EL2 Center in GaAs," Inst. Phys. Conf. Ser. 65, 41 (1983).

26. W. Walukiewicz, J. Lagowski and H. C. Gatos, "On the Optical Evaluation of the EL2 Deep Level Concentration in Semi-Insulating GaAs," Appl. Phys. Lett. 43, 192 (1983).

27. M. Kaminska, M. Skowronski, J. Lagowski, J. M. Parsey and H. C. Gatos, "Intracenter Transitions in the Dominant Deep Level (EL2) in GaAs," Appl. Phys. Lett. 43, 302 (1983).

28. M. Kaminska, J. M. Parsey, J. Lagowski and H. C. Gatos, "Current Oscillations in Semi-Insulating GaAs Associated with Field-Enhanced Capture of Electrons by the Major Deep Donor EL2," Appl. Phys. Lett. 41, 989 (1982).

29. J. Lagowski, M. Kaminska, J. M. Parsey, H. C. Gatos and M. Lichtensteiger, "Passivation of the Dominant Deep Level (EL2) in GaAs by Hydrogen," Appl. Phys. Lett. 41, 1078 (1982).

30. C.H. Gatos, J.J. Vaughan, J. Lagowski, and H.C. Gatos, "Cathodoluminescence in InP," J. Appl. Phys. 52, 1464 (1981).

31. E. Kamieniecki, T. E. Kazior, J. Lagowski and H. C. Gatos, "A Study of GaAs-Native Oxide Interface States by Transient Capacitance," presented at 7th Annual Conference on the Physics of Compound Semiconductor Interfaces, Estes Park, Colorado, January 1980; J. Vac. Science & Technology 17, 1041 (1980).

32. J. Lagowski, T. E. Kazior, W. Walukiewicz, H. C. Gatos and J. Siejka, "GaAs-Oxide Interface States: Gigantic Photoionization via Auger-like Process," J. Vac. Sci. Technol. 19, 519 (1981).

33. J. Lagowski, W. Walukiewicz, T. E. Kazior, H. C. Gatos and J. Siejka, "GaAs-Oxide Interface; Gigantic Photionization Effect and Its Implications to the Origin of These States," Appl. Phys. Lett. 39, 240 (1981).

34. E. Kamieniecki, T. E. Kazior, J. Lagowski and H. C. Gatos, "Study of GaAs-Oxide Interface by Transient Capacitance Spectroscopy: Discrete Energy Interface States," J. Vac. Sci. Technol. 17, 1041 (1980).

35. T. E. Kazior, J. Lagowski and H. C. Gatos, "The Electrical Behavior of GaAs-Insulator Interfaces - A Discrete Energy Interface State Model," J. Appl. Phys. 54, 2533 (1983).

36. H. C. Gatos, J. Lagowski and T. E. Kazior, "GaAs MIS Structures - Hopeless or Promising?" Jpn. J. Appl. Phys. 22, 11 (1983).

37. P. K. Kashkarov, T. E. Kazior, J. Lagowski and H. C. Gatos, "Interface States and Internal Photoemission in p-Type GaAs Metal-Oxide-Semiconductor Surfaces," J. Appl. Phys. 54, 963 (1983).

38. W. Walukiewicz, J. Lagowski, L. Jastrzebski and H. C. Gatos, "Minority-Carrier Mobility in p-Type GaAs," J. Appl. Phys. 50, 5040 (1979).

39. W. Walukiewicz, J. Lagowski, L. Jastrzebski, M. Lichtensteiger and H. C. Gatos, "Determination of Compensation Ratios in Semiconductors from Electron Mobility and Free Carrier Absorption; GaAs," 153d Electrochem. Soc. Meeting, Seattle, Washington, 1978.

40. W. Walukiewicz, J. Lagowski, L. Jastrzebski, M. Lichtensteiger and H. C. Gatos, "Electron Mobility and Free-Carrier Absorption in GaAs: Determination of the Compensation Ratio," J. Appl. Phys. 50, 899 (1979).

41. W. Walukiewicz, J. Lagowski, L. Jastrzebski, P. Rava, M. Lichtensteiger, C. H. Gatos and H. C. Gatos, "Electron Mobility and Free-Carrier Absorption in InP; Determination of the Compensation Ratio," J. Appl. Phys. 51, 2659 (1980).

42. W. Walukiewicz, J. Lagowski and H. C. Gatos, "77 K Electron Mobility in GaAs," J. Appl. Phys. 53, 769 (1982).

43. W. Walukiewicz, J. Lagowski and H. C. Gatos, "Reassessment of Space-Charge and Central Cell Scattering Contributions to GaAs Electron Mobility," J. Appl. Phys. 53, 5854 (1981).

44. W. Walukiewicz, J. Lagowski and H. C. Gatos, "Reply to Comment on Reassessment of Space Charge and Central-Cell Scattering Contributions to GaAs Electron Mobility," J. Appl. Phys. 53, 5346 (1982).

45. J. Lagowski, W. Walukiewicz, M. M. G. Slusarczuk and H. C. Gatos, "Derivative Surface Photovoltage Spectroscopy; A New Approach to the Study of Adsorption in Semiconductors; GaAs," J. Appl. Phys. 50, 5059 (1979).

46. M. M. G. Slusarczuk, "Study of Electronic and Optical Properties of Gallium Arsenide Surfaces and Interfaces," Sc.D. Thesis, M.I.T., 1979.

47. E. Kamieniecki, J. Lagowski and H. C. Gatos, "Wavelength Modulated Photocapacitance Spectroscopy," J. Appl. Phys. 51, 1863 (1980).

48. W. Walukiewicz, L. Pawlowicz, J. Lagowski and H. C. Gatos, "Characterization of Semi-Insulating GaAs," Proc. Semi-Insulating III-V Materials, Evian 1982, edited by S. Makram-Ebeid and B. Tuck, Shiva Publishing, Ltd., Nantwich, England, 1982.

49. H. C. Gatos, J. Lagowski and L. Jastrzebski, "Present Status of GaAs," NASA Contractor Report 3093, Jan. 1979.

50. H. C. Gatos, "Semiconductor Crystal Growth on Earth and in Space," Proc. of Mat. Processing Symp., Boston, Mass., 1981.

51. W. Walukiewicz, J. Lagowski and H.C. Gatos, "Shallow Donor Associated with the Main Electron Trap (EL2) in Melt-Grown GaAs," Appl. Phys. Lett. 43, 112 (1983).

52. W. Walukiewicz, H.E. Ruda, J. Lagowski and H.C. Gatos, "Electron Mobility Limits in a Two-Dimensional Electron Gas: GaAs-GaAlAs Heterostructures," Phys. Rev. B, 29, 4818 (1984).

53. J. Lagowski, H.C. Gatos, T. Aoyama and D.G. Lin, "On the Dislocation Density in Melt-Grown GaAs," presented at the Third Conference on Semi-Insulating III-V Materials, Warm Springs, Oregon, April 1984.

54. J. Lagowski, D.G. Lin, T. Aoyama and H.C. Gatos, "Oxygen-Related Midgap Level in GaAs," presented at the Third Conference on Semi-Insulating III-V Materials, Warm Springs, Oregon, April 1984.

55. J. Lagowski, D.G. Lin, H.C. Gatos, J.M. Parsey, Jr., and M. Kaminska, "Real and Apparent Effects of Strong Electric Fields on the Electron Emission from Midgap Levels EL2 and ELO in GaAs," Appl. Phys. Lett., in press.

56. J. Lagowski, H.C. Gatos, T. Aoyama and D.G. Lin, "Fermi Energy Control of Vacancy Coalescence and Dislocation Density in Melt-Grown GaAs," Appl. Phys. Lett., in press.

57. W. Walukiewicz, H.E. Ruda, J. Lagowski and H.C. Gatos, "Electron Mobility in Modulation Doped Heterostructures," submitted to Physical Review B1.

58. J. Lagowski and H.C. Gatos, "Partially-Confined Configuration for Crystal Growth from the Melt in Zero Gravity Environment," submitted to J. Electrochem. Soc.

APPENDIX

Reprints and preprints of papers which appeared in the literature or were submitted for publication since our last annual report are attached. They provide a more detailed account of some of the work discussed in the text of the present report.

On the optical evaluation of the EL2 deep level concentration in semi-insulating GaAs

W. Walukiewicz, J. Lagowski, and H. C. Gatos
Massachusetts Institute of Technology, Cambridge, Massachusetts 02139

(Received 7 February 1983; accepted for publication 27 April 1983)

We present a practical procedure for the evaluation of the Fermi energy in semi-insulating (SI)GaAs from electrical measurements. This procedure makes it possible to reliably extend the determination of the major deep level (EL2) concentration, by near-infrared absorption measurements, to SI GaAs. Employing this procedure, we showed that the EL2 concentration in Czochralski-grown GaAs increases monotonically with increasing As/Ga ratio (throughout the conversion from SI *n* type to semiconducting *p*-type crystals) rather than abruptly as previously proposed.

PACS numbers: 72.20.My, 72.80.Ey, 78.50.Ge

With the rapid progress in GaAs integrated circuits (IC) technology, based on semi-insulating (SI) GaAs, a great deal of effort has been devoted to studies of native deep donor (the EL2 level at $E_c - 0.76$ eV)[1–8] and its role in the compensation mechanism responsible for the semi-insulating behavior of "undoped" melt-grown GaAs.[9–13] The standard techniques for the determination of deep level concentrations, such as transient capacitance or transient current spectroscopies, are not readily applicable to SI material. Accordingly, the optical absorption method proposed in Ref. 1 has been widely used for the determinaton of the EL2 concentration.

In melt-grown GaAs a dominant contribution to the optical absorption in the spectral range $0.85\text{ eV} \lesssim h\nu \lesssim 1.3\text{ eV}$ has been attributed to the photoionization of the EL2,[1,9,14] i.e., to electron transitions from the occupied EL2 to the conduction band and hole transitions from the unoccupied EL2 to the valence band. Accordingly, the corresponding overall absorption coefficient $\alpha(h\nu)$ is

$$\alpha(h\nu) = N_{EL2} f_n \sigma_n^i + N_{EL2}(1 - f_n)\sigma_p^i, \tag{1}$$

where N_{EL2} is the EL2 concentration, σ_n^i and σ_p^i are the photoionization cross sections for electrons and holes respectively, f_n is the occupancy function of the EL2, $f_n = [1 + \exp(-E_F - E_{EL2}^i/kT)]^{-1}$, where E_F is the Fermi energy and E_{EL2}^i is the "effective" EL2 energy (which includes contribution from a degeneracy factor), and $E_{EL2}^i = 0.759 - 0.237 \times 10^{-3}\,T$, where T is the absolute temperature.[10]

The values of σ_n^i and σ_p^i as functions of the photon energy are discussed in Refs. 9 and 15. In the spectral region of highest sensitivity (1.1–1.25 eV) σ_n^i exceeds σ_p^i by a factor of 3–4. Thus, a transition from *n* to *p*-type material (a change of f_n from 1 to 0) leads to a decrease of α by a factor of 3–4 for a given EL2 concentration. It is also apparent that a change of EL2 occupation will lead to a change in the shape of the optical absorption spectrum, due to noticeable differences in $\sigma_n^i(h\nu)$ and $\sigma_p^i(h\nu)$. Thus, the Fermi energy in SI GaAs determines not only the value of the absorption coefficient but also the shape of the near-infrared absorption spectrum.

In the present letter we present a procedure for the determination of the Fermi energy in SI GaAs from electrical measurements. We show that the Fermi energy in typical SI GaAs ($\rho > 10^7\ \Omega$ cm) can vary between 0.65 and 0.85 eV below the conduction band; within this range the EL2 occupancy varies from 1 to nearly zero. We also employ the present results for the reevaluation of the magnitude of the effect of stoichiometry on the EL2 concentration and on the compensation of "undoped" Czochralski (CZ)-grown GaAs.

The major problem in the proper interpretation of electrical measurements on SI GaAs arises from the fact that both electrons and holes may contribute to electrical transport. Therefore, three quantities (e.g., Fermi energy and electron and hole mobilities) must be determined from the measured Hall constant and resistivity. As shown previously,[16] this difficulty can be overcome by utilizing theoretically calculated results of electron and hole mobilities. These mobilities depend mainly on the ionized impurity concentration, whereas the electron and the hole concentrations depend on the Fermi level position only. Thus, with the aid of theoretical calculations of the hole and electron mobilities, the ionized impurity concentration and the Fermi level position can be uniquely determined from electrical measurements.

The mobility calculations were carried out using a variational method in the form given in Refs. 16 and 17. All major scattering processes, i.e., polar optical, deformation potential, acoustical, piezoelectric, and ionized impurity, were included. Also in the hole mobility calculations the optical photon scattering via deformation potential has been taken into account. In some instances, where the hole to electron mobility ratio depends weakly on the ionized impurity concentration, the analysis of the experimental data can be quite accurately simplified by assuming a constant mobility ratio.

In Fig. 1(a) the resistivity and the Hall mobility are plotted as a function of the hole concentration. They are calculated from the standard expressions for mixed electron-hole conduction:

$$\frac{1}{\rho} = ne\mu_n\left(1 + \frac{p\mu_p}{n\mu_n}\right), \tag{2a}$$

$$\mu_H = \mu_n\left(\frac{n - p(\mu_p/\mu_n)^2}{n + p(\mu_p/\mu_n)}\right), \tag{2b}$$

 0003-6951/83/140192-03$01.00

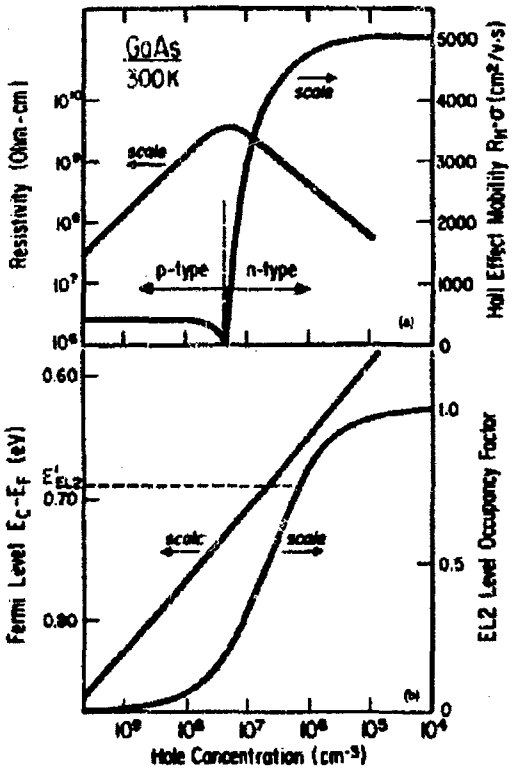

FIG. 1. (a) Dependence of resistivity and mobility on carrier concentration in the valence band; (b) dependence of Fermi level and EL2 occupancy on the carrier concentration in the valence band. The effective energy of EL2 at 300 K, E'_{EL2} is also indicated.

and

$$np = n_i^2, \tag{2c}$$

where[9] $n_i = 4.82\times10^{15}\ T^{3/2}\ (m_n m_p/m_0^2)^{3/4}\ e^{-E_g/2kT}$; the temperature dependence of the energy gap is given by[1]

$$E_g = 1519 - \frac{0.54T^2}{T+204}\ (\text{meV}), \tag{3}$$

m_n is the effective mass of conduction-band electrons and $m_p = (m_{lh}^{3/2} + m_{hh}^{3/2})^{2/3}$ is the density of states effective mass in the valence band (*lh* and *hh* refer to light and heavy holes, respectively).

The curves of Fig. 1 were calculated for a mobility ratio $\mu_n/\mu_p = 13$, which is a good approximation of theoretical results for ionized impurity concentrations of the order of $\sim10^{16}$ cm^{-3}, typical for the presently considered undoped SI GaAs. A value of 5000 cm^2/Vs was employed for the electron mobility, again typical for undoped SI GaAs.[10–12] It should be noted that the value of electron mobility affects only weakly the determination of the Fermi energy. Thus, the results presented below can be used very satisfactorily for electron mobilities ranging from 4000 to 6000 cm^2/Vs. The following values of effective masses were utilized: $m_n = 0.068m_0$, $m_{hh} = 0.55m_0$, and $m_{lh} = 0.08m_0$.

The Fermi level, measured with respect to the conduction band, as a function of the hole concentration is shown in Fig. 1(b). It is seen that the Fermi energy coincides with the "effective" EL2 energy [$E_c - 0.69$ eV (Ref. 10)] for a hole concentration of about 10^7 cm^{-3}, for which the Hall mobility is still determined mainly by electrons.

The occupancy function of the EL2 expressed in terms of the hole concentration is also plotted in Fig. 1(b). It should be noted that for SI GaAs with Hall mobility close to 0 (hole concentration 0.3×10^8 cm^{-3}) 85% of the EL2 level is unoccupied.

The results presented in Fig. 1(a) make possible the straightforward evaluation of the Fermi level position in SI GaAs of a given resistivity and Hall effect mobility. Consequently, the EL2 occupation can be determined from Fig. 1(b); thus, it becomes possible to reliably calculate the EL2 concentration from the optical absorption measurements if the absorption is due to the photoionization of EL2. The EL2 occupation by electrons decreases most noticeably in the region where the Hall effect mobility still remains very high and where the sign of the Hall constant indicates a dominant contribution from electrons. It is thus evident that occupation corrections to the optical absorption of the EL2 cannot be a priori ignored even in the region where the Hall effect measurements indicate an apparent strongly *n*-type character of the SI material.

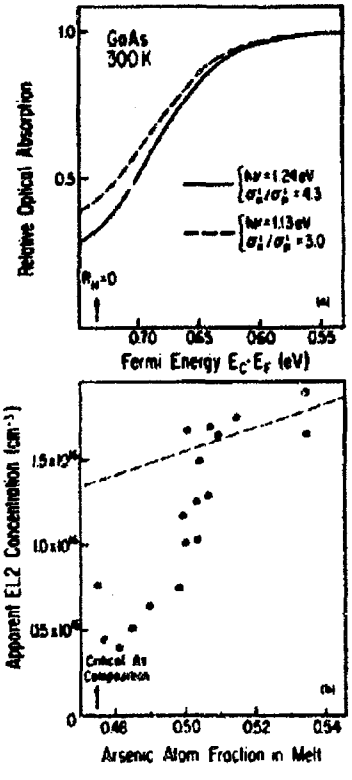

FIG. 2. (a) Calculated relative optical absorption (for two photon energies) due to the photoionization of a constant concentration of EL2 as a function of Fermi energy. $R_H = 0$ corresponds to vanishing Hall mobility. (b) Experimental results of optical absorption expressed as EL2 concentration as a function of arsenic atom fraction in melt after Ref. 2. Dashed line shows actual EL2 concentrations after experimental results are corrected for changes in the EL2 occupancy. Critical As composition corresponds to $R_H = 0$ in (a).

The results of the calculation of the absorption coefficient from expression (1) assuming N_{EL2} constant, but taking into account the changes in the Fermi energy are shown in Fig. 2(a). As seen in this figure, the optical absorption decrease caused by the downward shift of the Fermi level is quite pronounced for Fermi energies located in the vicinity of the effective EL2 energy.

For a comparison in Fig. 2(b) we show the reported decrease in the EL2 concentration,[3,12] as determined by the corresponding decrease of the optical absorption, as a function of changes in the melt composition (As/Ga ratio). The Fermi energy and the "arsenic atom fraction" scales of Figs. 2(a) and 2(b), respectively, were correlated using the data of Hall mobility and resistivity versus melt composition from Refs. 3 and 12, and the presently calculated results of Fig. 1. A transition of the Hall mobility (or the Hall constant R_H through zero takes place at a critical As composition) which provides a convenient reference point in correlating both scales. At this point only about 15% of the EL2 is occupied with electrons, while for arsenic atom fractions in the melt higher than about 0.51, the occupation of the EL2 exceeds 90% and remains essentially unchanged.

The optical absorption changes in Refs. 3 and 12 have been attributed entirely to a decrease in the EL2 concentration [Fig. 2(b)]. However, a comparison with Fig. 2(a) clearly shows that most of the "apparent" change in the EL2 concentration is due to the decrease in its occupancy. When this contribution from the "occupancy change" is taken into consideration, the actual stoichiometry-induced change in the EL2 concentration is represented by the dotted line in Fig. 2(b).

The results of Fig. 2(b) analyzed in the light of the presently proposed procedure show that in the entire range of melt composition the EL2 concentration in CZ-grown GaAs decreases monotonically with decreasing As/Ga ratio in the melt. This behavior is consistent with the results of a similar study of Bridgman-grown GaAs where a gradual decrease of the EL2 concentration was observed with decreasing As pressure above the melt.[7]

The above dependence is also consistent with the model of the EL2 formation in melt-grown GaAs which attributes the EL2 to a native defect complex involving the antisite defect As_{Ga} and arsenic vacancies.[18] This model considers a two-step process, i.e., (1) the creation of gallium vacancies, V_{Ga}, during the solidification process; (2) the post-solidification migration of the V_{Ga} to a neighboring As site leading to the formation of the EL2 defect complex. The experimentally observed decrease of the EL2 concentration with decreasing As/Ga ratio in the melt is, accordingly, due to a corresponding decrease of the V_{Ga} concentration during solidification.

The present results show that the melt stoichiometry-induced conversion of GaAs from SI *n* type to semiconducting *p* type is most likely due to the increase in the residual shallow acceptor concentration with decreasing As/Ga ratio rather than to the rapid decrease of the EL2 concentration proposed previously.[3,12,13] Such shallow acceptor concentration increase, determined from photoluminescence and Hall effect measurements, has indeed been reported[19–21] and has been attributed to point defects.[20,21]

In summary, we showed that, if the near-infrared absorption in GaAs is to be taken as being due to the photoionization of EL2, then the use of this absorption for the determination of the EL2 concentration in SI GaAs requires knowledge of the Fermi energy (EL2 occupancy). A practical method was presented for the determination of the Fermi energy in SI GaAs from electrical measurements.

The authors are grateful to the National Aeronautics and Space Administration for financial support.

[1]G. M. Martin, Appl. Phys. Lett. 39, 747 (1981).
[2]J. Lagowski, H. C. Gatos, J. M. Parsey, K. Wada, M. Kaminska, and W. Walukiewicz, Appl. Phys. Lett. 40, 342 (1982).
[3]D. E. Holmes, R. T. Chen, K. R. Elliott, and C. G. Kirkpatrick, Appl. Phys. Lett. 40, 46 (1982).
[4]E. J. Johnson, J. Kafalas, R. W. Davis, and W. A. Dyes, Appl. Phys. Lett. 40, 993 (1982).
[5]M. Kaminska, J. M. Parsey, J. Lagowski, and H. C. Gatos, Appl. Phys. Lett. 41, 989 (1982).
[6]P. W. Yu and D. C. Walters, Appl. Phys. Lett. 41, 863 (1982).
[7]J. Lagowski, M. Kaminska, J. M. Parsey, Jr., H. C. Gatos, and M. Lichtensteiger, Appl. Phys. Lett. 41, 1078 (1982).
[8]G. M. Martin, P. Terriac, S. Makram-Ebeid, G. Guillot, and M. Gavand, Appl. Phys. Lett. 42, 61 (1983).
[9]G. M. Martin, in *Proceedings of the Semi-Insulating III-V Materials Conference, Nottingham 1980*, edited by G. J. Rees (Shiva, Orpington, United Kingdom, 1980), p. 13.
[10]G. M. Martin, J. P. Farges, G. Jacob, and J. P. Hallais, J. Appl. Phys. 51, 2840 (1980).
[11]L. B. Ta, H. M. Hobgood, A. Rohatgi, and R. N. Thomas, J. Appl. Phys. 53, 5771 (1982).
[12]D. E. Holmes, R. T. Chen, K. R. Elliott, C. G. Kirkpatrick, and P. W. Yu, IEEE Trans. Electron Devices ED-29, 1045 (1982).
[13]D. E. Holmes, K. R. Elliott, R. T. Chen, and C. G. Kirkpatrick, in *Semi-Insulating III-V Materials, Evian 1982*, edited by S. Makram-Ebeid and B. Tuck (Shiva, Nantwich, 1982), p. 19.
[14]G. M. Martin, G. Jacob, G. Poiblaud, A. Goltzene, and C. Schwab, Inst. Phys. Conf. Ser. 59, 281 (1981).
[15]A. Chantre, G. Vincent, and D. Bois, Phys. Rev. B 23, 5335 (1981).
[16]W. Walukiewicz, L. Pawlowicz, J. Lagowski, and H. C. Gatos, in *Semi-Insulating III-V Materials, Evian 1982*, edited by S. Makram-Ebeid and B. Tuck (Shiva, Nantwich, 1982), p. 121.
[17]W. Walukiewicz, J. Lagowski, L. Jastrzebski, M. Lichtensteiger, and H. C. Gatos, J. Appl. Phys. 50, 899 (1979).
[18]J. Lagowski, J. M. Parsey, M. Kaminska, K. Wada, and H. C. Gatos, in *Semi-Insulating III-V Materials, Evian 1982*, edited by S. Makram-Ebeid and B. Tuck (Shiva, Nantwich, 1982), p. 154; J. Lagowski, M. Kaminska, J. Parsey, and H. C. Gatos, 10th Int. Conf. on GaAs and Related Compounds, September 1982, Albuquerque, New Mexico (in press).
[19]L. B. Ta, H. M. Hobgood, and R. N. Thomas, Appl. Phys Lett. 41, 1091 (1982).
[20]P. W. Yu, W. C. Mitchel, H. G. Mier, S. S. Li, and W. L. Wang, Appl. Phys. Lett. 41, 533 (1982).
[21]K. R. Elliott, D. E. Holmes, R. T. Chen, and C. G. Kirkpatrick, Appl. Phys. Lett. 40, 898 (1982).

Inst. Phys. Conf. Ser. No. 65: Chapter 1
Paper presented at Int. Symp. GaAs and Related Compounds, Albuquerque, 1982

Microscopic model of the EL2 level in GaAs

J. Lagowski, M. Kaminska*, J.M. Parsey, H.C. Gatos and W. Walukiewicz**

Massachusetts Institute of Technology, Cambridge, Massachusetts 02139

Abstract. It was found that the defect responsible for the dominant deep donor E_c-0.76 eV (EL2) in melt-grown GaAs also introduces a shallow donor level at E_c-0.025 eV. This finding makes possible the refinement of our antisite defect As_{Ga} model of the EL2 formation in melt growth to a microscopic model which accounts for the, thus far, observed electronic behavior of EL2 (including its metastable state). In addition to the antisite defect As_{Ga}, the proposed defect center involves an arsenic vacancy V_{As} on a neighboring site. This complex is similar to a DX center exhibiting a large lattice relaxation energy.

1. Introduction

The high resistivity of "undoped" melt-grown GaAs crystals is caused by a donor-type native defect which introduces a deep level (commonly referred to as EL2) located at E_c-0.76 eV (Martin et al 1980). This level was originally assigned to oxygen impurity (Milnes 1973) and later on to Ga vacancy (Watanabe 1981). Recent studies have related EL2 with the antisite defect As_{Ga} (Kaminska 1981, Chou 1981, Lagowski et al 1982 a,b,c, Schneider 1982, Johnson et al 1982). In our study of the EL2 formation we have proposed that the antisite defect As_{Ga} (expected to act as a double donor) is formed as a result of Ga vacancy migration to a neighboring As site during the post-growth cooling of the crystal (Lagowski et al 1982, a,b,c). The assignment of EL2 to this antisite defect made it possible to successfully explain the dependence of the EL2 concentration on growth parameters such as As/Ga ratio in the melt, Ga_2O pressure and concentration of shallow donors and acceptors. It is also consistent with the results of paramagnetic resonance studies (Wagner et al 1980, Schneider 1982). The assignment of the EL2 to a simple antisite defect As_{Ga}, however, does not fully account for the electronic properties of the EL2, and in particular, for its observed dual nature, i.e., its introduction of normal and metastable states (Vincent and Bois 1978, Vincent et al 1982).

In this paper we report results which provide the first experimental evidence of the introduction of an additional shallow donor by EL2 centers. These results are discussed in conjunction with a refined defect model of the EL2 center which considers not only the antisite defect As_{Ga} but also

* Present address: Institute of Experimental Physics, Warsaw University, Warsaw, Poland.

** Permanent address: Institute of Physics, Polish Academy of Sciences, Warsaw, Poland.

0305-2346/83/0065-0041 $02.25

a neighboring arsenic vacancy, V_{As}. This model accounts for the observed growth-property relationships just as the antisite defect model. In addition, however, it makes it possible to explain all observed electronic properties of the EL2.

2. Experimental

Our study was carried out on GaAs crystals grown using a Bridgman-type apparatus which allowed very precise control of the growth parameters (Parsey et al 1982). The electron concentration was varied between 5×10^{16} and $10^{18}cm^{-3}$ by intentional doping with Si, S, Se, Te (shallow donors). The As pressure during the growth was adjusted by selecting an As source temperature between 613 and 619°C. The temperature 617°C (under which the crystals with minimum dislocation density are obtained) apparently corresponds to optimum stoichiometry (Parsey et al 1982). Raising (lowering) the As source temperature was used to increase (decrease) the concentration of the EL2. It should be noted that the sensitivity of the EL2 concentration to the As source temperature (i.e., to the melt composition) decreases with increasing electron concentration, n. For n exceeding $3\times10^{17}cm^{-3}$ the melt-grown crystals had an EL2 concentration below the detection limit of about $2\times10^{14}cm^{-3}$, irrespective of the As source temperature.

The crystals were characterized using: (a) Hall effect and conductivity measurements in the temperature range of 77-300 K; (b) Schottky diode DLTS measurements of deep levels; (c) precise determinations of EL2 parameters using the measurements of total capacitance transient as a function of temperature, bias and the magnitude of filling pulses. For high electron concentration ($n>10^{17}$) optical absorption measurements of EL2 concentration were also carried out using very thick samples (up to 5 cm). Such measurements enable the elimination of high field effects, which may lead to an apparent decrease of the deep level concentration at high electron concentrations. In addition, SIMS analysis was employed for the determination of impurity concentrations.

3. Results and Discussion

Hall effect measurements revealed systematic differences between the temperature dependence of electron concentration in GaAs crystals containing EL2 and in the EL2-free crystals. The results are summarized in Fig. 1, where the ratio of room temperature to liquid nitrogen temperature electron concentration $\gamma = n(300\ K)/n(77\ K)$ is plotted as a function of the 300 K electron concentration. Samples containing EL2 exhibit a noticeable decrease of n at lower temperatures, as manifested by γ values larger than 1. Such a freezeout is not observed for EL2-free samples for which $\gamma = 1.00\pm0.03$ in the concentration range of $3\times10^{16}<n<10^{18}cm^{-3}$. Using results from (Rode 1975) it can be shown that in this concentration range the Hall factor, r, does not differ significantly from unity (i.e., $r = 1$ at 77 K due to degeneracy of electron gas and $1<r<1.05$ at 300 K). Thus, the Hall factor can be safely ignored in the interpretation of Fig. 1a.

In Fig. 2 the difference $n(300\ K) - n(77\ K)$ is plotted as a function of the EL2 concentration, N_{EL2}. It is seen that the change in electron concentration increases nearly proportionally to the increase in EL2 concentration. This, approximately, one-to-one correlation implies the presence of donor levels with a concentration identical to the EL2 concentration. This donor level, however, must be much shallower than the deep EL2 donor, $E_c-0.76$ eV, in order to become filled or emptied upon relatively small

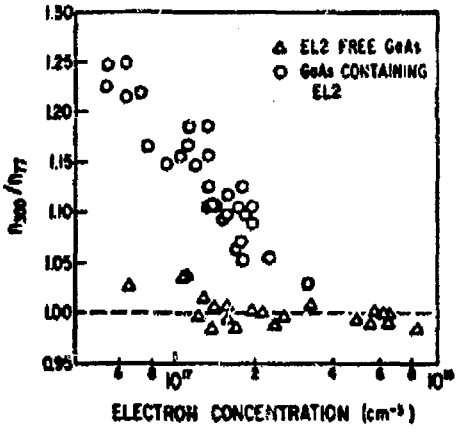

Fig. 1. Relative change in electron concentration between 300 K and 77 K in GaAs in the presence and absence of EL2

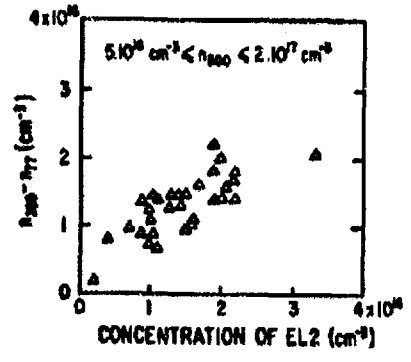

Fig. 2. Electron freezeout ($n_{300}-n_{77}$) vs. the concentration of EL 2 level

shifts of the Fermi level (within 50 meV from the conduction band edge) brought about by the change of n and/or of the temperature.

It should be pointed out that the concentration of other electron traps (EL4, EL5, and EL6) in the samples investigated was about one order of magnitude smaller than N_{EL2}. Thus, their contribution to the observed changes of n can be neglected.

The temperature dependence of electron concentration, n(T), can be obtained by considering the charge neutrality conditions, which for n-type material becomes:

$$n(T) = n_o + N_{EL2}\,[1-f_n(T)] \qquad (1)$$

where $n_o \equiv N_D^+ - N_A^-$, N_D^+ and N_A^- are the concentrations of ionized shallow donors and acceptors, respectively; and $N_{SD}^+(T) = N_{EL2}\,[1-f_n(T)]$ is the concentration of ionized shallow donor related to EL2; $f_n(T)$ is the occupational function for this level $f_n(T) = 1/[1 + g \exp(E_t - E_F/kT)]$; E_t is the energy level, E_F is the Fermi energy, and g is the degeneracy factor. The Fermi energy E_F is temperature dependent and its value can be obtained from n using the standard relationships $n = 5.44\times10^{15}(m^*T/m_o)^{3/2}F_{1/2}(E_F/kT)$, where $F_{1/2}(E_F/kT)$ is the Fermi Dirac Integral. In Figure 3, the temperature dependence of the electron concentration is shown for two samples with different doping levels (different values of electron concentrations) and also different concentrations of the deep EL2 donor. Curves were calculated from expression (1) taking $E_t - E_F = 25$ meV and $g = 2$. For both samples a good agreement is obtained between experimental and calculated dependences of electron concentration. It should be noted that qualitative evidence of the involvement of a shallow donor level in the EL2 center has been also provided by our recent study of the passivation of

EL2 by atomic hydrogen (Lagowski et al 1982c). It was found that a decrease of EL2 concentration results in a decrease not only of the concentration of the deep donors, but also of the shallower donors.

4. Microscopic Model of EL2

The experimentally established characteristics of the EL2 center are summarized in Tables I and II. Table I includes relationships between EL2 and crystal growth parameters, while Table II lists key characteristics derived from electrical and photoelectrical phenomena. We have recently proposed (Lagowski et al 1982, a,b) that EL2 is formed by the migration of a Ga vacancy to an As site during the post-growth cooling of the crystal and the subsequent formation of the antisite defect As_{Ga} and a neighboring arsenic vacancy as shown in Fig. 4. The concentration of

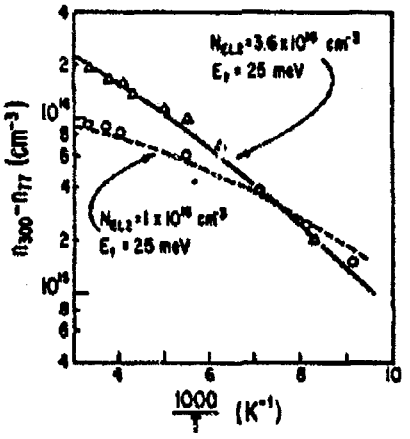

Fig. 3. Experimental (points) and theoretical (curves) dependences of electron concentration on $10^3/T$ for GaAs with $n_{300}=1.98\times10^{17}$cm^{-3} (triangles) and $n_{300}=6.10\times10^{16}$cm^{-3} (circles)

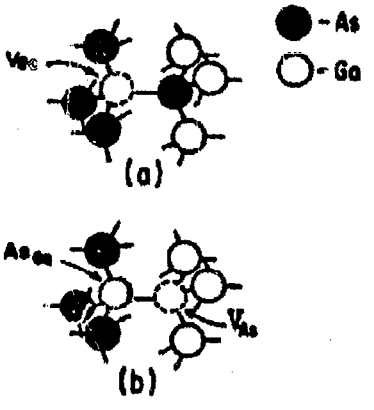

Fig. 4. Formation of the EL2 complex; (a) gallium vacancy, (b) $As_{Ga}V_{As}$ complex formed as a result of As_{Ga} V_{Ga} migration to As site.

this complex is a strong function of the electron concentration, n^{-4}. Thus, by assigning EL2 to an antisite defect As_{Ga} we explained unique features of EL2 such as: the suppression and annihilation of EL2 upon doping with shallow donors, the increase in EL2 concentration upon counterdoping with acceptors, and an increase in EL2 concentration with the increase of Ga_2O pressure during growth. This model also explained the decrease in EL2 concentration upon increasing the Ga/As ratio in the melt (decrease of gallium vacancy concentration).

The above growth-property relationships can be equally well explained when the EL2 center consists not only of an antisite defect As_{Ga}, but also of a neighboring arsenic vacancy. According to Van Vechten 1975 and Lagowski 1982a, the concentration of an antisite defect $[As_{Ga}]$ and of the concentration of a complex $[As_{Ga}V_{As}]$ formed during V_{Ga} migration can be expressed as

$$[As_{Ga}] = K_1[V_{Ga}]n^{-4}/[V_{As}] \qquad (2a)$$

Table I. Dependence of EL2 on Growth Factors

Growth Factor	Effect on EL2	References
As pressure or As/Ga ratio in the melt	Concentration decreases with decreasing As pressure or the As/Ga ratio	Lagowski et al 1982a Holmes et al, 1982a
Ga_2O pressure	Concentration increases with increasing Ga_2O pressure	Kaminska et al, 1981
Doping with shallow donors	Suppression at concentrations exceeding $\sim 10^{17} cm^{-3}$	Lagowski et al, 1982a,b
Counterdoping with shallow acceptors	Increase of EL2 concentration	Lagowski et al, 1982b

Table II. Electronic Properties of EL2

Property	Comments	Reference
Deep donor level at E_c-0.76 eV	Compensating deep level responsible for high resistivity of "undoped" GaAs	Mircea et al, 1976
Shallow donor level at E_c-0.025 eV	Its concentration is identical to concentration of deep donor level	Present work
Normal state with a configurational barrier (~70 meV) for capture of electrons	Only state observed at high electron concentrations	Henry & Lang, 1977
Metastable state	Observed at T<120K and only at low electron concentration	Vincent & Bois, 1978 Vincent et al, 1982

and

$$[As_{Ga}V_{As}] = K_2[V_{Ga}]\, n^{-4} \qquad (2b)$$

where K_1 and K_2 are the reaction constants. (2a) and (2b) indicate identical dependence of both centers on the electron concentration (i.e., doping with shallow donors and/or acceptors) and on the concentration of gallium vacancies. To account for the electronic properties of the EL2, the complex $As_{Ga}V_{As}$ seems to be more suitable than a simple antisite defect As_{Ga}.

The most significant electronic properties of the EL2 include: (1) the deep donor level at E_c-0.76 eV; (2) the shallower donor at E_c-0.025 eV discussed above; (3) the configurational barrier for capture of free electrons (Henry and Lang 1977, Kaminska et al 1982); (4) the dual nature of the center characterized by two states--i.e., a normal state and a metastable state (Vincent and Bois 1978, Vincent et al 1982). The latter state is observed at low temperatures (T<120 K) with sufficiently low electron concentration.

In a configurational coordinate (cc) diagram a stable state can be represented by a low relaxation energy (Fig. 5a), while a metastable state corresponds to a large relaxation energy (Fig. 5b). A combined cc diagram

of EL2 center proposed by Vincent and Bois 1978 is shown in Fig. 5c. As indicated by an arrow, the transition from a metastable to the stable state is thermally activated, i.e., the metastable state can be observed only at reduced temperatures (T<120 K). In III-V compounds with mostly covalent bonding the states with a large lattice relaxation energy cannot be readily explained. An explanation can be apparently provided by the

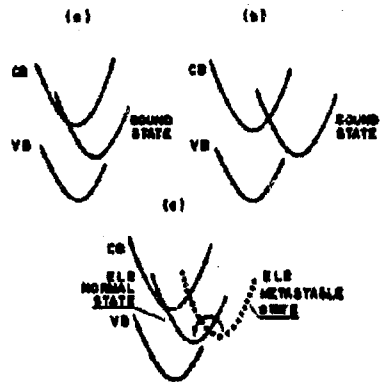

Fig. 5. Configuration coordinate (cc) diagrams for: (a) low lattice relaxation energy; (b) large lattice relaxation energy; (c) EL2 center involving both cases.

DX centers in $Al_xGa_{1-x}As$ and $GaAs_{1-x}P_x$ extensively studied in conjunction with donor-impurity-induced persistent photoconductivity (Lang and Logan 1979, Lang 1980). There are two striking similarities between DX centers and the EL2 center. (1) According to the microscopic model of Lang and Logan 1979, the DX center consists of a donor on a cation site plus an anion vacancy. The complex shown in Fig. 4 (the As_{Ga} donor plus arsenic vacancy) does belong to the same defect category; (2) the proposed cc diagram of DX center is of the same type as the cc diagram of a metastable EL2 state.

Thus by analogy to DX centers the complex of Fig. 4 can be considered as responsible for the metastable state of the EL2 center. This metastable state, however, is observed only at low electron concentration, which implies that the metastable state corresponds to the EL2 center with an ionized shallow donor level at E_c-0.025 eV. For high electron concentration only a normal state is observed which implies that only this state is possible for an occupied shallow donor. Accordingly, an increase of electron concentration (e.g., by a filling pulse in a Schottky diode) which increases the occupation of the E_c-0.025 eV donor should lead to the recovery of the EL2 center from the metastable state. Such an effect has been indeed reported, however, it was interpreted as being due to some unspecified Auger-like process. It is apparent that other models of the EL2 origin, i.e., the oxygen impurity or the Ga vacancy models, are in conflict with the experimental characteristics listed in Table I. The same is also true for the "Ga interstitial" microscopic model suggested by Vincent et al 1982, according to which the transition from a normal to a metastable state is realized by transfer of a Ga interstitial from a position with Ga atoms as nearest neighbors to a position with As atoms as nearest neighbors. This model cannot explain the "group A" properties of Table I, and the effects of electron concentration on the metastable state.

5. Summary and Conclusions

We propose a model of a defect center, consisting of an antisite defect As_{Ga} and V_{As}, which, for the first time, consistently explains the unique electronic properties of the EL2 and the relationships between the EL2 con-

centration and crystal growth parameters. Such an assignment renders the EL2 center very similar to DX centers characterized by a large lattice relaxation and extensively studied in III-V ternary compounds in conjunction with a persistent photoconductivity phenomena. Our finding of the existence of a shallow donor level associated with the EL2 was used to explain the two states of the EL2, i.e., a normal state and a metastable state. It should also be noted that the presence of a shallow donor level associated with the EL2 was not considered in previous studies of SI GaAs (Martin et al 1980, Holmes et al 1982a,b). Important consequences of this level for the compensation mechanism of GaAs will be presented elsewhere (Lagowski et al 1982d).

6. Acknowledgement

The authors are grateful to the National Aeronautics and Space Administration and to the National Science Foundation for financial support.

References

Chou Y 1981 GaAs and Related Compounds, Inst. Phys. Conf. Ser. 63, 185
Henry C H, Lang D V 1977 Phys. Rev. B 15, 989
Holmes D E, Chen R T, Elliot K R, and Kirkpatrick C G 1982a Appl. Phys. Lett. 40m 46
Holmes D E, Chen R T, Elliott K R, Kirkpatrick and Phil Won Yu 1982b IEEE Transactions on Electron Devices Vol. ED-29, No 7, 1045
Johnson E J, Kafalas J, Davies R W and Dyes W A 1982 Appl. Phys. Lett. 40, 933
Kaminska M, Lagowski J, Parsey J, Wada K and Gatos H C 1981 GaAs and Related Compounds, Inst. Phys. Conf. Ser. 63, 197
Kaminska M, Parsey J M, Lagowski J and Gatos H C 1982 Appl. Phys. Lett. in press
Lagowski J, Gatos H C, Parsey J M, Wada K, Kaminska M and Walukiewicz W 1982 a Appl. Phys. Lett. 40 342
Lagowski J, Parsey J M, Kaminska M, Wada K and Gatos H C 1982b, Proc. of 2d Conf. on Semi-Insulating III-V Materials, Evian, France, Shiva Publishing Limited in press.
Lagowski J, Kaminska M, Parsey J M, Gatos H C and Lichtensteiger M, 1982c, Appl. Phys. Lett. in press
Lagowski J, Walukiewicz W and Gatos H C 1982d submitted to Appl. Phys. Lett.
Lang D V and Logan R A 1979 Inst. Phys. Conf. Ser. No 43, 433
Lang D V 1980 J. Phys. Soc. Japan 49, Sippl. A, 215
Martin F H, Fargeo J P, Jacob G, Hallais J P, Poiblaud G 1980 J. Appl. Phys. 51, 2840
Milnes A G 1973 Deep Impurities in Semiconductors Wiley, New York, p. 59
Mircea A, Mitonneau A, Hollan L, Briere A 1976 Appl. Phys. 11, 153
Parsey J M, Nanishi Y, Lagowski J and Gatos H C 1982 J. Electrochem. Soc. 129, 388.
Rode D L 1975 Semiconductors and Semimetals Ed. R K Willardson and A C Beer, Academic Press, New York, Vol. 10, ch. 1
Schneider J 1982 Proc. 2d Int. Conf. on Semi-Insulating III-V Materials, Evian, France, Shiva Publishing Limited, in press
Van Vechten J A 1975 J. Electrochem. Soc. 122, 419 and 432
Vincent G and Bois D 1978 Solid State Commun. 27 431
Vincent G, Bois D and Chantre A 1982 J. Appl. Phys. 53, 3643

Watanabe M B, Tabaka A, Nakanisi T, and Zohta Y 1981 Jpn. J. Appl. Phys. 20, L429
Wagner R Y, Krebs J J, Strauss G H and White M A 1980 Solid State Commun. 36, 15

Proceedings of the 14th Conference (1982 International) on Solid State Devices, Tokyo, 1982;
Japanese Journal of Applied Physics, Volume 22 (1983) Supplement 22-1, pp. 11-19

(Invited) GaAs MIS Structures—Hopeless or Promising?

Harry C. GATOS, Jacek LAGOWSKI and Thomas E. KAZIOR

Massachusetts Institute of Technology, Cambridge, Massachusetts 02139, U.S.A.

High density of interface states introduces uncertainties in the study of GaAs MIS structures; the complex chemical nature of the Ga-As-oxide system has posed an additional problem. The interface states were found to have discrete energy positions about 0.7 and 0.9 eV below the conduction band minimum (rather than a continuous spectrum of energies) which are also characteristic of GaAs "real" surfaces and independent of the insulator. On the basis of the energy position and dynamic parameters of interface states the commonly observed anomalous behavior (e.g., frequency dispersion and capacitance hysteresis) of GaAs MIS structures can be accounted for. Results and arguments are presented indicating that these deep states are the main problem in GaAs MIS structures. Substantial decrease of their density is considered quite feasible and thus the development of GaAs MIS technology appears promising indeed.

§1. Introduction

The potential of GaAs for electronic applications above and beyond those achievable by Si has been recognized for at least 25 years. Its high and direct energy gap and high carrier mobility render GaAs suitable for exciting applications such as integrated optoelectronics, very fast electronic logic, and other circuits and monolithic microwave systems. Although GaAs devices (optoelectronic microwave and others) have been developed and have found significant applications, considering its potential, GaAs has remained essentially the "material of the future."

Extensive efforts have, of course, been made to develop GaAs MIS structures, which are fundamental to exploiting this material's potential. Sucess can hardly be claimed. Is it for reasons inherent to the material or because of limited research and development effort that GaAs applications have not advanced beyond their infancy stage? We need to consider this equation.

The intent of this paper is to present the highlights of the results of MIT's electronic materials group in the overall context of the results of other groups, rather than to review comprehensively all of the published studies on the subject.

§2. Complexities in GaAs MIS Structures—Inherent and Extrinsic

The bulk semiconductor characteristics (e.g., carrier mobility and lifetime) as well as those of the insulator (e.g., dielectric constant, ionic charge mobility and chemical stability) are certainly important parameters in the design and performance of MIS structures; the semiconductor-insulator interface properties, however, are critical and are the controlling factor. Yet these properties are not necessarily determined by the bulk properties of the two materials, although in some respects they are dependent on them. Accordingly, detailed characterization of the interface properties, understanding of their origin, and achieving their control are fundamental to the development of MIS structures. The individual components of the GaAs MIS structures asd the importance of their detailed characterization will be briefly considered below.

2.1 *The semiconductor*

With its high mobility (about an order of magnitude greater than that of Si) GaAs is a superior material for high-speed devices. In principle, crystallographically and electronically it is also a relatively simple material. However, its prepration in "high quality" single crystal form presents substantial difficulties. Achieving perfect stoichiometry is perhaps the major problem. Deviation from stoichiometry leads to a defect structure[1] all aspects of which are not as yet recognized, nor, of course, understood. Excess of two types of vacancies are introduced which can lead to macrodefects (dislocations) and a multitude of point defects and point defect complexes, either intrinsic or involving impurities, which in turn, introduce

traps, recombination centers and carrier compensation effects. No bulk single crystal approaching crystalline and chemical perfection has as yet been grown.

Of course, high quality epitaxial layers have been achieved on poor quality bulk substrates and respectable device technology has been developed on subh layers. However, in contrast to the earlier prevailing views, epitaxial layers are not immune to the substrate defects.[2] Diffusion of these defects can readily degrade the epitaxial layers as devices perform demanding functions (e.g., at high temperature, high carrier injection, and under high energy radiation).

We do not believe that the problems associated with bulk crystal growth are insurmountable; simply research and development commensurate with these problems has not been carried out. For example, the number of publications in the period 1971–1980 recorded in the Chemical Abstracts on the bulk crystal growth remained at an average of ten per year. Paradoxically, during the same period publication of GaAs devices increased from less than 100 (in 1971) to more than 1000 (in 1980). It is encouraging to record, however, that in the last three years research on bulk crystal growth and bulk crystal studies has increased sharply worldwide.

2.2 *The semiconductor surfaces and interfaces*

Intrinsic surface states are to a large measure determined by the electronic configuration of the surface atoms. In the case of Si each surface atom has a dangling electron (resulting from the termination of lattice). These electrons generate surface states (energy levels) within the gap.[3] In GaAs the surface atoms have no dangling electrons; for reasons discussed many years ago[4] the As surface atoms have a pair of unshared electrons, whereas the Ga atoms have no unshared electrons. Indeed, no intrinsic surface states were found within the gap.[5] States introduced by the As atoms are in the valence band (As sublattice) and those by the Ga atoms are in the conduction band (Ga sublattice).

It would, thus, appear that the GaAs surfaces would present less of a problem with respect to surface states than Si. In practice, however, the reverse is true.

Surface states in "clean" and especially in "real" surfaces of Si have been studied extensively and effectively.[3] The field effect proved to be a most powerful tool. In "clean" surfaces the density of states was found to be about 10^{15} cm^{-2}, a value close to the density of surface atoms, confirming their association with dangling bonds. On "real" surfaces the density of these states decreased by 3 to 4 orders of magnitude and varied only within a narrow range upon various surface treatments; this decrease was attributed to the saturation of dangling bonds by oxygen and to a nearly matching between Si and its native oxide. Thermal oxidation decreased the density even further. In today's Si MOS structure the density of interface states is insignificantly small (typically 10^9 cm^{-2} or smaller).

Studies on GaAs "real" surfaces have been very limited.[6] Perhaps the major reason has been the fact that standard field effect analysis cannot be carried out because a minimum in surface conductance could not be obtained. Employing pulsed field measurements we identified in an early study[7] surface states about 0.4, 0.7 and 0.9 eV below the conduction band. In a later study,[8] employing pulsed field techniques, the main state was found to be 0.7 and about 1 eV below the conduction band; these states were found to be essentially insensitive to crystallographic orientation, etching treatment and gas ambient. We concluded in that study that the surface states are associated with crystalline defects in the space charge region rather than with particular abrupt termination of the lattice at the surface. By means of surface photovoltage spectroscopy, surface states 0.7 and 0.9 eV below the conduction band were also found. Again, no variations in the energy position of the surface states or the surface barrier (0.55 eV) were observed in various ambients.[9]

Thus, from the above studies (allowing for inherent small errors) it is clearly shown that, on the real surfaces of GaAs, there are two main discrete surface states; their energy positions at 0.7 and 0.9 eV below the conduction band are independent of chemical treatments, ambients and doping level of the crystals. These various treatments and ambient have only relatively small effects on their characteristics such as their capture cross

sections and densities.

In extensive X-ray photoemission studies, employing "clean" surfaces, Spicer and coworkers[10] have found that submonolayer coverage of oxygen and various metals introduces two main discrete surfaces with the above energies. They attributed these states to missing Ga and As atoms at the surface as a result of the interaction of these clean surfaces with the ambient species. They also found that these states lead to pinning of the Fermi level at the surface.

A number of studies have been devoted to electronic characteristics of GaAs-insulator interfaces employing C-V and I-V techniques, thermal and optical transients, and DLTS. The results of these studies are not in general agreement regarding the interface states. Thus employing C-V measurements on GaAs–Si_3N_4 structures, a U-shaped distribution of surface states was reported extending over the entire gap.[11] Studies on C-V and I-V GaAs–SiO_2 and GaAs–$Si_xO_yN_z$ and GaAs-oxide structures showed a U-shaped distribution localized in the upper half of the gap with a minimum at 0.36 eV.[12] Similar results were reported from studying GaAs-oxide structures with saturation surface photovoltage measurements.[13] On the other hand, a U-shaped distribution within the lower part of the gap with a minimum near 1.1 eV below the conduction band was reported on GaAs-Si_3N_4 and GaAs-oxide structures.[14,15,16] On the basis of DLTS studies on MIS structures discrete interface states were reported in the vicinity of 0.4[16] and 0.65 eV below the conduction band.[17]

The discussion of the models proposed in the above investigations to account for the experimental results (Fig. 1) and conclusions is beyond the scope of this paper. However, in view of the inconsistency of the reported results, the inevitable question must be asked. Is this inconsistency due to the complexity of the GaAs-insulator interface in the MIS structures, or is it due to uncertainties stemming from the measurement techniques? This question will be addressed.

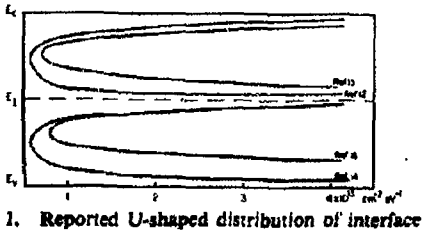

Fig. 1. Reported U-shaped distribution of interface states.

2.3 *The insulator*

As pointed out earlier, excellent characteristics in the Si–SiO_2 interface are readily attained because of the nearly perfect compatibility of the Si with its oxide. The GaAs-native oxide system to begin with is very complex from a thermodynamic as well as from a kinetic point of view. Numerous phases can exist as a function temperature, and moreover As_2O_3 is thermally unstable in the presence of GaAs leading to the formation of elemental As.[18] The build-up of As at the interface has been reported[19] and models have been proposed to account for the kinetics of this build-up, which has been observed after oxidation, as well as after subsequent annealing treatments. The introduction of interface states by free As has, of course, been considered.

Oxide formation has been obtained by thermal oxidation, anodic oxidation and plasma annealing. Anodic oxides have exhibited the most satisfactory dielectric properties[20] although results obtained with plasma oxidation[21,22] are quite good.

In a number of instances anomalous C-V behavior of the GaAs-oxide interfaces has been reported.[16,23,23] Some aspects of the anomalous behavior we have accounted for by establishing that significant negative electric charge, as high as 10^{12} q/cm^{-2}, is present in oxides formed anodically or by plasma discharge;[24] by thermal annealing at 70–180°C we were successful in eliminating this charge.

Although Ga–As oxides with satisfactory dielectric properties have been achieved[24], it is unlikely that they will serve as an insulator for MIS structures because they are thermally unstable and chemically reactive.

Numerous other insulating films have been studied, among them, Si_3N_4, SiO_2, $Si_xO_yN_z$, and Al_2O_3. Although Si_3N_4 appears quite promising, sufficient work has not been carried out as yet leading to a definitive conclusion.

Thus, we believe that the problems associated with the insulator properties are both inherent

and extrinsic. Ga–As oxides, for reasons unrelated to their dielectric properties (chemical reactivity and thermal instability) appear to be inherently unsuited for GaAs MIS structures. Regarding other insulating films such as Si_3N_4, the problems could very well be extrinsic and further, extensive, research and development work might lead to their resolution.

2.4 *Measurements*

The availability of only limited definitive results, the prevailing uncertainties and inconsistencies in experimental data and fundamental understanding regarding surface states both on real surfaces and at interfaces, are to a large measure associated with experimental techniques and measurements. Actually, the high densities of these states and their energy position deep into the gap render powerful experimental techniques unsuitable or impair their precision, accuracy, and/or reliability.

For the investigation of surface states on real surfaces, d.c. or a.c. field effect techniques have proven to be powerful indeed in the case of Ge and Si[3,6] and also InSb[25] surfaces, as they provide accurate insight into the energy position, as well as into the dynamic parameters of the surface states. As pointed out earlier, these techniques are not applicable to GaAs surfaces. Surface photovoltage spectroscopy capable of providing a very detailed analysis of the surface state structure of high energy gap semiconductors[26] becomes much less effective in the study of GaAs surfaces because of the relatively good communication of the surface states with the bulk.[27] Other, generally powerful, techniques, such as those based on pulsed fields, X-ray, and UV-electron emission spectroscopy[10] lead only to a partial characterization of the surface states.

Regarding the study of interface states in actual MIS structures, the majority of the investigations have relied on capacitance based methods. However, in those investigations the electronic behavior of the MIS structures has exhibited a large majority carrier hysteresis and a significant frequency dispersion[16,21,23] of the positive gate bias capacitance. Although these investigations have revealed important aspects of the GaAs MIS structures, no entirely consistent models have emerged relating the observed anomalous behavior to the interface state structure. it is a very difficult problem indeed to determine conclusively unknown parameters from anomalous characteristics, particularly when the nature of the anomaly itself is not clearly understood.

DLTS, even as applied for the characterization of deep levels in bulk crystals, is unique for its probing power, rather than for its precision in determining the dynamics of deep levels.

Thus, much of the uncertainty and controvery associated with MIS structures is due to the limitations of the available techniques. However, limited as the techniques may be generally, we believe that the strong points of each technique have not as yet been utilized in a complimentary mode from which a composite but reliable picture may emerge.

§3. Invariably Discrete Energy Interface States

We hypothesized that non-equilibrium charging and discharging of the interface states in capacitance-based techniques might be the major cause of the reported discrepancies between the surface state configuration on GaAs real surfaces (discrete energy states) and at the GaAs-insulation interface state configuration (continuous energy distribution) and also of the inconsistencies in the results of many investigations on GaAs MIS structures. It was this hypothesis that motivated our investigation of interface states through the analysis of the spectral and transient responses of photostimulated currents in MIS structures.[28]

The measurement procedure is schematically illustrated in Fig. 2. Figure 2(a) represents the

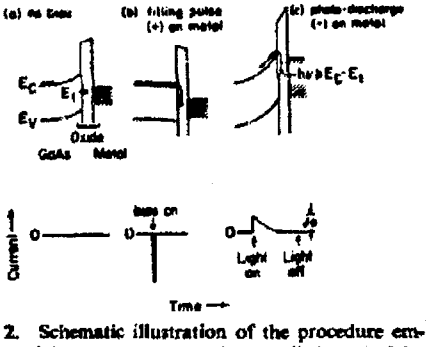

Fig. 2. Schematic illustration of the procedure employed in measurements of photodischarge of interface states.

MOS structure with a residual amount of charge trapped at the interface. A large positive bias filling pulse is applied to the gate, Fig. 2(b), creating an instantaneous current spike. This spike represents the lowering of the surface potential barrier and filling of the interface states. The gate voltage is then switched to a negative bias to drive the GaAs into depletion; since thermal generation is negligible, the states remain filled. The structure is then illuminated with subbandgap monochromatic light and the current monitored, Fig. 2(c). When $he \gtrsim E_c - E_t$, (E_t is the energy position of the trap relative to the conduction band minimum) electrons are excited from the trap to the conduction band, where they are swept away from the interface by the large electric field, and are recorded as discharge current. In the absence of thermal generation (low temperature) and negligible concentration of recombination centers (high surface barrier and no minority carriers) the photodepopulation of interface states can be described as:[28]

$$dn_t/dt = -I\sigma_i n_t, \tag{1a}$$

or

$$n_t = n_{t0}e^{-t/\tau};\ \tau = (I\sigma_i)^{-1} \tag{1b}$$

where I is the photon flux, σ_i is the photoionization cross section, n_t is the concentration of electrons in a discrete interface state, and n_{t0} their initial concentration. Thus, the photodischarge current $J = q\,dn/dt$ becomes

$$J(t) = J_0 e^{-t/\tau} \text{ where } J_0 = -qI\sigma_i n_{t0}. \tag{2}$$

It is thus apparent that the relaxation time τ, of the discharge provides a measure of the photoionization cross section, while the product $J_0\tau$ gives the initial discharge in the interface states. The total charge transferred from the interface upon illumination can also be obtained as

$$\Delta Q_{ss} = \int_0^\infty J\,dt \tag{3}$$

For a single state totally depopulated $|\Delta Q_{ss}| = qn_{t0}$.

It should be noted that this experimental procedure provides a simple means for distinguishing between discrete states and states continuously distributed in energy. For a discrete state, only τ (or σ_i) depends on photon energy, while n_{t0} is a constant independent of the energy of the photons utilized in the photodischarge process. Thus, ΔQ_{ss} should exhibit a step-like energy dependence, i.e., $\Delta Q_{ss} = 0$ for $he < E_c - E_t$ and $|\Delta Q_{ss}| = qn_{t0}$ for $he > E_c - E_t$. For states with continuous energy distribution both τ (or σ_i) and n_{t0} depend on energy.

Figure 3(a) shows a typical current transient. By repeated filling and photodischarging of the interface traps at various photon energies and by determining the integrated area of each current transient, the total charge, ΔQ_{ss}, removed from the interface is obtained as a function of he shown in Fig. 3(b). A definite step-like threshold in ΔQ_{ss} is found at 0.7 eV remaining constant until 0.85 eV where a second threshold appears with Q_{ss} again becoming constant. Identical step-like behavior as a function of photon energy was exhibited by the independently measured roduct $J_0\tau$ (as pointed out above $|\Delta Q_{ss}| = J_0\tau = qn_{t0}$). This behavior is characteristic of discrete traps.

A quantitative analysis based on eq. (2) yields the following trap parameters: $E_{t1} = 0.73 \pm 0.03$ eV, $N_{t1} = 6 \times 10^{12}$ cm^{-2}, $\sigma_{t1}^{max} = 3 \times 10^{-18}$ cm^2; and $E_{t2} = 0.87 \pm 0.03$ eV, $N_{t2} = 7.5 \times 10^{11}$ cm^{-2}, $\sigma_{t2}^{max} = 10^{-17}$ cm^2.

The energy position of these deep interface states is in good agreement with those reported for real surfaces as well as those with submonolayer oxygen coverage and deposited metals as seen in Table I.

In contrast to surfaces with low oxygen

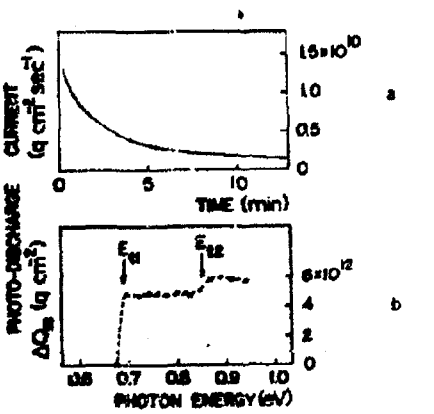

Fig. 3. (a) Photodischarge current transient for $h\nu = 0.9$ eV and $I = 10^{13}$ photons cm^{-2}s; (b) charge removed from interface states by photodischarge as a function of photon energy.

Table I. Main GaAs Discrete Surface/Interface States.

	Real Surfaces		Adatom Induced (Sumbonolayer Coverage)		GaAs-Oxide Interfaces	
Clean Surfaces	E_c-E_i (eV)	N_i (cm^{-2})	E_c-E_i (eV)	N_i (cm^{-2})	E_c-E_i (eV)	N_i (cm^{-2})
No states[31] in the energy gap	0.70 to 0.75[7,8,9]	—	0.7 ± 0.05[10]	$\sim > 10^{12}\ cm^{-2}$	0.7 ± 0.05[28]	$5 \times 10^{12}\ cm^{-2}$
	0.9 to 1.0[7,8,9] States only weakly affected by ambient		0.9 ± 0.05[10]		0.85 ± 0.05[28] High density shallow states in the vicinity of conduction and valence band edges	$5 \times 10^{11}\ cm^{-2}$

coverage, the GaAs-thick oxide interfaces exhibited a high density ($\sim 10^{14}\ cm^{-2}$) of shallow donors and acceptor pairs; photoexcitation of these pairs led to a gigantic photoionization of deep interface states with rates 10^3 times greater than direct transitions into the conduction band as a result of energy transfer from the excited donor-acceptor pairs to deep states.[28]

Similar results on deep interface states were obtained on p-type GaAs MOS structures[29] and on MIS structures with GaAs-Si_3N_4 interfaces.[30] We consider these findings significant, as they lead to the important conclusion, inferred by investigations on real surfaces, that the energy positions of interface states are independent of the conductivity type of the semiconductor and the nature of the insulator (Fig. 4).

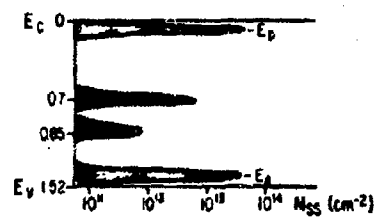

Fig. 4. Discrete interface states in GaAs MIS structures.

A summary of the results obtained on p-type GaAs MOS structures with photodischarge of interface states and internal photoemission measurements[29] is shown in Fig. 5.

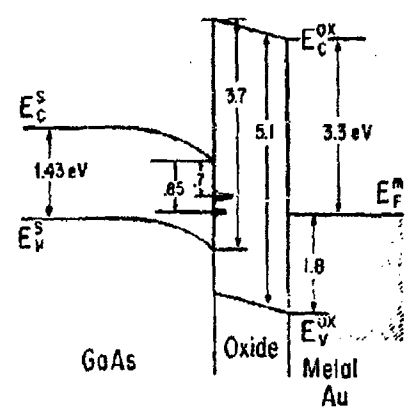

Fig. 5. Summary of energy diagram of p-type GaAs MOS structure.

§4. Resolution of Extrinsic Complexities

We believe some important problems contributing to the complexity of the analysis of experimental results, of the understanding of the behavior of GaAs MIS structures, and thus assessing the application potential of such structures have been resolved.

The finding that the interface states are independent of the nature of the insulator, but are characteristic of the real GaAs surfaces, essentially eliminates the need to consider the insulator as a significant factor in the behavior of the MIS structures and identifies the major controlling parameter. Interference from electric charges in the insulator can now be diagnosed and eliminated.

The establishment of the presence of discrete energy interface states led us to an investigation where capacitance measurements were carried out on GaAs MOS structures in conjunction with photo- a well as thermal emission.[30] We found that all essential features of the anomalous behavior of GaAs MIS structures, such as the frequency dispersion and the C-V hysteresis, could be explained on the basis of the pinning of the Fermi level and the time con-

Table II. Role of Interface States in Electrical Behavior of GaAs MIS Structures.

Effect	Explanation	Comment
Appearance of plateau in C-V characteristics[31]	Pinning of Fermi level by high density interface states	Surface potential variation
Frequency-temperature dispersion	Frequency-temperature dependence of time constants associated with charging and discharging of interface states	Characteristics of MIS devices change with operation frequency and/or temperature
Capture of free carriers at interface	Thermal activation over surface barrier	At low temperature surface potential varies with temperature
C-V hysteresis	Strong time dependence of emission of carriers from interface states	Causes drift in MIS devices with time

stants of the charging and discharging of the high density discrete energy interface states. A brief summary of some of the results is presented in Table II.

We certainly do not intend to imply that the resolution of the main complexities associated with the study of the GaAs MIS structures means that all extrinsic problems are solved. We do believe, however, that investigations on GaAs MIS structures can now be more sharply and effectively focused.

§5. Inherent Problem and Potential Promise

The high density of discrete energy interface states is indeed an inherent problem in GaAs MIS as they are essentially "intrinsic" in GaAs real surfaces. Their energy positions 0.7 and 0.9 eV below the conduction band (these values should not be considered more accurate than ± 0.05 eV) appear to be invariable. Surfaces, of any orientation, cut, polished, and etched exhibit the same states regardless of etchant, etching procedure, or ambient to which they are subsequently exposed.[7,8,9] The same stated are formed on cleaved (110) state free surfaces upon submonolayer coverage with oxygen or various metals.[10] Even when thick oxides are grown[28] or other insulators are deposited[30] on these surfaces, no basic change takes place in their surface state configuration. The high density of shallow donor and acceptor pairs we reported at GaAs-thick oxide interfaces[28] may be part of the basic surface structure, but they cannot be detected by techniques employed on real surfaces.

The conclusion is inevitable: the GaAs surface or interface states originate in lattice defects. Spicer and coworkers[10] have assigned them to missing Ga and As atoms as a result of interactions of the surface with chemical species.

Deep levels are not unique to the GaAs surfaces. A number (more than 5) of deep levels, both donor and acceptor types and unrelated to impurity atoms, are present in melt-grown GaAs crystals.[32] Although they have been attributed to lattice point defects (and their complexes) no assignments to specific defects have been made with certainty with the exception of the major and most studied deep level (referred to as EL2, 0.82 eV below the conduction band) which we have assigned to the antisite defect AsGa,[33] an assignment being widely accepted.

We will outline briefly the behavior of these levels. Their density is significantly affected by high temperature treatments,[34] apparently due to lattice defect interactions. Even more interesting we consider the finding that their concentration is affected by the stoichiometry of the crystals and the presence of shallow donor and acceptor impurities.[35] In fact, by controlling the stoichiometry and the impurity concentration we have grown deep level-free crystals[35] apparently as the result of minimizing the point defect concentration. More recently we found that by introducing hydrogen in GaAs crystals in a hydrogen plasma discharge of 300°C, the EL2 level is completely passivated.[36]

At thing time there are no sound reasons to lead us to the conclusion that the deep interface states and the bulk deep levels are identical or different. However, some extrapolation of our knowledge on deep bulk levels to the interface states, even on a speculative basis, we believe to be appropriate, as both types of levels must be directly or indirectly vacancy

related.

Vacancies are inevitably "frozen in" in GaAs crystals; they must then be present in the surface region. The fact that no surface states are found in clean cleaves surfaces[3] simply suggests that either their concentration is below the detection limits of the experimental techniques (if the surface states are due to vacancies) or their concentration is below a critical value necessary for the formation of point defect complexes (if the surface states are due to point defect complexes). In either case, it is reasonable to assume that the "frozen in" concentration of vacancies should play a role in the density of surface and interface states. Unfortunately, no systematic studies have been carried out on the density of surface states for crystals with relatively low vacancy concentration (LPE layers) and for crystals with high vacancy concentration (melt-grown crystals).

Thus, it is reasonable to hypothesize that the density of surface states can be decreased, hopefully to an acceptable value for high quality MIS structures, by the growth of "appropriate" crystals, by special treatments of GaAs-insulator interface or both. Appropriate crystals should be as close to stoichiometry as possible and contain vacancy-gettering impurities such as Si. Special treatments can involve the introduction of vacancy-gettering impurities (such as Si) during the formation of the GaAs-insulator interface, the introduction of deep level passivating species, such as hydrogen, and heat treatments of the GaAs-insulator structure.

We believe that our hypothesis is justified on the basis of present knowledge; we must, therefore, conclude that GaAs-MIS structures, far from being inherently hopeless, are most promising for an exciting GaAs-MIS technology. We also believe, however, that much more extensive and intensive research and development efforts, than in the past, must be devoted to all "components" of GaAs-MIS structure.

§6. Summary

The immense potential of GaAs for MIS applications, far beyond those of Si MIS technology has not been realized because of the high density of interface states and because GaAs and its native oxides lack the electronic compatibility of Si and SiO_2. However, it has been established that the interface states have discrete energy positions, which are independent of the surface treatment or the insulator, and they originate in lattice defects.

The knowledge of the energy positions and dynamic parameters of the interface states made it possible to understand the perplexing anomalous behavior of the GaAs MIS structures (e.g., frequency dispersion and capacitance hysteresis). Thus, these states constitute the main inherent problem in the development of device quality GaAs-MIS structures.

However, with further understanding of the origin of these states and their relationship to the defect structure of the crystals, it appears quite possible that control of their density to desired values is achievable. Thus, GaAs MIS structures, far from being hopeless, present real promise for new breakthroughs in MIS technology.

Acknowledgement

The authors are grateful to the National Science Foundation and to the National Aeronautics and Space Administration for financial support.

References

1) J. M. Parsey, Y. Nanishi, J. Lagowski and H. C. Gatos: J. Electrochem. Soc. 129 (1982) 388.
2) L. Jastrzebski, J. Lagowski and H. C. Gatos: J. Electrochem. Soc. 128 (1981) 697.
3) A. Many, Y. Goldstein and N. B. Grover: *Semiconductor Surfaces* (North-Holland Publishing Co., Amsterdam, 1965).
4) H. C. Gatos and M. C. Lavine: J. Electrochem. Soc. 107 (1960) 427; H. C. Gatos: J. Appl. Phys. 32 (1961) 1232.
5) A. Huijser and J. Van Laar: Surface Sci. 52 (1975) 202; W. E. Spicer, I. Lindau, J. N. Miller, D. T. Ling, P. Pianetta, P. W. Chye and C. M. Garner: Phys. Scr. 16 (1977) 388; D. J. Chadi: Phys. Rev. Lett. 41 (1978) 1062.
6) D. R. Frankl: *Electrical Properties of Semiconductor Surfaces*, (Pergamon Press, New York, 1967).
7) S. Kawaji and H. C. Gatos: Surf. Sci. 1 (1964) 407.
8) T. M. Valahas, J. S. Sochanski and H. C. Gatos: Surface Sci. 26 (1971) 41.
9) J. Lagowski, I. Baltov and H. C. Gatos: Surf. Sci. 40 (1973) 216.
10) W. E. Spicer, I. Lindau, P. Skeath, C. Y. Su and P. Chye: J. Vac. Sci. Technol. 17 (1980) 1019; Phys. Rev. Lett. 44 (1980) 420.
11) J. E. Foster and J. M. Swartz: J. Electrochem. Soc. 117 (1970) 1416.
12) C. R. Zeisse, L. J. Messick and D. L. Lile: J.

Vac. Sci. Technol. 14 (1977) 957.
13) A. Shimano, A. Moritani and J. Nakai: Jpn. J. Appl. Phys. 15 (1976) 939.
14) L. G. Meiners: J. Vac. Sci. Technol. 15 (1978) 1402.
15) T. Sawada and H. Hasegawa: Thin Solid Films 56 (1979) 183; Phys. Stat. Sol. 54 (1979) 689.
16) H. Hasegawa and T. Sawada: IEEE Trans. Electron. Devices ED 27 (1980) 1055; J. Vac. Sci. Technol. 16 (1979) 1478.
17) E. Kamieniecki, T. E. Kazior, J. Lagowski and H. C. Gatos: J. Vac. Sci. Technol. 17 (1980) 1041.
18) C. D. Thurmond, G. P. Schwartz, G. M. Kammlott and B. Schwartz: J. Electrochem. Soc. 127 (1980) 1366.
19) C. W. Wilmsen, R. W. Kee and K. M. Gleb: J. Vac. Sci. Technol. 16 (1979) 1434.
20) H. Hasegawa, K. E. Forward and H. L. Hartnagel: Appl. Phys. Lett. 15 (1975) 567; Thin Solid Films 32 (1976) 65.
21) F. Kashiga and T. Sugano: Thin Solid Films 56 (1979) 39.
22) S. Gourrier, A. Mircea and M. Bucal: Thin Solid Films 65 (1980) 415.
23) G. Weiman: Thin Solid Films 56 (1979) 39.
24) J. Siejka, A. Morawski, J. Lagowski and H. C. Gatos: Appl. Phys. Lett. 38 (1981) 552.
25) H. Huff, S. Kawaji and H. C. Gatos: Surface Sci. 5 (1966) 399.
26) J. Lagowski, C. L. Balestra and H. C. Gatos: Surface Sci. 29 (1972) 213.
27) H. C. Gatos and J. Lagowski: J. Vac. Sci. Technol. 10 (1973) 130.
28) J. Lagowski, T. E. Kazior, W. Walukiewicz, H. C. Gatos and J. Siejka: J. Vac. Sci. Technol. 19 (1981) 519.
29) P. K. Kashkarov, T. E. Kazior, J. Lagowski and H. C. Gatos: J. Appl. Phys., in press.
30) T. E. Kazior: *Electrical Properties of the GaAs-Insulator Interface*, Ph.D. Thesis, Massachusetts Institute of Technology, June 1982.
31) J. G. Simmons and L. S. Wei: Solid-State Electron. 16 (1973) 43.
32) C. M. Martin, A. Mitonneau and A. Mircea: Electron. Lett. 13 (1977) 191.
33) J. Lagowski, H. C. Gatos, J. M. Parsey, K. Wada, M. Kaminska and W. Walukiewicz: Appl. Phys. Lett. 40 (1982) 342.
34) T. Ikoka, M. Takikawa and M. Taniguchi: *GaAs and Related Compounds, Japan, 1981*, Inst. Phys. Conf. Ser. (1982) No. 63, p. 191.
35) J. M. Parsey, Y. Nanishi, J. Lagowski and H. C. Gatos: J. Electrochem. Soc. 128 (1981) 936.
36) J. Lagowski, M. Kaminska, J. M. Parsey, Jr., H. C. Gatos and M. Lichtensteiger: Appl. Phys. Lett. in press.

Shallow donor associated with the main electron trap (EL2) in melt-grown GaAs

W. Walukiewicz, J. Lagowski, and H. C. Gatos
Massachusetts Institute of Technology, Cambridge, Massachusetts 02139

(Received 14 February 1983; accepted for publication 19 April 1983)

A systematic analysis of Hall effect measurements on a large number of melt-grown GaAs crystals with different concentrations of the major deep trap (EL2) revealed the presence of a new shallow donor level (20–30 meV below the conduction band) with concentrations similar to those of the EL2. This finding indicates that the EL2 center is a double donor consisting of the deep EL2 donor at $E_c - 0.76$ eV and a shallow donor state. The presence of the shallow donor state should have important consequences in the formulation of a compensation mechanism in semi-insulating GaAs.

PACS numbers: 72.20.My, 72.80.Ey, 78.50.Ge

It is commonly accepted that the high resistivity of "undoped" semi-insulating GaAs results from the compensation of shallow acceptors by deep donors (EL2) located at $E_c - 0.76$ eV.[1–4] The shallow acceptors are most likely due to residual carbon impurities.[2,4] The question of the origin of the EL2 donor is more uncertain.[5–9] Most recently, EL2 has been attributed to the antisite defect As_{Ga} complexed with a native defect (e.g., an arsenic vacancy on a neighboring lattice site) rather than to any impurity or to a simple native defect.[10] The first indication of the association of an additional donor with EL2 was provided by our recent finding that the EL2 is passivated by atomic hydrogen; this passivation is accompanied by a greater decrease in a free-electron concentration than expected from the elimination of a single charge deep donor state at $E_c - 0.76$ eV.[6] The question of the charge state of the EL2 complex is critical not only in the understanding of the origin of this center, but also in the quantitative explanation of the compensation mechanism of semi-insulating (SI) GaAs (Ref. 2).

In this letter we report the results of a systematic study on a large number of Bridgman-grown crystals, aimed at establishing the presence and the parameters of the shallow donor associated with EL2.

The study was performed on semiconducting n-type GaAs since the deep levels can be readily determined with Schottky barrier capacitance (current) transient measurements and the shallow donors can be conveniently measured from the temperature dependence of the Hall effect and the conductivity. Samples were grown using a Bridgman-type apparatus which allowed very precise control of the growth parameters.[11] The electron concentration was varied between 10^{15} and 10^{18} cm^{-3} by intentional doping with Si, S, Se, and Te. The As partial pressure during the growth (i.e., the As/Ga ratio in the melt) was adjusted by selecting an As source temperature T_{As} between 613 and 619 °C. Raising (lowering) T_{As} was used to increase (decrease) the concentration of the EL2.[7] For crystals with electron concentration of about 10^{16} cm^{-3} the employed range of T_{As} enabled the modulation of the EL2 concentration by a factor of 2. The EL2 concentration and its sensitivity to the As source temperature (i.e., to the melt composition) decreases with increasing electron concentration n. In fact, for n exceeding 3×10^{17} cm^{-3} the melt-grown crystals had an EL2 concentration below the detection limit of about 2×10^{14} cm^{-3}, irrespective of the source temperature.

Representative experimental data of the Hall constant versus temperature for two samples containing EL2 are shown in Fig. 1. It is seen that there is a systematic increase of the electron concentration with increasing temperature. This behavior indicates the existence of a donor level the occupancy of which changes substantially in the temperature range employed. For EL2-free samples, the changes of the electron concentration were found to be about one order of magnitude smaller.

For a quantitative treatment of the free-carrier freezeout caused by the shallow donor we have determined the temperature dependence of the total electron concentration from the expression

$$n(T) = n_0 + N_{SD}\,[1 - f_n(T)], \tag{1}$$

where $n_0 = N_D^+ - N_A^-$; N_D^+ and N_A^- are the concentra-

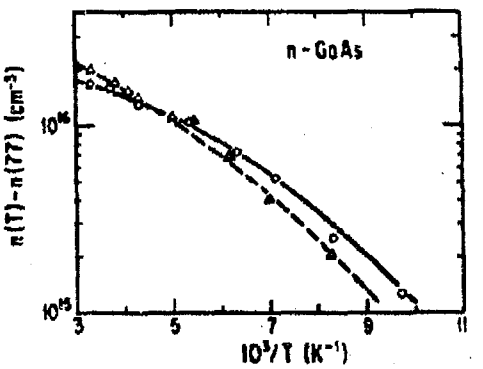

FIG. 1. Dependence of the electron concentration (freezeout), $n(T) - n(77)$ on temperature in GaAs containing EL2. (○)$n(300) = 1.25\times10^{17}$ cm^{-3}, $N_{EL2} = 2.2\times10^{16}$ cm^{-3}; (△)$n(300) = 1.98\times10^{17}$, $N_{EL2} = 3.0\times10^{16}$ cm^{-3}. Curves are theoretically calculated from Eqs. (2) and (3)—see text.

 0003-6951/83/130112-03$01.00

tions of the ionized donors and acceptors, respectively. N_{SD} is the total concentration of the EL2-related shallower donor; E_F is the Fermi energy determined from the free-electron concentration. It is assumed here that any shallow hydrogenic donors and acceptors (at concentrations N_D and N_A, respectively) are completely ionized in the considered temperature range (no measurable freezeout was found in the EL2-free material), while the new, less shallow donor N_{SD} determines the change of the electron concentration with temperature. The occupancy function for this donor is given by

$$f_n(T) = [g \exp(\alpha/k) \exp(-E^0_{SD} - E_F)/kT]^{-1}, \quad (2)$$

where g is the degeneracy factor. Here, it is assumed that the ionization energy E_{SD} is linearly dependent on temperature $E_{SD} = E^0_{SD} - \alpha T$.

The factor g depends on degeneracy of the shallow state. At present no information is available on values of the degeneracy factor and of the temperature coefficient α. Accordingly, the product $g \exp(\alpha/k)$ must be treated as a fitting parameter in the analysis of the experimental data. The calculated results of $n(T) - n(77)$ vs $1/T$ obtained from Eqs. (2)–(4) with $g \exp(\alpha/k) = 2$ are shown in Fig. 1 (dashed and solid lines); $n(77) \simeq N_D^+ - N_A^- = \text{const}$. In these calculations the following values of independent variables were used: $E^0_{SD} = 20$ meV, $N_{SD} = 2.2 \times 10^{16}$ cm^{-3} (solid line) and $E^0_{SD} = 25$ meV and $N_{SD} = 3.6 \times 10^{16}$ cm^{-3} (dashed line). The above concentrations of the new donor are in good agreement with the EL2 concentration in the two samples, i.e., 2.2×10^{16} (○) and 3.0×10^{16} (△), respectively. The value $g \exp(\alpha/k) = 2$ coresponds to a simplest case of a hydrogenic type donor ($g = 2$; $\alpha = 0$). It should be noted, however, that for $g \exp(\alpha/k)$ ranging from 2 to 6, a good fitting can be obtained by introducing a 30% change in the new donor concentration N_{SD} and taking E_{SD} values in the range 20–30 meV. For $g \exp(\alpha/k) < 1$ the experimental data cannot be satisfactorily fitted using expressions (2) and (4).

The association of a shallow donor with the EL2 center was further investigated employing about 200 samples in which the EL2 concentration varied from below the detection limit about 4×10^{16} cm^{-3}. On all these samples Hall effect and conductivity measurements at 77 and 300 K were carried out, and their EL2 concentration was determined by Schottky diode transient capacitance measurements. Representative results are shown in Fig. 2. The approximately one-to-one correlation between $n_{300} - n_{77}$ and EL2 concentration implies the presence of a donor level with concentrations which are the same as those of EL2.

Secondary-ion mass spectroscopy (SIMS) analysis carried out on 16 representative samples containing EL2 and EL2-free did not reveal any relationship between chemical impurities and the new shallow donor. It should be also pointed out that the concentration of other electron traps (EL4, EL5, and EL6) in the samples investigated was about one order of magnitude smaller than that of EL2. Thus, their contribution to the observed changes of n can be neglected.

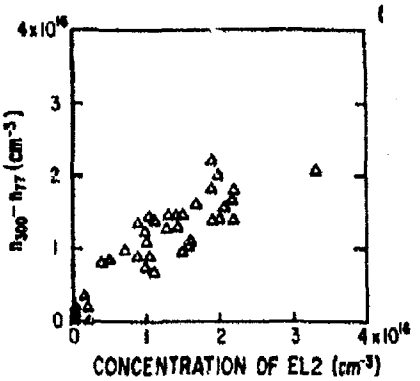

FIG. 2. Electron freezeout, $n(300) - n(77)$ vs EL2 concentration. The electron concentration $n(300)$ in the samples ranged from 5×10^{15} to 2×10^{17} cm^{-3}.

In Fig. 3 the concentration ratio $\gamma = n(300)/n(77)$ is plotted as a function of electron concentration $n(T)$ for a large number of samples. It is clearly seen that there is a systematic difference between the EL2-containing and EL-free samples. The samples containing EL2 exhibit a noticeable decrease of n at lower temperatures, as manifested by γ values larger than one. Such a freezeout is not observed for EL2-free samples for which γ remains 1.00 ± 0.03 in the concentration range $5 \times 10^{15} \leq n \leq 10^{18}$ cm^{-3}. This result provides further support for the one-to-one correspondence between N_{SD} and N_{EL2}.

With the aid of expressions (1) and (2) we have calculated the theoretical dependence of $n(300)/n(77)$ on the free-electron concentration (which determines the Fermi energy) assuming a constant concentration of $N_{SD} = 2 \times 10^{16}$ cm^{-3}, equal to the average concentration of the EL2 in the samples employed in Fig. 3. Other parameters were taken the same as in fitting the data of Fig. 1; i.e., $g \exp(\alpha/k) = 2$ and $E^0_{SD} = 20$ meV. The theoretical results are represented by the

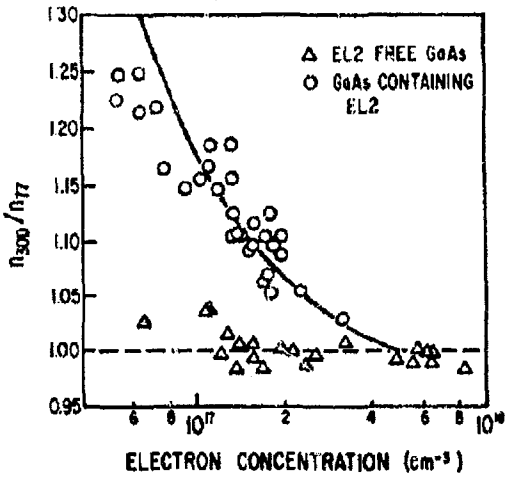

FIG. 3. Relative change of the electron concentration n_{300}/n_{77} vs electron concentration at 300 K in the presence and absence of EL2. Solid line was calculated using Eq. (2).

solid line on Fig. 3. It is seen that the theoretical curve is consistent with the general tendency of the experimental data. The scatter of the experimental points about this curve is expected, since there are differences in the EL2 concentration in the samples.

In our measurements we have assumed that the temperature dependence of the Hall coefficient is entirely determined by the changes of the electron concentration in the temperature range 77–300 K. This assumption is valid when the Hall factor defined as the Hall-to-drift-mobility ratio $r = \mu_H/\mu_d$ is temperature independent. The value of the Hall factor depends on the scattering mechanisms determining the electron mobility and on the electron statistics. The fact that the mobilities in the EL2-containing and EL2-free samples were similar indicates that the same scattering processes determine the mobilities in both cases; the electron statistics are also the same, since the samples had the same electron concentration (at 300 K). Accordingly, the observed changes in electron concentration as a function of temperature in the EL2-containing samples (Fig. 3) are not due to changes in the Hall factor. Indeed, measurements of the Hall constant carried out for several typical samples at very high magnetic fields (up to 140 kGs), at which $\mu_H B > 10^4$ and the Hall factor r_H approaches unity, showed that the concentration difference $n(300) - n(77)$ is within 15% the same as that determined at low magnetic fields.

The present findings have two important implications regarding the origin of the EL2 and the quantitative treatment of the compensation mechanism in SI GaAs. As pointed out above, there is increasing evidence that the EL2 involves the antisite defect AS_{Ga} not alone, but in a complex with another native defect (most likely an arsenic vacancy). The present discovery of an additional shallow donor state associated with the EL2 defect together with recent theoretical calculations on the antisite As_{Ga} energy levels[12] can be considered as additional evidence against the association of the EL2 with the antisite defect alone.

The increased concentration of ionized shallow centers indicated by the present finding accounts for the typical mobility values in SI GaAs. Let us consider SI GaAs with the EL2 concentration N_{EL2}. Since in this material all shallow donors must be ionized, the lowest ionized impurity concentration should exceed $2N_{EL2}$. On the other hand, the material will be semi-insulating as long as the concentration of acceptors does not exceed $2N_{EL2}$. The doubly ionized EL2-related defect will effectively scatter as four separate centers. Therefore, the effective concentration of ionized scattering centers will be $<6N_{EL2}$. However, in n-type undoped GaAs the deep EL2 level is often almost entirely unoccupied. Therefore, in such material the total ionized impurity concentration should be close to $2N_{EL2}$. Considering a typical EL2 concentration in SI GaAs between 10^{15} and 2×10^{16} cm^{-3}, one obtains a concentration of ionized impurities between 2×10^{15} and 4×10^{16} cm^{-3}. Employing the results of theoretical calculations of electron mobility in SI GaAs in Ref. 13, we find that mobilities in the samples employed in this study should range from 5500 to 3000 cm^2/Vs. This range is in good agreement with experimental values of electron mobilities measured in undoped Si GaAs.[1–3]

In summary, we found that a new shallow donor with the binding energy 20–30 meV is associated with the center responsible for the EL2. The concentrations of both the new shallow donor and that of the deep EL2 donor were found to be the same in a given sample. The present finding accounts for the reported mobilities of Si GaAs and indicates that compensation in SI GaAs must require shallow acceptor concentrations greater than those of EL2 rather than smaller, as previously supposed.

The authors are grateful to the National Aeronautics and Space Administration for finanacial support. Part of this work was performed at the Francis Bitter National Magnet Laboratory, which is supported at M.I.T. by the National Science Foundation.

[1]E. M. Martin, J. F. Farges, G. Jacob, J. P. Hallais, and G. Poiblaud, J. Appl. Phys. 51, 2840 (1980).
[2]D. E. Holmes, R. T. Chen, K. R. Elliott, C. G. Kirkpatrick, and Phil Won Yu, IEEE Trans. Electron Devices ED-29, 1045 (1982).
[3]G. M. Martin, in *Proceedings of the Semi-Insulating Materials Conference*, Nottingham, 1980, edited by G. J. Rees (Shiva, Nantwich, 1980), p. 13.
[4]H. M. Hobgood, A. Rohatagi, and R. N. Thomas, J. Appl. Phys. 53, 5771 (1982).
[5]M. Kaminska, J. M. Parsey, J. Lagowski, and H. C. Gatos, Appl. Phys. Lett. 41, 989 (1982).
[6]J. Lagowski, M. Kaminska, J. M. Parsey, Jr., H. C. Gatos, and M. Lichtensteiger, Appl. Phys. Lett. 41, 1078 (1982).
[7]J. Lagowski, H. C. Gatos, J. M. Parsey, K. Wada, M. Kaminska, and W. Walukiewicz, Appl. Phys. Lett. 40, 342 (1982).
[8]Y. Chou, Inst. Phys. Conf. Ser. 63, 185 (1981).
[9]J. Schneider, in *Semi-Insulating III-V Materials*, edited by S. Makram-Ebeid and B. Tuck (Shiva, Nantwich, 1982), p. 144.
[10]J. Lagowski, M. Kaminska, J. M. Parsey, H. C. Gatos, and W. Walukiewicz, 10th Conference on GaAs and RElated Compounds, 1982, Albuquerque, New Mexico.
[11]J. M. Parsey, Y. Nanishi, J. Lagowski, and H. C. Gatos, J. Electrochem. Soc. 129, 388 (1982).
[12]G. B. Bachelet, M. Schluuter, and J. A. Baraff, Phys. Rev. B 27, 2545 (1983).
[13]W. Walukiewicz, L. Pawlowicz, J. Lagowski, and H. C. Gatos, in *Semi-Insulating III-V Materials*, edited by S. Makram-Ebeid and B. Tuck (Shiva, Nantwich, 1982), p. 121.

The electrical behavior of GaAs-insulator interfaces: A discrete energy interface state model

T. E. Kazior,[a] J. Lagowski, and H. C. Gatos
Massachusetts Institute of Technology, Cambridge, Massachusetts 02139

(Received 5 November 1982; accepted for publication 24 January 1983)

The relationship between the electrical behavior of GaAs Metal Insulator Semiconductor (MIS) structures and the high density discrete energy interface states (0.7 and 0.9 eV below the conduction band) was investigated utilizing photo- and thermal emission from the interface states in conjunction with capacitance measurements. It was found that all essential features of the anomalous behavior of GaAs MIS structures, such as the frequency dispersion and the C–V hysteresis, can be explained on the basis of nonequilibrium charging and discharging of the high density discrete energy interface states.

PACS numbers: 73.40.Qv, 72.20.Jv

INTRODUCTION

The development of a GaAs Metal Insulator Semiconductor (MIS) technology has not thus far been realized because the *C–V* behavior of GaAs MIS structure is typically characterized by a large majority carrier hysteresis and a pronounced frequency dispersion. This anomalous behavior has been attributed to a high density of interface states with a continuous energy distribution throughout the energy gap.[1,2] However, no interface state distribution model has adequately or unambiguously explained this anomalous behavior.

A number of investigators have proposed a U-shaped continuous distribution of states with maxima near midgap and near the band edges [1–7]; most of these studies were performed using capacitance techniques, which present serious difficulties due to the anomalous capacitance behavior of the GaAs MIS structures. Deep Level Transient Spectroscopy (DLTS) measurements have led to inconsistent results such as the inconclusive identification of a state with an activation energy of 0.37 eV below the conduction band,[8] a continuous distribution of states with a peak of 0.43 eV below the conduction band,[9] and a discrete state with an activation energy of 0.38 eV assigned at midgap.[2] The latter state is part of the more complex Interface State Band (ISE) model in which the presence of interface state bands associated with the semiconductor bands are invoked in an attempt to explain the anomalous electrical behavior of the GaAs-insulator interfaces.[1,2,6,7] The above anomalous behavior has also been attributed to the existence of a compensated layer near the semiconductor surface which is the result of anodization-induced surface damage[10]; and also to an overcompensated surface layer which is caused by a high density of discrete interface states near midgap extending spacially into the semiconductor bulk.[11]

Investigations of "real" surfaces of GaAs by pulsed field effect techniques and surface photovoltage spectroscopy revealed the presence of two states with discrete energy positions at 0.7 and 0.9 eV below the conduction band[12–14]; their energy positions were found to be independent of orientation and surface preparation procedures. Surface states at these two energy positions were subsequently observed on GaAs surfaces with a submonolayer coverage of oxygen and of various metal adatoms[15]; it was proposed that these states must also be present in the GaAs-thick oxide interfaces.[16]

In an earlier study a high density (10^{12} cm^{-2}) of interface states with discrete energy of 0.65 eV below the conduction band ($E_c - E_t \sim 0.65$ eV) was identified at the GaAs-anodic oxide interface employing DLTS.[17] A similar high density discrete interface state was also found at GaAs–Si_3N_4 interfaces.[18] Employing a photoionization discharge current technique[19–21] the presence of the state was confirmed, and its density was determined to be about 5×10^{12} cm^{-2}; in addition a second state 0.9 eV below the conduction band was observed; furthermore, a gigantic photoionization process involving a highly effective indirect discharge of the deep states was discovered.[19] The interface state model which resulted from this latter study together with earlier proposed models are shown in Fig. 1.

In the present study a detailed analysis of the capacitance characteristics of GaAs-anodic oxide and GaAs–Si_3N_4 structures was carried out utilizing photo- and thermal-discharge of the high density discrete energy interface states to investigate the relationship between the characteristics of these states and the anomalous electrical behavior of GaAs MIS structures.

EXPERIMENT

High quality *n*-type Liquid Phase Epitaxy (LPE) and Vapor Phase Epitaxy (VPE) GaAs epitaxial layers were used in this study with electron concentrations ranging from 7×10^{14} to 8×10^{17} cm^{-3}. Epitaxial layers were chosen since melt-grown GaAs exhibits high densities of deep levels, often comparable to the free carrier concentration. DLTS analysis performed on metal semiconductor (MS) structures formed on adjacent samples from the same wafers showed that the concentration of bulk traps, when detectable, was $< 10^{-2}$ times that of the electron concentration. At worst, the bulk trap density corresponded to a density of trapped charge in the semiconductor space charge region 1.5 orders of magnitude less than that trapped at the interface. Thus, in this study, charge exchange with bulk traps played as insignificant role in comparison to that with interface traps.

[a] Present address: Raytheon Company, Lexington, Massachusetts 01773.

 0021-8979/83/052533-07$02.40

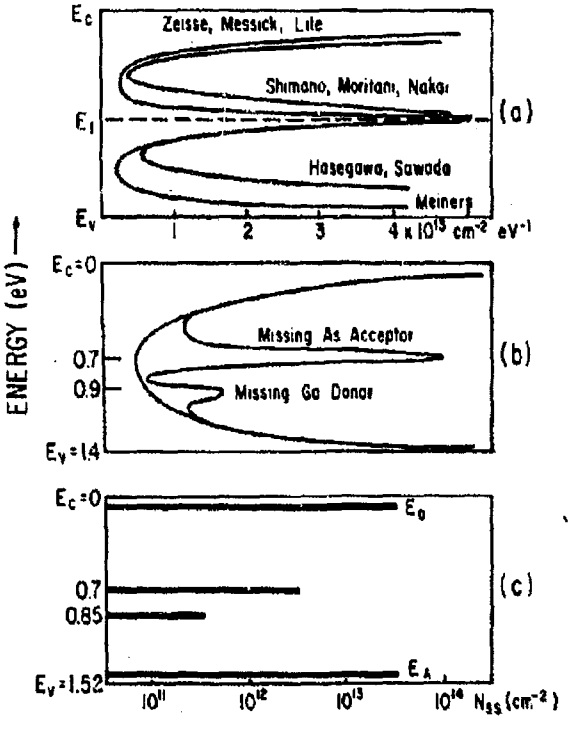

FIG. 1. GaAs interface state models: (a) U-shaped distributions obtained from capacitance based measurements (Refs. 1–4); (b) unified defect model (Ref. 16); (c) our model derived from photoionization discharge current analysis (Refs. 19–21).

For GaAs-anodic oxide structures, oxide layers were formed using the AGW process (Anodization in Glycol and Water)[22] in constant current mode ($j_a = 100\ \mu$ A cm^{-2}) until a predetermined thickness, typically 2000 Å, was formed. The anodization current was then allowed to decay to $<3\%$ j_a to complete the oxidation reaction. High resistivity oxides ($>10^{15}\ \Omega$ cm) were obtained from this procedure.

For GaAs–Si_3N_4 structures, the Si_3N_4 layers, typically 1000 Å, were deposited from a mixture of SiH_4, NH_4, and N_2 in a parallel plate R. F. plasma reactor (Plasma Enhanced Chemical Vapor Deposition). MIS structures were formed by evaporation of semitransparent Au layers on the insulator.

The MIS structures were mounted on a variable temperature cryostat (temperature range 10 to 500 K). *C–V* characteristics were recorded using a standard configuration (function generator-current preamplifier-lock-in amplifier). The variable parameters were probing frequency (2 Hz to 1 MHz), temperature, gate bias sweep rate and photon energy of sub-band-gap monochromatic illumination. The illumination was provided by a halogen lamp and a double prism monochromator.

RESULTS AND DISCUSSION

A. Fermi level pinning

Typical capacitance characteristics recorded as a function of probing frequency (5 Hz to 1 MHz) and temperature

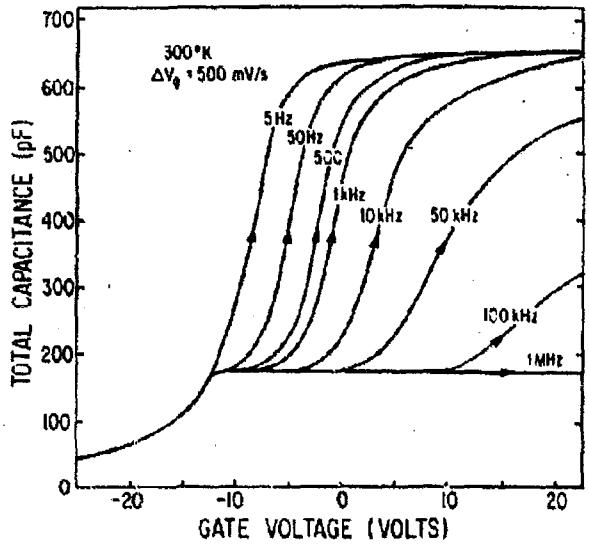

FIG. 2. Typical *C–V* characteristics of *n*-GaAs MIS structures obtained as a function of probing frequency.

(100 to 450 K) are presented in Figs. 2 and 3, respectively. As seen in these figures a "plateau" (an arrest in the capacitance increase with increasing voltage) appears in the *C–V* curves at values $C_p < C_i$ where C_i is the insulator capacitance; this "plateau" capacitance value, C_p, becomes the limit of both the high frequency and low temperature positive bias capacitance. As shown in Fig. 4, the ratio C_p/C_i increases with increasing electron concentration, for both the GaAs-oxide and GaAs–Si_3N_4 structures.

It has been postulated[23] that under equilibrium condi-

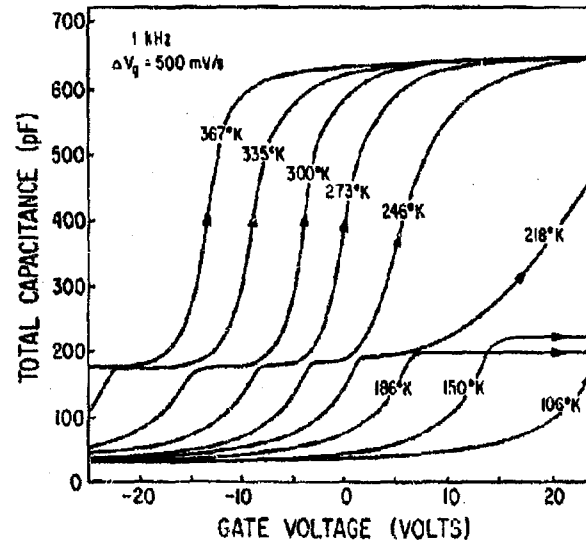

FIG. 3. Typical *C–V* characteristics of *n*-GaAs MIS structures obtained as a function of temperature, 100 to 400 K.

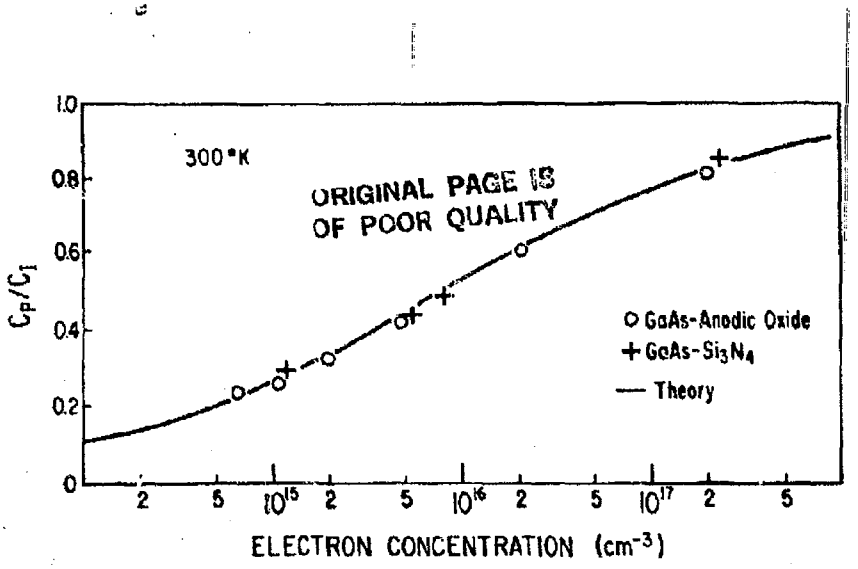

FIG. 4. Ratio of C_p/C_i vs electron concentrating; theoretical curve calculated from expression (2); experimental points were normalized to a constant value of $C_i = 3.25\times10^{-8}$ f cm^{-2}.

tions, a plateau can appear in the C–V characteristics of MIS structures due to the Fermi-level pinning by discrete traps at the interface. In the interfaces presently studied high density discrete traps were found to be present at $E_c - E_t \sim 0.7$ eV.

The relationship between the plateau and the discrete traps can be found by examining the capacitance relationships. For high probing frequencies the interface state capacitance becomes negligible and the total MIS capacitance, C_{TOT}, can be approximated as due to the depletion capacitance, C_D, and the insulator capacitance connected in series:

$$1/C_{TOT} = 1/C_D + 1/C_i, \tag{1}$$

where $C_D = (q\varepsilon_s/2V_s)^{1/2}\varepsilon_s$ is the semiconductor dielectric constant, and V_s is the surface potential.

When the Fermi (E_F) level is pinned by the discrete trap, E_t, the surface barrier becomes $q_s^V = E_t - E_F$. Thus, from Eq. (1) the plateau capacitance $C_p \simeq C_{TOT}$ is obtained as

$$C_p/C_i = C_i\left[\sqrt{2(E_t - E_F)/q^2n\varepsilon_s} + 1\right]^{-1}. \tag{2}$$

The Fermi energy in the bulk, E_F, (measured with respect to the conduction band edge) can be determined as a function of n from the relationship

$$n = 5.44\times10^{15}(m^*T/m_0)^{3/2}F_{1/2}(E_F/kT), \tag{3}$$

where $F_{1/2}$ is the Fermi–Dirac integral.

The dependence of C_p/C_i on the electron concentration calculated from Eqs. (2) and (3) is shown in Fig. 4 (solid line). It is seen that the agreement between the experimental data and the theoretical treatment is excellent, indicating that the Fermi level does become pinned by the $E_c - E_t = 0.7$ eV discrete states present in GaAs MIS structures. It is also of interest to note that the present model leads to a much better agreement with experimental data of Fig. 4 than the recent model of Ref. 11 based on a concept of interface traps extending spacially into the semiconductor bulk.

To further understand the effect of the interface states on the capacitance characteristics, we will consider the charge balance

$$Q_{bias} + Q_{sc} + Q_{ss} + Q_i = 0, \tag{4}$$

and the summation of the voltage throughout the structure:

$$V_{bias} = V_i + V_s + V_{ms}. \tag{5}$$

Here Q_{bias} and Q_i are the charges at the gate and in the insulator, respectively; $Q_{sc} = (2q\varepsilon nV_s)^{1/2}$ is the semiconductor space charge, $Q_{ss} = qn_t$ is the charge at interface states, n_t is the density of trapped carriers; V_{bias} and V_i are the bias and insulator voltages, and V_{ms} is the difference between the semiconductor and the metal work functions. Considering Gauss' law for a sheet of charge on an insulator we have

$$Q_{bias} = C_iV_i. \tag{6}$$

Combining Eqs. (4), (5), and (6), the following expression is obtained for the applied gate bias.

$$V_{bias} = qn_t/C_i - (2q\varepsilon_s nV_s)^{1/2}/C_i - Q_s/C_i + V_{ms}. \tag{7}$$

Charging of the initially empty interface traps begins when the Fermi level at the interface moves up to the vicinity of E_t (i.e., $qV_s \simeq E_t - E_F$). A corresponding value of the bias voltage $V_{bias} \equiv V_0$ defines the onset of the capacitance plateau in C–V characteristics.

$$V_0 = -\left[2\varepsilon_s n(E_t - E_F)\right]^{1/2}/C_i - Q_s/C_i + (E_t - E_F)/q + V_{ms}. \tag{8}$$

The voltage at which the traps become completely filled, $qn_t = qN_t$ (the Fermi level is still pinned), is

$$V_1 = qN_t/C_i + V_0. \tag{9}$$

A relation between the voltage increase $(V_1 - V_0)$ along the capacitance plateau and the density of interface traps, N_t, is obtained by combining Eqs. (8) and (9), assuming Q_s = constant:

$$N_t = C_i(V_1 - V_0)/q. \tag{10}$$

As seen in Fig. 2, the voltage increase along the plateau of the high frequency (1 MHz) curve is ~ 30 V. (V_0 is about -10 V, and $V_1 \sim 20$ V, is at the breakdown field of the insulator.) This voltage increase corresponds to a trap density, N_t, of about 6×10^{12} cm^{-2} (the insulator capacitance $C_i = 3.25\times10^{-8}$ f cm^{-2}) which agrees very well with the density, $N_t \simeq 5\times10^{12}$ cm^{-2}, of the trap, $E_c - 0.7$ eV reported in earlier studies.[19–21]

The above estimate and the results of Fig. 4 show that the capacitance plateau in C–V characteristics can be explained as due to the pinning of the Fermi level in the vicinity of the $E_c - 0.7$ eV interface trap. Along this plateau the semiconductor space charge region is in depletion even for large positive gate biases; the negative charge, induced in the semiconductor, accumulates in the interface traps rather than in the space charge region.

B. Capture of carriers

As pointed out above, the plateau capacitance C_p appears when the Fermi level at the surface approaches the empty interface traps. As shown in Fig. 5, C_p exhibits a lowest value at approximately room temperature, and it increases with decreasing temperature. Using $C(T)$ data from Fig. 5 and expression (2), one can calculate the surface barrier $V_s(T)$ corresponding to the capacitance plateau. Results are given in Fig. 6 for $T < 250$ K, V_s decreases linearly with decreasing temperature, whereas for $T > 250$ K it becomes independent of temperature.

The results in Fig. 6 indicate that the capture of carriers by the interface traps, and the associated Fermi-level pinning, is a temperature dependent process. This process can be explained by considering that an electron must overcome the surface barrier in order to be captured in an interface trap. The capture rate of electrons by the interface traps is described by the standard expression

$$d[\quad]/dt = [\quad]\exp(-qV_s/kt), \tag{11}$$

where σ is the cross section and v_T the thermal velocity. The level pinned by the discrete traps $qV_s = E_t - E_F$ ($E_c - E_F \simeq 0.1$ eV for $n = 5\times10^{15}$); the capture rate decreases with decreasing temperature as approximately $\exp(-0.6/kT)$ and it becomes negligible at low temperatures. In this case the interface traps and the conduction band can no longer be in dynamic equilibrium. The Fermi level is not pinned by these traps. In order to fill the traps the surface barrier must be lowered by increasing the gate bias to some new value. Accordingly, at the low temperature region, the onset of the capacitance plateau (which corresponds to the onset of electron capture by interface traps) will shift to more positive gate bias, i.e., to lower values of the surface barrier.

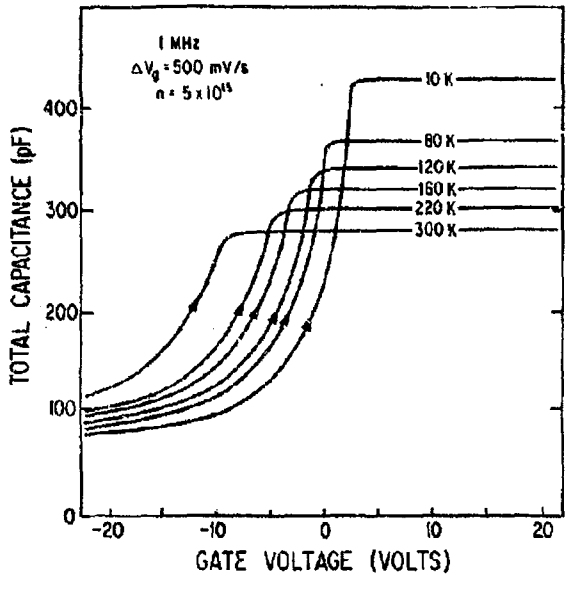

FIG. 5. C–V characteristics recorded as a function of temperature, 10 to 300 K.

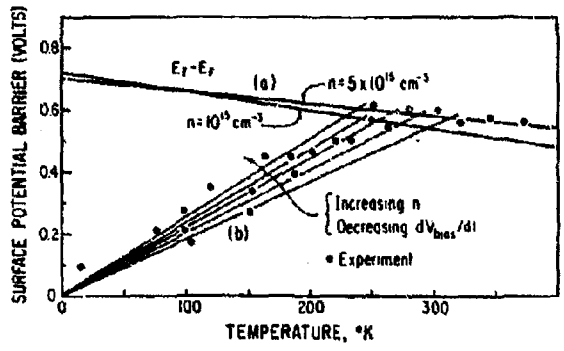

FIG. 6. Surface potential vs temperature: (a) predicted behavior based on temperature dependence of Fermi-level position; (b) O, observed behavior; solid line, approximately linear temperature dependence.

The value of V_s corresponding to the capacitance plateau can be obtained from the time derivative of Eq. (6)

$$dQ_{bias}/dt = C_i dV_i/dt. \tag{12}$$

Substituting Eqs. (4) and (5), and taking $d/dt = 0$, $dQ_t/dt = 0$, Eq. (12) becomes

$$(qdn_t/dt - dQ_{sc}/dt) = C_i(dV_{bias}/dt - dV_s/dt). \tag{13}$$

Along the plateau, $dV_s/dt = 0$ and $dQ_{sc}/dt = 0$; thus, Eq. (13) becomes

$$qdn_t/dt = q(N_t - n_t)e_n. \tag{14}$$

Substituting Eq. (11) into Eq. (14) and solving for V_s yields

$$V_s = -kT/q \ln\left[\frac{C_i dV_{bias}/dt}{\sigma_n v_T n(N_t - n_t)}\right]. \tag{15}$$

Thus, V_s varies linearly with temperature; the slope is weakly dependent on $\ln(dV_{bias}/dt)$ and $\ln(n)$, i.e., on the bias voltage sweep rate and on the carrier concentration. It should be noted that an order of magnitude change in either bias voltage sweep rate or carrier concentration [as determined from Eq. (3)] leads to only a 2% change in C_p, which is well within the experimental error of typical C–V measurements. As seen in Fig. 6, the experimental points $V_s(T)$ for T 200 K agree very well with values calculated from Eq. (15) (solid line).

This result confirms that the capture of carriers by the interface traps occurs through thermal activation over the surface barrier. For $T < 250$ K the interface traps and the conduction band are not in dynamic equilibrium and qV_s varies with temperature. For $T > 250$ K, the interface traps

and the conduction band remain in a dynamic equilibrium and the capacitance plateau corresponds to the pinning of the Fermi level (discussed above) and the surface barrier $qV_s \simeq E_i - E_F$ which varies only weakly with increasing temperature.

C. Frequency and temperature dependence of C–V behavior

It was shown in Figs. 2 and 3 that, for positive values of gate bias, C_{TOT} increases with increasing temperature and decreasing frequency. As seen in Fig. 7, C_{TOT} is also dependent on sub-band-gap illumination, because of the enhanced emission (photoionization) of carriers from the interface states. In fact, the increase in C_{TOT} is more pronounced under illumination $h\nu = E_g - 45$ meV, consistent with the finding that under such illumination the photoionization of the deep interface states is much more efficient than under $h\nu = 0.9$ eV.[19–21]

On the basis of the experimental results of Fig. 7 and the above discussion on the capacitance plateau we propose the frequency, temperature, and illumination dependence of the positive bias total capacitance can be explained in terms of the frequency, temperature, and illumination dependence of the interface trap capacitance, C_{ss}.

According to the treatment of Ref. 23, C_{TOT} can be expressed in terms of the probing frequency, and the time constant, τ, of the interface states, as follows

$$C_{TOT} = \frac{C_I}{C_I + C_D + C_{ss}} \left[C_D + C \frac{(C_I + C_D + C)^2 + \omega^2\tau^2 C_D(C_I + C_D)}{(C_I + C_D + C_{ss})^2 + \omega^2\tau^2(C_I + C_D)} \right], \quad (16)$$

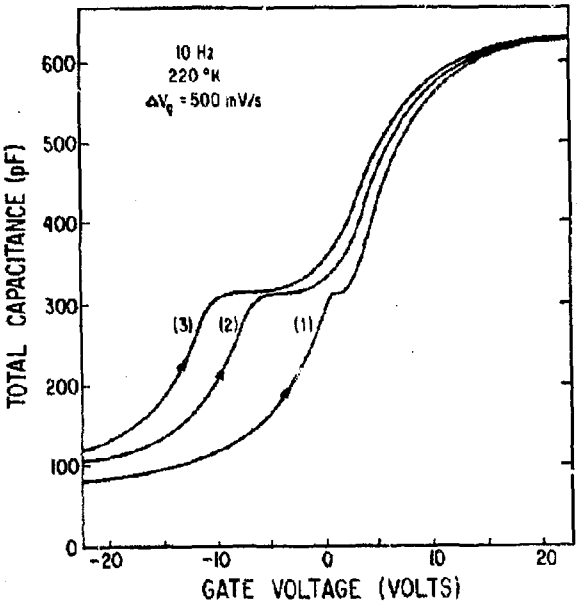

FIG. 7. C–V characteristics obtained under the influence of sub-band-gap monochromatic illumination: (1) in the dark; (2) $h\nu = 0.9$ eV and $I = 10^{15}$ photons/cm² s; (3) $h\nu = E - 45$ meV and $I = 10^{15}$ photons/cm² s.

where C_{ss} is the interface capacitance. An expression for τ can be derived from the expression for trap occupancy changes

$$\frac{1}{q}\frac{dQ_n}{dt} = \frac{dn_t}{dt} = \sigma_n v_T n \exp\left(-\frac{qV_s}{e_T kT}\right)(N_t - n_t) - (e_T + e_I)n_t. \quad (17)$$

The solution of Eq. (17) yields:

$$n_t(t) = N_T\tau r + N_T\tau(e_T + e_I)\exp(-t/\tau), \quad (18)$$

where $\tau = 1/(e_T + e_I + r)$; $e_T = \sigma_n v_T N_c \exp -(E_C - E_t)/kT$ is the thermal emission rate; $e_I = \sigma_I I$ is the photoemission rate; σ_I is the photoemission cross section; I is the photon intensity, and N_c the density of states in the conduction band.

Thus, τ is both temperature and illumination dependent.

Returning to Eq. (16), the term $\omega\tau$ is of major importance. For $\omega\tau \gg 1$, Eq. (16) reduces to Eq. (1). This limit is achieved for very high frequencies (in this case 1 MHz) and/or very low temperatures; in both cases $C_{TOT} \to C_{ledge}$. For $\omega\tau \ll 1$, $1/C_{TOT} = 1/(C_D + C_{ss}) + 1/C_I$. This limit is obtained at low frequencies (< 10 Hz) and/or high temperatures (in both cases $C_{TOT} \to C_I$). For $\omega\tau \sim 1$, intermediate frequency and/or temperature, the full expression of Eq. (16) is used, and C_{TOT}, for positive gate bias, satisfies inequality $C_I < C_{TOT} < C_p$, as observed in Figs. 2 and 3.

Thus, with increasing temperature (τ decreases as e_n increases) and/or decreasing frequency the value of C_{TOT} increases. Under illumination, e_I contributes to the decrease of τ and consequently C_{TOT} increases.

It must, thus, be concluded that the temperature and frequency dependence of the electrical behavior of GaAs MIS structures is due to the temperature and frequency dependence of the time constant, τ, i.e., of the rate of change of the charge trapped by the interface states. This dependence is observed in the positive bias capacitance characteristics where C_{TOT} varies with ω, τ and C_{ss} and not with C_D (V_s = constant).

D. Dependence of hysteresis on charging and discharging of interface states

As seen in Fig. 8, the capacitance behavior is characterized by a large hysteresis. This hysteresis is dependent on the bias voltage sweep rate, dV_{bias}/dt, (see Fig. 9) and it becomes especially pronounced at low temperatures (see Fig. 10) whereby a thermal release of electrons trapped at the interface is negligible. At 10 K the dark capacitance (Fig. 10, curve 1) is shifted by approximately 20 V with a reverse bias sweep. On the basis of Eq. (10) this shift corresponds to Δn_t of about 4×10^{12}/cm². Curve 2 (Fig. 10) represents the dark capacitance behavior following the reverse bias sweep of case 1; it is seen that the capacitance curve for the second forward bias sweep is shifted to large positive values of gate bias indicating that charge remained stored in the interface states. Subsequently, the MIS structure was illuminated with sub-band-gap light to remove the charge trapped on the interface

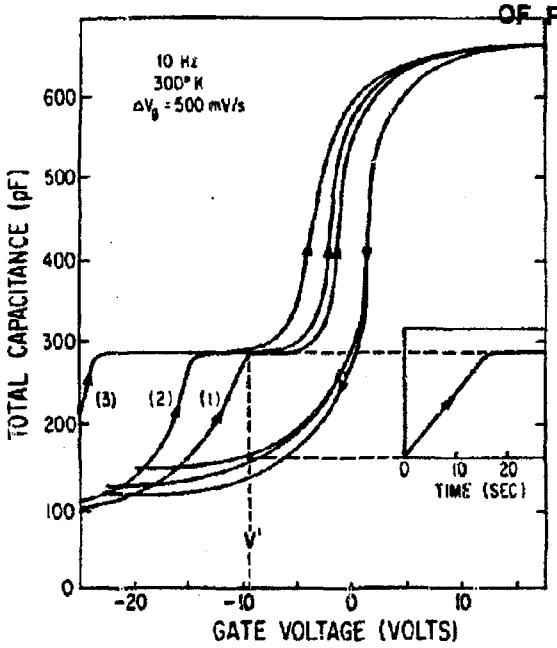

FIG. 8. *C–V* characteristics demonstrating hysteresis and time dependence of emission of carriers from interface states. Inset: restoration of dynamic equilibrium and reduction of hysteresis.

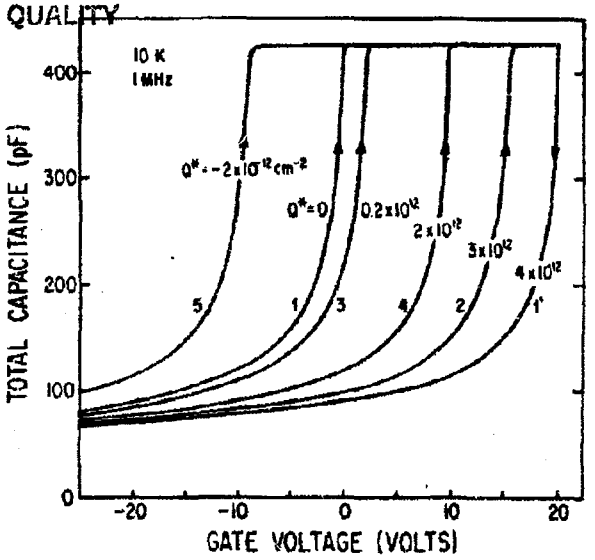

FIG. 10. Low temperature *C–V* characteristics demonstrating hysteresis: (1) dark characteristics; (2) repeat of dark characteristic; (3)–(5) repeat after partial photodischarge of interface states with $h\nu \approx 0.9$ eV. Q^* indicates estimated values of $qn_s - Q_f$.

states. As curve 3 shows, the capacitance returned close to its original behavior represented by curve 1. Depending on the amount of charge optically removed from the interface, the reduction of hysteresis can be controlled and the low temperature capacitance behavior can be shifted to any position along the voltage axis (curves 4 and 5).

At elevated temperatures hysteresis becomes less pronounced as thermal generation begins to play an increasing role in the discharge of the interface states.

The dependence of the hysteresis on the bias sweep rate (Fig. 9) indicated that the emission of trapped carriers from the interface is time dependent. This time dependence was further confirmed by the following experiment. The reverse bias sweep was arrested at a voltage V' (Fig. 8) and C_{TOT} was recorded versus time (insert Fig. 8). C_{TOT} increased with time until it reached the value of C_{TOT} of the forward bias sweep (in this case C_p). The rate of this discharge was found to be enhanced by sub-band gap illumination. Thus, it appears that for sufficiently long times (very slow sweep rates) the hysteresis becomes negligible.

The time dependent hysteresis indicates that the traps

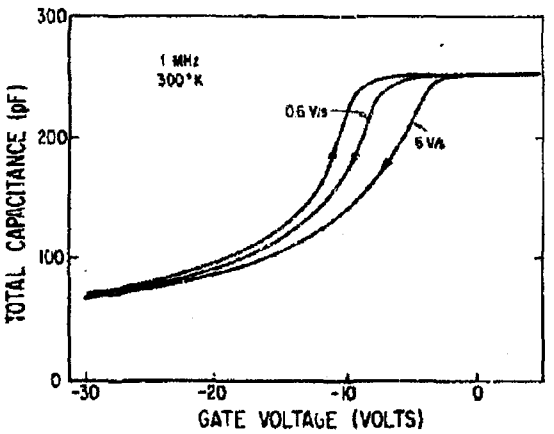

FIG. 9. *C–V* characteristics as a function of gate sweep rate.

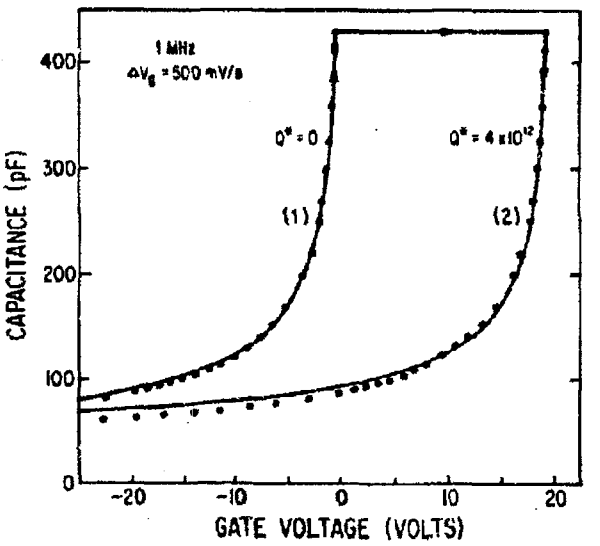

FIG. 11. *C–V* characteristics, $T = 10$ K; $Q^* = qn_s - Q_f$; O, theoretical points; solid line, experimental characteristics.

TABLE I. Role of interface states in electrical behavior of GaAs MIS structures.

Effect	Explanation	Comment
appearance of plateau in capacitance characteristics	pinning of Fermi level by high density interface state at $E_t - E_v = 0.7$ eV	surface potential variation restricted to depletion space-charge region, semiconductor never reaches accumulation
frequency/temperature dispersion	frequency/temperature dependence of time constant associated with charging and discharging of interface states	characteristics of MIS devices change with operation frequency and/or temperature
capture of free carriers at interface	thermal activation over surface barrier	for low temperature operation, surface potential varies with temperature
C–V hysteresis	slow release of carriers trapped by interface states	causes drift in MIS devices

are not in dynamic equilibrium with the conduction band; the surface potential V_s changes with gate bias and filled traps move above the Fermi level; their discharge is then only weakly dependent on gate bias but strongly dependent on time. In the high frequency limit, the total capacitance behaves as

$$1/C_{\rm TOT} = (2V_s/qn\epsilon_s)^{1/2} + 1/C_i, \tag{19}$$

where V_s is determined by Eq. (7) and where $n_s(t) = n_s \exp(-t/\tau)$.

Thus, the emission of charge from the interface states, in addition to its dependence on temperature, frequency, and illumination, is also strongly dependent on time.

E. Capacitance characteristics: theory versus experiment

Low temperature experimental capacitance characteristics will now be compared with theoretical results calculated from Eqs. (1) and (7). Low temperature was chosen to eliminate thermal emission of trapped carriers and to achieve the condition $\omega\tau \gg 1$ where $C_{\rm TOT} = C_p$ for positive bias. Solution of Eqs. (1) and (7) for $q_t^N = 0$ and $n = 5\times10^{15}/{\rm cm}^3$ yielded the results (points) indicated in curve 1 in Fig. 11. The capacitance behavior is simply ideal for deep depletion of the semiconductor space-charge region. The points along curve 2 were obtained assuming an increase of the interface charge n_s by $4\times10^{12}/{\rm cm}^2$. (In both cases the calculations were carried out for $q_t^V > 0.12$ eV, i.e., the value of C_p at this temperature). The agreement between the calculated points and the experimental curves is very good.

SUMMARY AND CONCLUSIONS

The influence of the high density interface states with discrete energy on the electrical behavior of GaAs MIS structures is summarized in Table I. At temperatures $T > 250$ K the high density of these states pins the Fermi level near midgap and restricts surface potential variations. At lower temperatures the capacitance plateau shifts to lower surface barrier values to allow electron capture by interface traps. The main features of the anomalous electrical behavior of the GaAs MIS structures, especially the frequency dispersion and the large hysteresis can be readily explained on the basis of the dependence of the time constant associated with the charging and discharging of discrete interface states at $E_c - 0.7$ eV on the probing frequency, on temperature, on illumination, and on time. The presently observed effects of the interface states on the C–V behavior of GaAs MIS can account for the conflicting results (obtained by capacitance-based techniques) reported in the literature on the distribution of the GaAs-insulator interface states.

ACKNOWLEDGMENTS

The authors are grateful to the National Aeronautics and Space Administration and to the National Science Foundation for financial support.

[1]T. Sawada and H. Hasegawa, Thin Solid Films 56, 183 (1979).
[2]H. Hasegawa and T. Sawada, J. Vac. Sci. Technol. 16, 1478 (1979).
[3]L. G. Meiners, J. Vac. Sci. Technol. 15, 1402 (1978).
[4]C. R. Zeisse, L. J. Messick, and D. L. Lile, J. Vac. Sci. Technol. 14, 957 (1977).
[5]G. Weiman, Thin Solid Films 56, 173 (1979).
[6]T. Sawada and H. Hasegawa, Phys. Status Solidi 54, 689 (1979).
[7]H. Hasegawa and T. Sawada, J. Vac. Sci. Technol. 21, 462 (1982).
[8]J. Stannard, J. Vac. Sci. Technol. 15, 1508 (1978).
[9]K. Yamasaki and T. Sugano, Appl. Phys. Lett. 35, 932 (1979).
[10]S. Varadarajan, M. A. Littlejohn, and J. R. Hauser, Thin Solid Films 56, 255 (1979); J. Electron. Mater. 9, 819 (1980).
[11]E. Kamieniecki and G. Cooperman, J. Vac. Sci. Technol. 19, 453 (1981).
[12]T. M. Valahas, J. S. Sochanski, and H. C. Gatos, Surf. Sci. 26, 41 (1971).
[13]J. Lagowski, I. Baltov, and H. C. Gatos, Surf. Sci. 40, 216 (1973).
[14]H. C. Gatos, J. Lagowski, and T. E. Kazior, presented at 1982 International Conference on Solid State Devices, Tokyo, 1982.
[15]W. E. Spicer, I. Lindau, P. Skeath, C. Y. Su, and P. Chye, Phys. Rev. Lett. 44, 420 (1980).
[16]W. E. Spicer, I. Lindau, P. Skeath, C. Y. Su, and P. Chye, J. Vac. Sci. Technol. 17, 1019 (1980).
[17]E. Kamieniecki, T. E. Kazior, J. Lagowski, and H. C. Gatos, J. Vac. Sci. Technol. 17, 1044 (1980).
[18]T. E. Kazior, Ph.D. Thesis, Massachusetts Institute of Technology, Cambridge, Massachusetts, 1982.
[19]J. Lagowski, T. E. Kazior, W. Walukiewicz, H. C. Gatos, and J. Siejka, J. Vac. Sci. Technol. 19, 714 (1981).
[20]J. Lagowski, W. Walukiewicz, T. E. Kazior, H. C. Gatos, and J. Siejka, Appl. Phys. Lett. 39, 242 (1981).
[21]P. K. Kashkarov, T. E. Kazior, J. Lagowski, and H. C. Gatos, J. Appl. Phys. 54, 963 (1983).
[22]H. Hasegawa and H. L. Hartnagel, J. Electrochem. Soc. 123, 713 (1976).
[23]J. G. Simmons and L. S. Wei, Solid-State Electron. 16, 43 (1973).

PHYSICAL REVIEW B VOLUME 29, NUMBER 8 15 APRIL 1984

Electron mobility limits in a two-dimensional electron gas: GaAs-GaAlAs heterostructures

W. Walukiewicz,* H. E. Ruda, J. Lagowski, and H. C. Gatos
Massachusetts Institute of Technology, Cambridge, Massachusetts 02139
(Received 26 January 1984)

A theoretical model was formulated for electron scattering in a two-dimensional electron gas confined in a triangular potential well. For the first time, the effects of intersubband scattering were included. An inherent mobility limit is imposed by phonon, alloy, and remote impurity scattering. Intersubband scattering was found to play a significant role in determining this mobility limit. The model accounted very satisfactorily for the reported electron mobility characteristics in GaAs-GaAlAs heterostructures.

The two-dimensional electron gas confined at a GaAlAs-GaAs interface has received a great deal of attention[1–8] because its unique transport characteristics play a key role in a new generation of ultra-high-speed semiconductor devices. Thus, in "selectively doped" GaAlAs-GaAs heterostructures, electrons confined at the GaAs side of the interface and separated from their parent donors, which are in GaAlAs, have exhibited mobilities as high as 2×10^6 cm^2/Vs;[7] this value is about one order of magnitude greater than that achieved in the highest-purity bulk GaAs.[8]

Two-dimensional electron transport in a triangular potential well was originally formulated for silicon inversion layers.[9] In subsequent publications[10–12] different scattering mechanisms which contribute to the electron mobility in GaAs-GaAlAs heterostructures have been discussed. In this Rapid Communication we report on the first calculation of the mobility limits for the two-dimensional electron gas using a triangular well approximation, and considering the first-excited subband. All major scattering processes were included.

We will consider a GaAlAs-GaAs heterostructure with a triangular potential well on the GaAs side as shown schematically in the insert of Fig. 1. Electrons are supplied to the well from the "selectively doped" GaAlAs; an undoped GaAlAs "spacer" region separates GaAs from the *n*-type doped GaAlAs region. The momentum of electrons in the potential well is quantized in the z direction (perpendicular to the interface) resulting in the splitting of the three-dimensional conduction band into a series of two-dimensional subbands. In our treatment of electron transport parallel to the interface we take into account two energy subbands: the ground subband and the first excited one. The corresponding electron wave functions are described using variational solutions whereby wave-function parameters are related to the electron field within the triangular well.[10] The electric field, in turn, is related to the concentration of ionized remote impurities in GaAlAs, N_I, to the spacer thickness d, and to the concentration of ionized acceptors in the lightly *p*-type GaAs bulk region. Relationships between the pertinent parameters are established using standard electrostatic consideration.[9,11]

The excited subband becomes of importance when the Fermi energy equals the energy separating the ground and the excited subband. In this case, in addition to states in the ground subband, the states within the excited subband become available for electron scattering leading to an abrupt increase in the scattering rates. The electron concentration at which such intersubband scattering occurs is determined by the electric field in the well.

For the considered gas density $0.1–1\times10^{12}$ cm^{-2} the occupation of the excited subband is limited only to the states at the very bottom of the subband. These states correspond to very small wave vectors. Thus, the momentum transfer for intersubband scattering can be taken, to a good approximation, as equal to the wave vector of electrons in the ground subband. Deformation-potential and piezoelectric acoustic phonon scattering rates were calculated, assuming that the two-dimensional electron states are coupled through a spherically symmetric scattering potential. Intersubband

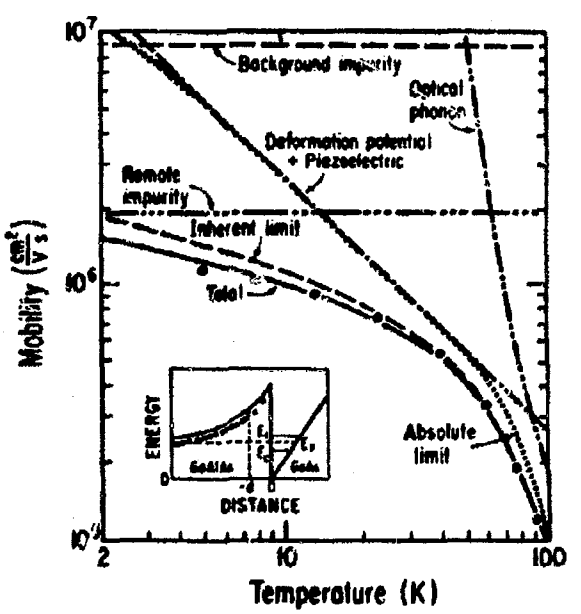

FIG. 1. Temperature dependence of the electron mobility in GaAlAs-GaAs heterostructures, with 200-Å-wide undoped spacer. Points are experimental data from Ref. 7 for an interface carrier density of 3×10^{11} cm^{-2}. The curves are calculated mobilities at this carrier density, with a remote ionized impurity concentration of 8.6×10^{16} cm^{-3}. In the insert the energetic structure of a modulation-doped heterostructure is given schematically. E_0 and E_1 refer to the ground and first-excited subbands, respectively; E_F is the Fermi energy and d the spacer width.

scattering for both scattering mechanisms results in a mobility drop of about 30%, compared with just intrasubband scattering.

Alloy disorder scattering arises from electrons which have penetrated into the GaAlAs. Since the penetration strongly depends on the electron energy, the resulting electron mobility decreases rapidly with increasing electron gas density. The intersubband scattering effect becomes very pronounced in this case owing to a strong overlap of the parts of ground and excited subband wave functions describing the penetration into the barrier. The scattering rates for remote and background-screened ionized scatterings were calculated by modifying the approach, originally developed for silicon inversion layers.[9] Intersubband contributions to background and remote ionized impurity scattering were found to be important; however, in the case of remote ionized impurity scattering, its contribution is diminished with increasing spacer width d. At low electron densities the parameter defining screening of ionized impurity scattering depend on temperature, resulting in a temperature increase of the ionized impurity contribution to the mobilities.[13] This effect becomes significant at temperatures exceeding about 40 K. Since at these temperatures the mobility is phonon limited, the weak temperature dependence of ionized impurity scattering does not affect the temperature dependence of the total mobility.

In our approach the remote impurity concentration is determined by the equilibrium condition for the Fermi energy.[11] Therefore, the only fitting parameters in our calculations are the background-ionized impurity concentration and the remote ionized impurity concentration in the spacer. In practice, the aim is to minimize residual impurity concentration in both the spacer and in the well. In the following mobility calculation we will neglect the spacer contribution, since at similar residual impurity levels the scattering efficiency by background impurity in the well is far greater than by those located in the spacer.[12] Polar optical phonon scattering in a three-dimensional approximation, appropriate for bulk GaAs (Ref. 14) was included at higher temperatures. We did not include interface roughness scattering[11] since extremely flat interfaces are fabricated by molecular-beam epitaxy (MBE); in these structures alloy disorder scattering (inherently present and included in our calculation) can be more important than scattering by surface roughness.

Electron mobilities were calculated assuming that the electron gas remains degenerate over the considered range of temperatures and electron densities. Therefore, the total relaxation time was obtained from the sum of the individual scattering rates. Parameters used in calculations were taken from Refs. 15 and 16.

The contribution of the various scattering processes to the temperature dependence of the electron mobility in the range 2–100 K is shown in Fig. 1. It is seen that with decreasing temperature the predominant scattering mechanism shifts from polar optical phonons (dominant for $T > 90$ K) to acoustic phonons (for the range of $80 \gtrsim T > 15$ K) and finally to ionized impurity scattering, which determines the mobility near 0 K.

The temperature dependence of the total electron mobility, resulting from the contributions of all scattering mechanisms, is shown as a solid line in Fig. 1. Experimental mobility data are also shown (solid circles) from measurements on state-of-the-art, very-high-purity GaAs-GaAlAs structures. It is seen that the agreement between theory and experiment is very good. If the contribution from background impurity scattering is deducted from total electron mobility, then we obtain a mobility limit which we refer to as "inherent." As seen in Fig. 1, at low temperatures the total mobility values are somewhat lower than the inherent mobility values, as are the experimentally obtained values. This difference is, of course, readily accounted for by the presence of impurities in GaAs at a level of about 8×10^{13} cm^{-3}. An absolute mobility limit can be arrived at by deducting from the total electron mobility the scattering contributions from background and remote impurities (Fig. 1). This absolute limit, however, is not realizable since the presence of remote impurities is necessary as they provide the electrons to the two-dimensional gas in GaAs; thus, the "inherent" mobility must be considered as a realistic limit.

At constant temperature the electron mobility in a two-dimensional gas depends on the gas density. This dependence results primarily from the energy dependence of the scattering rates. However, as seen in Fig. 2, in the case of alloy disorder scattering a strong additional electron density dependence derives from the increased penetration of the electron gas into the GaAlAs layer, with increasing electron density. As has been discussed previously, a pronounced

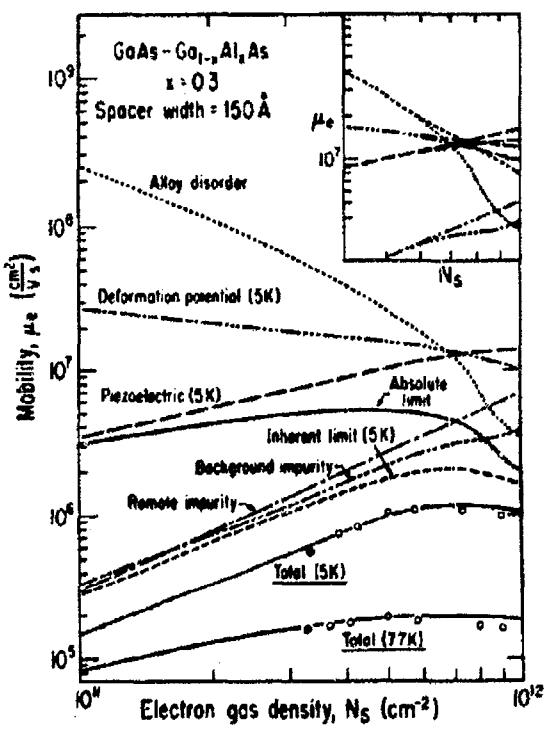

FIG. 2. Electron mobility at 5 and 77 K vs interface carrier density. Solid and open circles correspond to the experimental data of Ref. 7 measured in the dark, and under illumination, respectively. Theoretical mobilities were calculated using remote and background-ionized impurity concentrations of 8.8×10^{16} and 1×10^{15} cm^{-3}, respectively. The insert shows the effect of intersubband scattering. The upper curves correspond to the intrasubband mobility, while the lower curves include the effect of intersubband scattering with broadening parameter $\Gamma = 0.5$ meV.

drop in electron mobility occurs at about 7×10^{11} cm^{-2}, resulting from the onset of the intersubband scattering. The contributions of the intersubband scattering to individual scattering processes are shown in the insert of Fig. 2. The total electron mobility, obtained from the sum of all contributions to electron scattering, is shown for 5 and 77 K in Fig. 2, together with experimental results of Ref. 7 which were obtained using persistent photoconductivity to vary the electron density;[17] it is seen that the agreement is very good, assuming a background impurity concentration of 1×10^{15} cm^{-3}. It should be noted that the experimental mobilities, as a function of electron concentration, exhibit a maximum at about $N_s\approx7\times10^{11}$ cm^{-2} consistent with our theoretical finding (Fig. 2). The inherent mobility limit (i.e., assuming no background impurity scattering) at 5 K is also shown in Fig. 2. It is seen that the upper limit is approximately 2×10^6 cm^2/Vs for $N_s\approx7\times10^{11}$ cm^{-2}. Although it is of no practical significance, we also show in Fig. 2 the absolute mobility limit, i.e., assuming neither background nor remote mobility scattering.

A very important characteristic of the GaAlAs-GaAs structure is the undoped GaAlAs spacer width; by increasing the spacer width, the efficiency of remote impurity scattering is decreased and concurrently the density of electrons transferred to the well is decreased. Therefore, there must be an optimum spacer width, at which point the conductivity (the product of mobility and electron density) reaches a maximum.

The dependence of the electron mobility on spacer width at 5 K is shown in Fig. 3. It is seen that the total mobility reaches a maximum; the spacer width at which this maximum occurs decreases with increasing background impurity concentration. Actually, the inherent mobility limit (no background impurity scattering) increases with spacer width and tends towards a phonon-limited value at large spacer width, which is also in agreement with experimental trends, as reported in Ref. 7.

In conclusion, we proposed a model for the electron mobility in two-dimensional electron gas which took into consideration intersubband scattering. Mobility limits were thus determined as functions of temperature, electron density, and spacer width in GaAlAs-GaAs heterostructures. These calculations provided a good description of recently reported high electron mobility characteristics in such heterostructures.

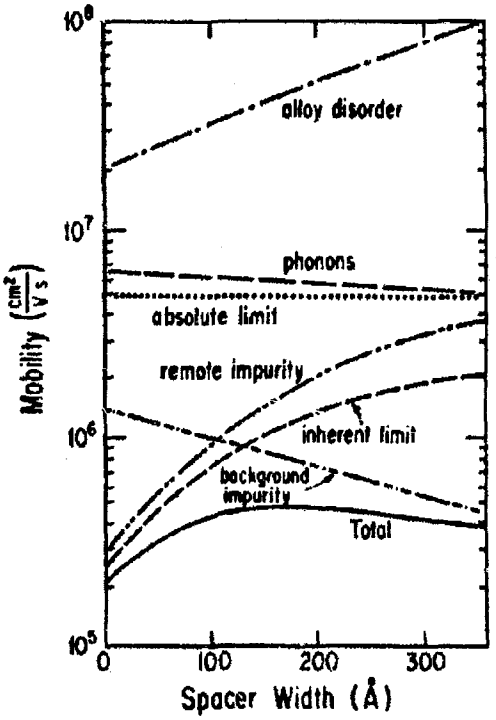

FIG. 3. Electon mobility values at maximum conductivity ($eN_s\mu_e$) vs spacer width for $Ga_{0.7}Al_{0.3}As$-GaAs heterostructure at 5 K. The "total" curve corresponds to a background impurity concentration of 1×10^{15} cm^{-3}.

The authors gratefully acknowledge Dr. Hiyamizu for furnishing experimental data prior to publication. The authors are also grateful to the National Aeronautics and Space Administration for financial support.

*Permanent address: Institute of Physics, Polish Academy of Sciences, aleja Lotnikow 32/46, 02-668 Warsaw, Poland.

[1]R. Dingle, H. L. Störmer, A. C. Gossard, and W. Wiegmann, Appl. Phys. Lett. 33, 665 (1978).
[2]Z. Schlesinger, J. C. M. Hwang, and S. J. Allen, Phys. Rev. Lett. 50, 2098 (1983).
[3]H. L. Störmer, Z. Schlesinger, A. Chang, D. C. Tsui, A. C. Gossard, and W. Wiegmann, Phys. Rev. Lett. 51, 126 (1983).
[4]S. Hiyamizu, R. Mimura, T. Fujii, H. Nanbu, and H. Hashimoto, Jpn. J. Appl. Phys. 20, L245 (1981).
[5]T. J. Drummond, H. Morkoc, and A. Y. Cho, J. Appl. Phys. 52, 1380 (1981).
[6]J. V. DiLorenzo, R. Dingle, M. Feuer, A. C. Gossard, R. Handel, J. C. M. Hwang, A. Kastalski, V. G. Keramides, R. A. Kelhl, and P. O'Connor, IEDM Tech. Dig. 25, 578 (1982).
[7]S. Hiyamizu, J. Saito, K. Nanbu, and T. Ishikawa, Jpn. J. Appl Phys. 22, L609 (1983).
[8]C. M. Wolfe, G. E. Stillman, and W. T. Lindley, J. Appl. Phys. 41, 3088 (1970).
[9]F. Stern and W. Howard, Phys. Rev. 163, 816 (1967).
[10]P. J. Price, Surf. Sci. 113, 199 (1982).
[11]T. Ando, J. Phys. Soc. Jpn. 51, 3900 (1982).
[12]F. Stern, Appl. Phys. Lett. 43, 974 (1983).
[13]F. Stern, Phys. Rev. Lett. 44, 1469 (1980).
[14]W. Walukiewicz, J. Lagowski, L. Jastrzebski, M. Lichtensteiger, and H. C. Gatos, J. Appl. Phys. 50, 889 (1979).
[15]D. L. Rode, in *Semiconductors and Semimetals*, edited by R. K. Willardson and A. C. Beer (Academic, New York, 1975), Vol. 10.
[16]J. S. Blakemore, J. Appl. Phys. 53, R123 (1982).
[17]H. L. Störmer, A. C. Gossard, W. Wiegmann, and K. Baldwin, Appl. Phys. Lett. 39, 912 (1981).

ON THE DISLOCATION DENSITY IN MELT-GROWN GaAs

J. Lagowski, H. C. Gatos, T. Aoyama[a] and D. G. Lin
Massachusetts Institute of Technology
Cambridge, Massachusetts 02139

ABSTRACT

We have discovered a striking relationship between the dislocation density and the Fermi energy in melt-grown GaAs. Thus, a shift of the Fermi energy from 0.1 eV above to 0.2 eV below its high temperature (1100 K) intrinsic value increases the dislocation density by as much as 5 orders of magnitude. The Fermi energy shift was brought about by n- and p-type doping at a level of about $10^{17}cm^{-3}$ i.e. one to two orders of magnitude below that commonly employed for impurity hardening. The pronounced role of the Fermi energy in dislocation densitites must be associated with the dependence of the point defect interactions on the charge state of these defects, i.e. on the occupancy of the associated electronic levels. It appears most likely that these interactions and thus the dislocation density are controlled in a critical manner by the concentration of gallium vacancies. Similar post-solidification defect interactions were recently proposed in order to explain the formation of the antisite defect As_{Ga} and the associated midgap level EL2. Our findings permit the identification of regimes of thermal stress, stoichiometry, Fermi energy and impurity hardening which are of fundamental importance in the formation of dislocation in the melt-grown GaAs.

[a] On leave from Hitachi Research Laboratories, Ibaraki, Japan.

Presented at the Third Conference on Semi-Insulating III-V Materials, Warm Springs, Oregon, April, 1984.

INTRODUCTION

A reduction of the dislocation density in melt-grown single crystals is perhaps the most important materials problem in GaAs IC's technology. Dislocation free GaAs is commercially available but only heavily doped with a donor concentration ranging from 10^{18} to 10^{19} cm^{-3}. Semi-insulating material, currently used for IC's has been recently obtained dislocation-free by utilizing doping with isoelectronic impurities (group III and V elements) at a level of 10^{19} to 10^{20} cm^{-3}.(1)

It has been a common trend to treat dislocations in melt-grown crystals, and particularly in crystals grown by the Czochralski liquid encapsulated (LEC) technique, within a framework of critical stress models.(2,3) Such models assume that dislocations are generated in the solidified material when thermal stress exceeds certain critical values, which is supposed to be a well-defined characteristic of the material.

Impurity effects on dislocation density(1,4) have been attributed to various mechanisms of blocking the propagation of dislocations (e.g. strong localized bounding;(5) differences in tetrahedral radii between the impurity and the host atoms;(6) and impurity-defect blocking complexes.(7) They are phenomenologically treated as impurity hardening effects which increase the value of the critical stress. Such treatment is an extention of that developed for elemental semiconductors (Ge and Si) and it does not take into account the unique stoichiometry aspects of GaAs related to a finite existance region. It is of interest to note that the effects of stoichiometry on the dislocation density in GaAs were originally reported in the mid 60's.(8) The systematic demonstration of the critical role of

stoichiometry in the generation of dislocation has been provided in our recent study on GaAs grown under minimized thermal stress by the horizontal Bridgman method in which stoichiometry is controlled (and varied) by controlling (varying) the arsenic source temperature, T_{As}. We have found that the dislocation density exhibits a sharp and very pronounced minimum at an optimum arsenic temperature T_{As} = 617 ± 1°C.[9] We have further found that growth under "off stoichiometry" conditions leads to high dislocation densities which exceed those found in crystals grown under pronounced thermal stress.[9,10] It has been suggested that stoichiometry also plays an important role (in the form of stoichiometry dependent critical stress) in dislocation formation during LEC growth of GaAs.[11]

In the present communication we present experimental results which shed a new light on the role of defects in the dislocation formation in GaAs grown under low thermal stress; we show that in moderately doped crystals the dislocation density is controlled by the Fermi energy.

EXPERIMENTAL

Single crystals of GaAs with a cross-sectional area up to $2cm^2$ were grown using a horizontal Bridgman apparatus especially designed for the precise control of growth parameters.[9] The growth was carried out in a high purity fused quartz boat (specially treated to prevent the melt from wetting the boat) or in a pyrolytic boron nitride boat.

A series of experiments were carried out to investigate the effects of stoichiometry on the properties of GaAs. In these experiments the arsenic source T_{As}, temperature was decreased (increased) from 623°C to 610°C (from 610°C to 623°C) in discrete steps of 1°C to 2°C at 1 to 2 hour

intervals corresponding to 1 to 2 cm of growth. The corresponding melt composition ranged from approximately 0.49 (610°C) to 0.51 (623°C) atom-fraction of arsenic.

Undoped, Si-doped and Zn-doped growth melts were employed in these experiments. The crystals with free carrier concentrations (both holes and electrons) below $5 \times 10^{16} cm^{-3}$ were grown with addition of Ga_2O_3 to the melt in order to reduce the silicon contamination. The carrier concentration was determined from Hall effect and conductivity measurements. Dislocations were revealed using molten KOH etching.

RESULTS AND DISCUSSION

Effect of Stoichiometry

Our previous investigation of lightly doped n-type crystals has shown a striking correlation between deviations from stoichiometry and dislocation density. We have established an optimum arsenic source temperature, 617 ± 1°C, which leads to a minimum dislocation density.[9,10] The present growth experiments confirm these results and further show that the same behavior is also characteristic in ligthly doped p-type GaAs crystals.

In Fig. 1 we show the dependence of the dislocation density on the arsenic temperature T_{As} for p-type and n-type GaAs crystals with a free carrier concentration of about $10^{16} cm^{-3}$. A minimum dislocation density of about $10^{3} cm^{-2}$ is obtained at an optimum temperature 617 ± 1°C. Deviation from this temperature leads to an increase of the dislocatin density by as much as two orders of magnitude i.e. to dislocation densities which are comparable to (or even higher than) those found in GaAs crystals grown under large thermal stresses.[1-3]

In Fig. 2 we show Nomarski contrast photomicrographs of etched surfaces of three segments of a p-type crystal. These photomicrographs show sharp changes in the dislocation density during growth in response to stoichiometry changes. Dislocations rapidly vanish in the crystal as T_{As} becomes closer to the optimum value. On the other hand dislocations are generated as T_{As} is shifted away from an optimum value. Exactly the same behavior has been observed previously in lightly doped n-type GaAs. These findings indicate that non-stoichiometry induced dislocations do not readily propagate with progressing crystal growth; accordingly they must be in a form of dislocation loops rather than edge dislocations.

Effects of Doping

We have reported previously that, in crystals grown under carefully minimized thermal stress, n-type doping constitutes a very effective means for the virtual elimination of non-stoichiometry induced dislocations.[10] This dramatic effect of doping is observed for a donor concentration of about $10^{17}cm^{-3}$ i.e. significantly smaller than those involved in impurity hardening phenomena believed to block the propagation of stress induced dislocation.[1,4-7] This relatively low level of doping is quite sufficient to convert crystals with high dislocation densities, N_0, grown under arsenic deficient conditions ($T_{As} \approx 613°C$, $N_D \sim 10^5-10^6cm^{-3}$) to dislocation free material ($N_D < 100cm^{-2}$). The same is also true for crystals grown under arsenic rich conditions.

The effect of p-type doping is very different from that of n-type doping. The differences are evidenced by the Nomanski contrast photomicrographs of Fig. 3. It is seen that for crystals grown under optimum

stoichiometry increase in the acceptor concentrators increases the dislocation density in contrast to the effect resulting from an increase of the donor concentration. It is also seen in Fig. 3 that GaAs with a hole concentration of about 5×10^{17} exhibits a high dislocation density (5×10^{4} to $5 \times 10^{5} cm^{-2}$) which could not be minimized to any significant extent by the optimization of the arsenic source temperature. The effects of the conductivity type and carrier concentration on the dislocation density in GaAs grown under optimum T_{As} are quantitatively summariz in Fig. 4. It is seen that the transition form n-type to p-type material enhances the dislocation density by as much as five orders of magnitude.

The Role of Fermi Energy

The key to understanding the formation of dislocation in GaAs grown under low thermal stress lies in the finite existence region of GaAs. Accordingly the type and concentration of point defects (especially of vacancies and their complexes) in a solidifying crystal is controlled by the melt composition (i.e. the arsenic source temperature). During the post-solidification cooling defects in the crystal become supersaturated and interact forming other defects such as defect complexes and dislocations.

We have suggested, in conjunction with the antisite defect model of EL2, that the relevant defect interactions are controlled by the migration of gallium vacancies.[12] The same model of gallium vacancy migration can explain the effects of the conductivity type and of the carrier concentration on the dislocation density in GaAs. The formation of dislocations in GaAs upon condensation of vacancies requires the participation

of defects from both the Ga and As sublattices. However, the process can be initiated by only one type of defect, such as V_{Ga}, since the corresponding defect, V_{As}, can be created upon migration of V_{Ga}. The point defects in GaAs lead to localized electronic levels. The occupancy of the levels, i.e., the charge state of defects is controlled by the Fermi energy. The charge state of defects determines their concentration, migration and ability to coalesce.

Transition from p- to n-type GaAs caused by intentional doping shifts the Fermi energy upwards in the energy gap increasing the concentration of negatively charged acceptor-type defects and decreasing the concentration of ionized deep donor levels. According to ref. 12 critical post-solidification defect interactions take place at a temperature of about 1100 K. Thus, in Fig. 4 we have indicated the Fermi energy values of 1100 K corresponding to the carrier concentration at 300 K.[13] The correlation between the Fermi energy and dislocation density is evident. The plateau of dislocation density coincides with a constant Fermi energy. On the n-type region the dislocation density decreases when the added donor concentration becomes comparable to (or higher than) the intrinsic carrier concentration at 1100 K; n_i(1100 K); while on the p-type region the dislocation density increases when the acceptor concentration becomes comparable to n_i(1100 K). This relationship is consistent with the critical role of a gallium vacancy which in GaAs leads to an acceptor level close to the middle of the energy gap. The downward shift of Fermi energy caused by n- to p-type transistion increases the fraction of neutral gallium vacancies which promote condensation and migration of vacancies required for

the formation of dislocations.

It is of interest to note that the importance of gallium vacancy has previously been suggested in accounting for the stoichiometry effects[8] and also in conjunction with donor impurity hardening in dislocation blocking by complexes of donor atom-gallium vacancy.[7] The role of Fermi energy has been discussed in the dislocation model as a factor altering the propagation of dislocation and thus also affecting the low temperature value of the critical stress.[4] To our knowledge the correlation between Fermi energy and dislocation formation in GaAs reported here is established for the first time.

Different Regimes of Impurity Effects on Dislocations

The present finding together with literature data made it possible to define regimes of fundamental importance in the formation of dislocations in melt-grown GaAs. Two mechanisms of dislocation formation should be distinguished: (1) stress-induced glide dislocations which are generated by an excessive thermal stress; and (2) nonstoichiometry-induced dislocations which are generated upon condensation of excessive vacancies into dislocation loops. As shown in Fig. 5, dislocation densities corresponding to both of these mechanisms overlap over a wide range of the dopant concentration. In strictly undoped material (without electrically active or isoelectronic impurities) the lowest dislocation density is controlled by the stoichiometry. The Fermi energy effects on the nonstoichiometry induced dislocations are significant for dopant concentrations exceeding about $8 \times 10^{16} cm^{-3}$. Donor-type impurity at concentration $2 \times 10^{17} cm^{-3}$ is sufficient to eliminate completely nonstoichiometry dislocations while

acceptor impurity increases the dislocation density.

The thermal stress-induced dislocations are generated at a temperature which is much closer to the melting point than 1100 K corresponding to nonstoichiometry dislocations. Thus, the effects of Fermi energy on propagation and multiplication of stress-induced dislocations would require high concentration of electrically active dopant, exceeding $10^{18}cm^{-3}$. As shown in Fig. 5, this concentration range overlaps with that considered in other "impurity hardening" phenomena. GaAs free of stress-induced dislocations is typically grown with electrically active dopant of concentration well above $10^{18}cm^{-3}$ or with even higher concentration of isoelectronic dopants. The effectiveness of impurity hardening in GaAs is a function of stoichiometry.

ACKNOWLEDGEMENT

The authors are grateful to the National Aeronautics and Space Administration and the Airforce Office of Scientific Reaearch for financial support.

REFERENCES

1. G. Jacob, Semi-Insulating III-V Materials, edited by S. Makram Ebeid and B. Tuck (Shiva, London, 1982) p. 2.
2. A. S. Jordan, R. Caruso and A. R. Von Neida, The Bell System Technical Journal, 59, 593 (1980).
3. M. G. Mil'Vidskii and E. P. Bochkarev, J. Crystal Growth 44, 61 (1978).
4. M. G. Mil'Vidsky, V. B. Osvensky and S. S. Shifrin, J. Crystal Growth 52, 396 (1981).
5. Y. Seki, H. Watanabe and J. Matsui, J. Appl. Phys. 49, 822 (1978).
6. P. A. Kirkby, IEEE J. Quantum Electron. QE-11, 562 (1975).
7. V. Swaminathan and S. M. Copley, J. Appl. Phys. 47, 4405 (1967).
8. J. C. Brice and G. D. King, Nature 209, 1346 (1966); J. Brice, J. Crystal Growth 7, 9 (1970).
9. J. M. Parsey, Jr., Y. Kanishi, J. Lagowski and H. C. Gatos, J. Electrochem. Soc. 128, 936 (1981); 129, 388 (1982).
10. J. M. Parsey, Jr., J. Lagowski and H. C. Gatos, J. Electrochem. Soc. (1984) in press.
11. M. Duseaux and G. Jacob, Appl. Phys. Lett. 40, 789 (1982).
12. J. Lagowski, H. C. Gatos, J. M. Parsey, K. Wada, M. Kaminska, and W. Walukiewicz, Appl. Phys. Lett. 40, 342 (1982).
13. Fermi energy values were calculated using GaAs parameters compiled by J. S. Blakemore, J. Appl. Phys. 53, R123 (1982).

FIGURE CAPTIONS

Fig. 1. Dislocation density vs. arsenic source temperature (stoichiometry) for lightly doped n- and p-type GaAs.

Fig. 2. Photomicrographs of etched crystal surfaces from different segments of a GaAs crystal.

Fig. 3. Photomicrographs of etched surfaces of GaAs crystals grown under different arsenic source temperatures and under different doping conditions.

Fig. 4. Dislocation density vs. 300 K free carrier concentration. Upper portion shows the corresponding values of the Fermi energy at 1100 K.

Fig. 5. Schematic diagram of dislocation density in GaAs vs. free carrier concentration and conduction type.

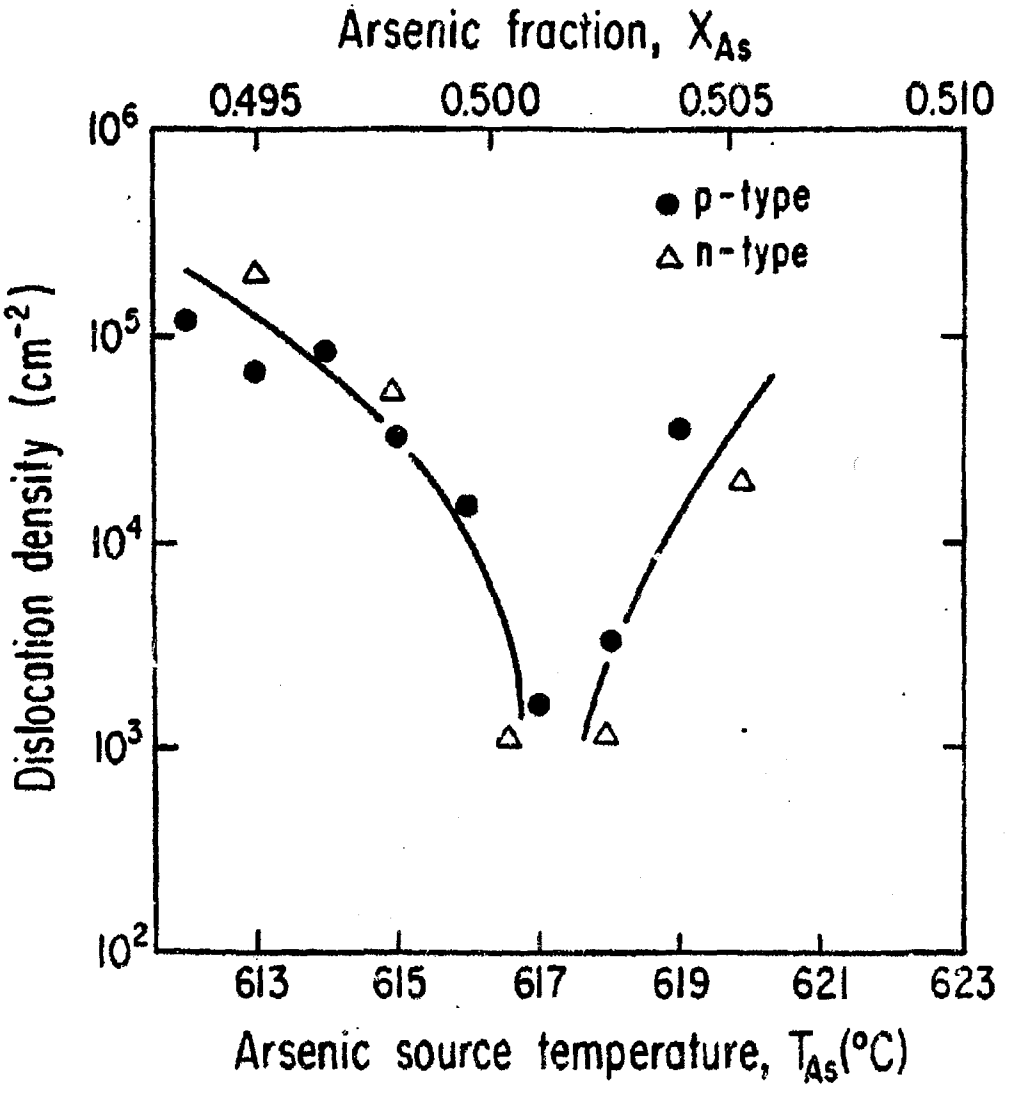

Fig 1.

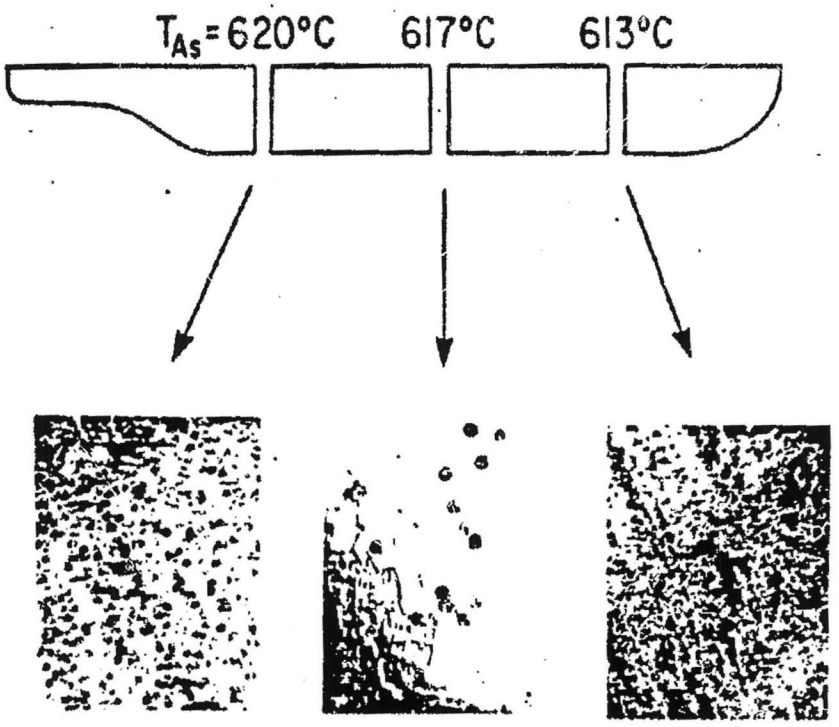

Fig. 2

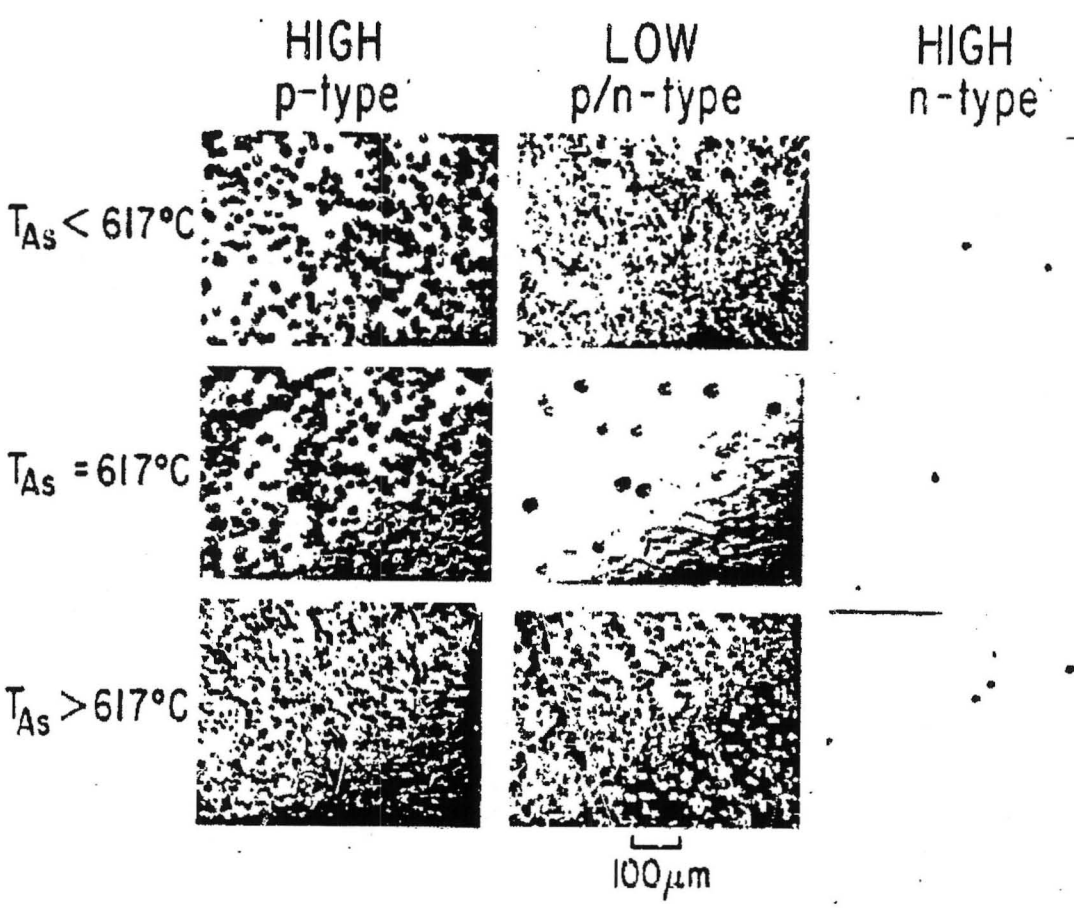

Fig. 3

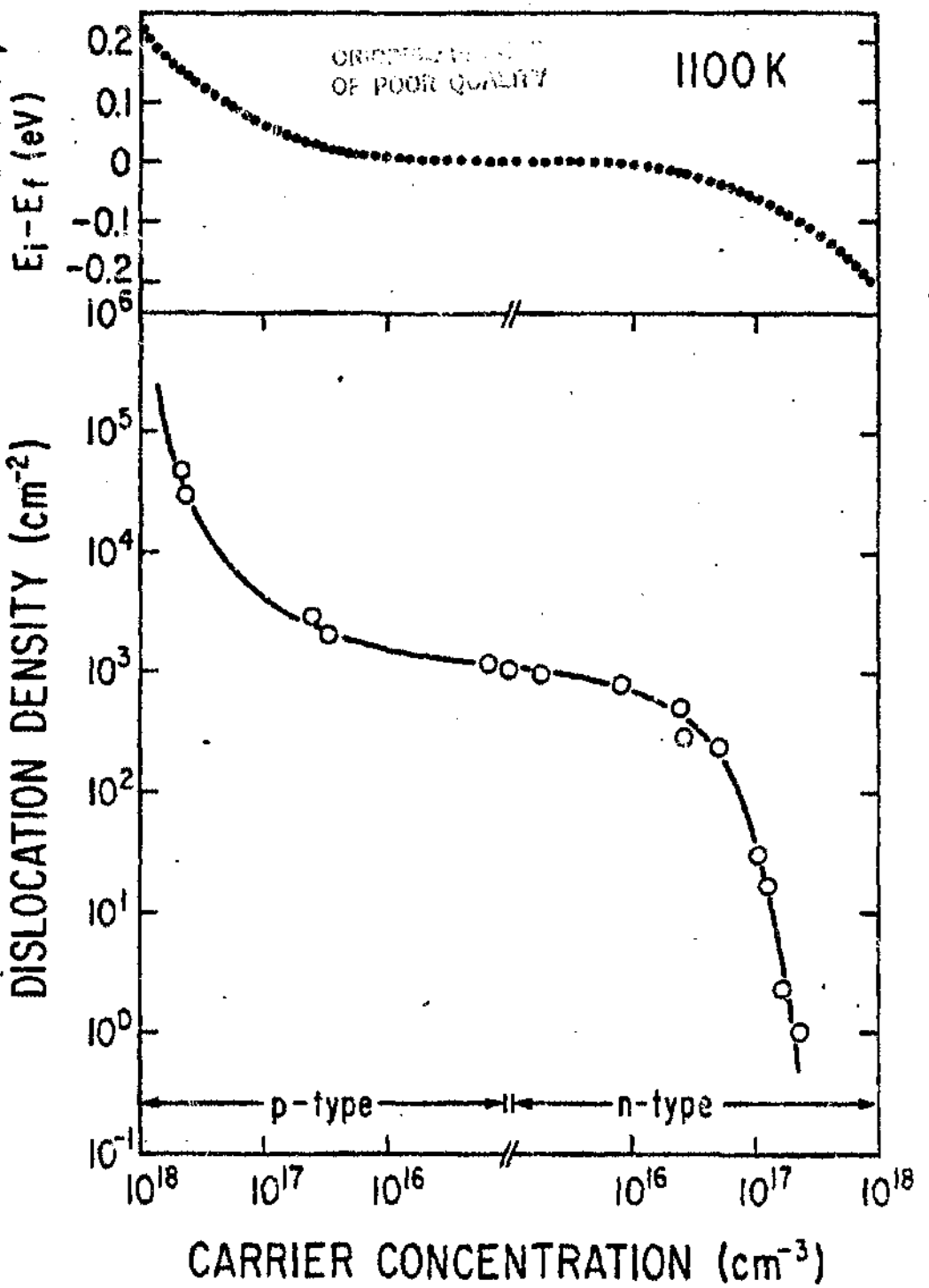
FERMI ENERGY, $E_i - E_f$ (eV)
0.2
0.1
0
-0.1
-0.2
1100 K
DISLOCATION DENSITY (cm^{-2})
10^6
10^5
10^4
10^3
10^2
10^1
10^0
10^{-1}
p-type
n-type
10^{18}
10^{17}
10^{16}
10^{16}
10^{17}
10^{18}
CARRIER CONCENTRATION (cm^{-3})

Fig. 4.

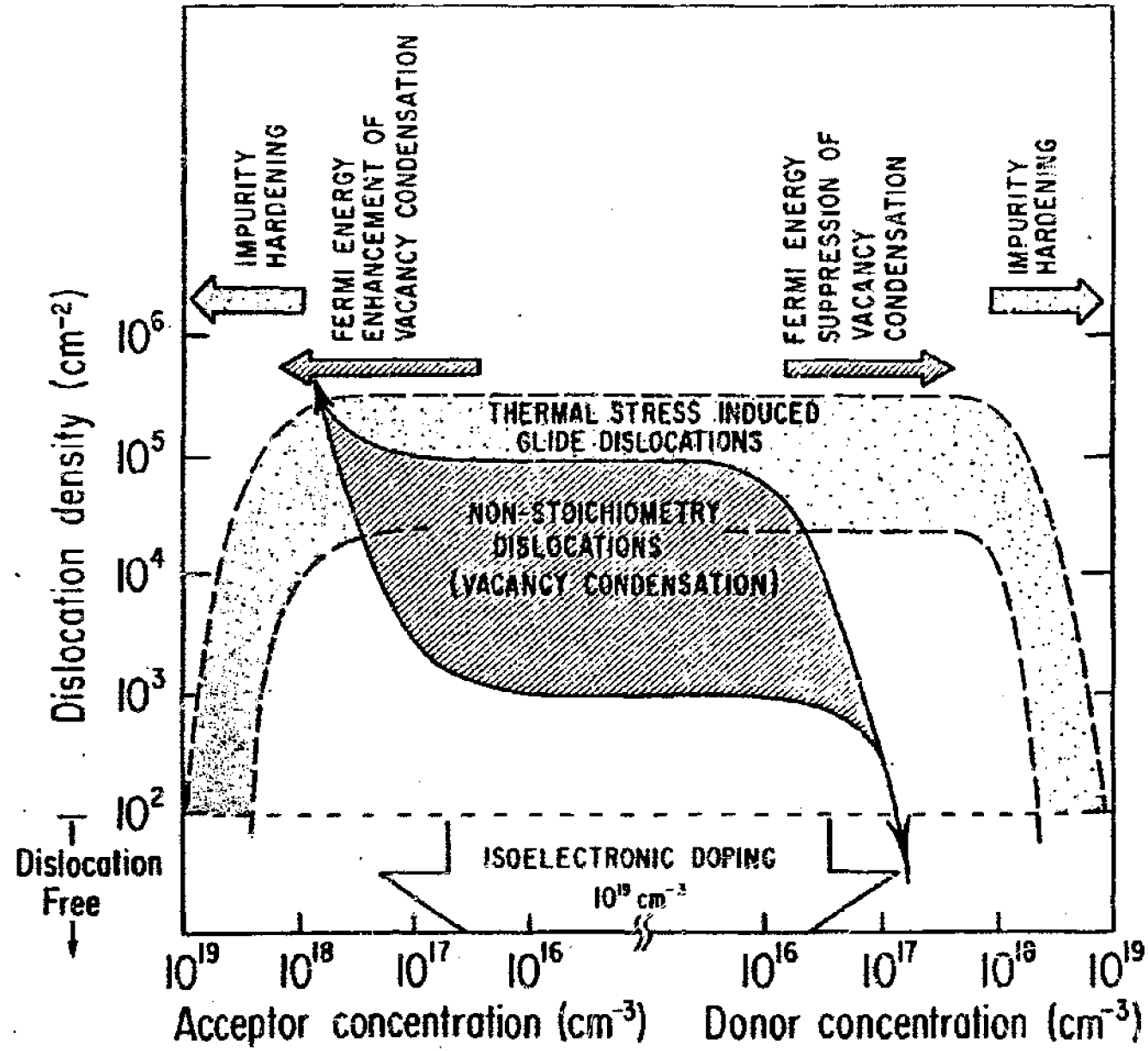

Fig. 5

OXYGEN-RELATED MIDGAP LEVEL IN GaAs

J. Lagowski, D. G. Lin, T. Aoyama[(a)] and H. C. Gatos
Massachusetts Institute of Technology
Cambridge, Massachusetts 02139

ABSTRACT

We established that in Bridgman- as well as in Czochralski-LEC-grown GaAs there is a deep level related to oxygen, ELO, with essentially the same activation energy (825 ± 4 meV) as EL2; however, the electron capture cross section of ELO is four times greater than that of EL2. In conjunction with measurements on "oxygen-free crystals" containing only EL2 we formulated practical procedures for the evaluation of the [EL2]/[ELO] concentration ratio from DLTS measurements. The IR absorption spectra of GaAs containing only EL2 and EL2 + ELO were found to be essentially the same indicating the need to re-examine the absorption characteristics of EL2. The present results answer the question of long standing as to whether or not oxygen is responsible for a deep level and confirm recent finding that EL2 is not the only midgap level in melt-grown GaAs.

[(a)]On leave from Hitachi Research Laboratories, Ibaraki, Japan.

Presented at the Third Conference on Semi-Insulating III-V Materials, Warm Springs, Oregon, April, 1984.

INTRODUCTION

Deep energy levels in melt-grown GaAs have received a great deal of attention as compensating centers responsible for the high resistivity material required for IC applications. The complex electrical and optical properties of this material have been commonly interpreted in terms of "the one deep level model" with only one midgap donor referred to as EL2. However, most recent discoveries of midgap levels other than EL2 (1), and especially of the oxygen-related level ELO, (2-4) have demonstrated that the simplistic one midgap level (EL2) concept of melt-grown GaAs cannot be valid. These findings raised once again the question of long standing. Is oxygen involved in midgap energy levels in melt-grown GaAs? We have addressed this question in our extensive experimental studies in the last three years. Our results (5) confirmed the earlier findings (6) of the oxygen-induced suppression of Si contamination. We have also identified indirect effects of oxygen doping (5) such as increase of the electron trap concentration, a decrease of the excess carrier lifetime and the suppression of the 1.2 eV luminescence band. These effects resulted from gettering the silicon impurity from the GaAs melt rather than from direct oxygen involvement in electrically active centers.

In our most recent study (3) we have succeeded in the identification of an oxygen-related midgap level, ELO, in Bridgman-grown GaAs which appears to be very similar to the midgap level in oxygen implanted GaAs (2) and in LEC GaAs (1). In the present communication we discuss the properties of ELO and compare them with those of the native defect level EL2.

We also present practical means for distinguishing between the two midgap levels.

EXPERIMENTAL

"Oxygen-doped" GaAs crystals were grown in a horizontal Bridgman-type (HB) apparatus utilizing quartz or PBN boats. Oxygen doping was realized by adding Ga_2O_3 to the GaAs charge material at a weight fraction ratio $W_{Ga_2O_3}/W_{GaAs}$ varying from zero ("oxygen free" crystals) up to 10^{-3}, or by filling the growth ampul with oxygen gas to a pressure up to 300 Torr (at room temperature). The upper limits of added oxygen exceeded by about one order of magnitude the doping range utilized in the study of ref. 7 which failed to recognize any midgap levels other than the EL2.

The oxygen concentration in our "oxygen free crystals" was below $10^{16}cm^{-3}$, and in the heavily doped ones it was 1 to 4 x $10^{16}cm^{-3}$, as determined by SIMS analysis. Our heavily oxygen-doped crystals remained conducting (electron concentration ranging from 0.5 to 2 x $10^{16}cm^{-3}$) due to the presence of sulfur impurity in the starting material.

Deep level characterization was carried out using transient capacitance measurements, photocapacitance transients (induced by monochromatic light) and optical absorption measurements. The features of our transient capacitance system included: (a) DLTS with variable duration filling pulses; (b) direct determination of the capacitance relaxation, c(t), by recording with a signal averaging technique; the various measurements could be electronically stored and directly compared, (c) precise temperature control and monitoring with an absolute accuracy and reproducibility better than 0.1°C.

RESULTS AND DISCUSSION

Midgap Level Parameters

The primary difficulty in studying EL0 stems from the striking similarity between its parameters and those of EL2. Accordingly, when both EL0 and EL2 are simultaneously present their unique separation is hardly possible without reference to standard material containing only one midgap level.

In our study the crystals grown without oxygen doping and containing only EL2 were used as reference. In Fig. 1 we present Schottky barrier capacitance transients corresponding to electron emission from midgap levels in oxygen-free and in heavily oxygen-doped GaAs. The capacitance relaxation, C(t), in oxygen-free material (Fig. 1a) is perfectly exponential consistent with the standard emission equation for a single deep level $\delta C=\delta C^{\circ}e^{-te_1}$, where t is time, δC° is the magnitude of capacitance change, and e_1 is the emission rate. The oxygen-doped crystal (Fig. 1b) exhibits a two-component exponential transient: $\delta C=\delta C_1^{\circ}e^{-te_1} + \delta C_2^{\circ}e^{-te_2}$, with the slow component corresponding to EL2 emission as measured in oxygen-free material. By subtracting the EL2 component we separated the transient corresponding to EL0 and thus we were able to determine the EL0 emission constant e_2 and the EL0 concentration (from δC_2°). We have carried out such analysis of capacitance transients recorded over a wide temperature range 270-450 K. The results are summarized in Fig. 2 in the form of thermal activation plots T^2e^{-1} vs $10^3/T$ for EL2 and EL0 levels. Least square analysis yields for EL2 an activation energy E_A = 815 ± 2 meV and an electron capture cross section σ_{na} = (1.2 ± 0.1) x 10^{-13} cm^2; the

corresponding values for ELO are E_A = 825 ± 5 meV and $\sigma_{na} = (4.8 \pm 0.6) \times 10^{-13} cm^2$. Empirical formulas for emission rates are:

$$\text{for EL2: } e_1^{-1} = \frac{3.53 \times 10^{-8}}{T^2} \exp\left(\frac{9450}{T}\right) \text{ sec}^{-1} \qquad (1)$$

$$\text{for ELO: } e_?^{-1} = \frac{6.84 \times 10^{-9}}{T^2} \exp\left(\frac{9580}{T}\right) \text{ sec}^{-1} \qquad (2)$$

where T is the absolute temperature in K.

We consider the above EL2 parameters more accurate than any previously published ones due to a much greater range of experimental data (8). We propose that these values be used as standards for midgap level identification in GaAs.

It is not clear at present whether oxygen is directly and solely responsible for the midgap ELO level. Theoretical study (9) and experimental data extrapolated from $GaAs_{1-x}P_x$ (10) indicated that an energy level of oxygen atom on arsenic site should be located in GaAs about 0.79 eV below the conduction band, i.e., very close to ELO energy.

ELO Concentration

As pointed out above, the activation energies of the electron emission rates are very similar for ELO and EL2. Accordingly, both individual levels exhibit DLTS peaks of identical shape. However, the ELO peak temperature T_{ELO} is shifted to a temperature lower than that of the EL2 peak, T_{EL2}, due to the larger value of the electron capture cross section ($\sigma_{na}(ELO) \approx 4\sigma_{na}(EL2)$). Using the emission rate formulas 1 and 2, the DLTS peaks can be exactly calculated for any given boxcar gate setting

t_1/t_2 (or an emission rate window $(t_2-t_1)/\ln t_2/t_1$). When EL0 and EL2 are simultaneously present at concentrations N_{EL0} and N_{EL2}, respectively, the resulting DLTS peak will occur at a temperature, T_{eff}, dependent on the concentration ratio of the two levels. As shown in Fig. 3, the involvement of two levels in an overal DLTS peak is not by any means evident. The half width of the overall peak is only marginally larger than the half width of the component peaks corresponding to the individual levels. It is thus clear that the involvement of two levels of similar energies can be recognized more readily from direct capacitance transient measurements C(t) (Fig. 1) than from DLTS measurements. Nevertheless, when the sample temperature is precisely monitored, the ratio N_{EL0}/N_{EL2} can be accurately determined by deconvolution of a DLTS peak into components with emission rates described by eqns. 1 and 2 (as done in Fig. 3).

The relative concentration of midgap levels can be quickly evaluated from the position of an overall DLTS peak using the calculated values given in Fig. 4. It is seen in that figure that increase of EL0 concentration gradually shifts T_{eff} from a temperature characteristic for EL2 peak down to a temperature of EL0 peak. The shift is linear with $X \equiv N_{EL0}/(N_{EL0}+N_{EL2})$ up to $X \approx 0.6$. Furthermore, the shift is very similar for all rate windows. Thus, X can be very well approximated by a simple relation:

$$X = 0.05 \times \Delta T \qquad (3)$$

where $\Delta T(^\circ C)$ is a difference between the actually measured peak position and the position corresponding to EL2 only, e.g., measured in oxygen-free GaAs. (Both measurements should be made with the same emission rate window.)

ELO Identification Using Short Filling Pulses

The above procedure assumes the identical initial occupation of ELO and EL2 within a depletion layer. In our recent work on ELO identification (3) we have discussed a very effective means for enhancement of the relative contribution of ELO to overall transient capacitance signal based on utilization of short duration filling pulses, which preferentially fill ELO and not EL2. As shown in Fig. 5a the magnitude of capacitance transient corresponding to EL2 decreases when a short duration filling pulse is used. A corresponding decrease of the EL2 peak height is seen in the DLTS spectrum of Fig. 5b. However, there is no shift in a peak position and no change in emission rate is observed in Figs. 5b and 5a, respectively. In oxygen-doped GaAs (Figs. 5c and 5d) a decrease of the filling pulse duration produces more significant changes. The increased contribution to ELO in respect to that of EL2 (the effect is due to larger capture cross section of ELO than that of EL2) is clearly seen in capacitance transients of Fig. 5c. A corresponding shift of an overall DLTS peak toward lower temperature is visible in Fig. 5d.

Using the procedures discussed above, we have identified ELO not only in the heavily oxygen-doped HB GaAs grown in our laboratory, but also in commercial HB GaAs (typically $N_{ELO}/N_{EL2} \lesssim 0.3$) and in LEC-grown GaAs ($N_{ELO}/N_{EL2} \sim 0.25$). The presence of ELO in these crystals is not surprising, since they were grown from melts containing oxides (usually arsenic oxide added in HB melt) or encapsulated in B_2O_3 (LEC).

Apparent Effects of Electric Field

Preferential filling of ELO (as compared to that of EL2) is also

observed for long duration filling pulses, when the magnitude of employed pulses is smaller than the barrier heigh (i.e., insufficient to complete the filling of all levels within the depletion region. DLTS results obtained under such conditions could be easily misinterpreted as anomalous phenomena such as: an increase of the emission in low electric fields, non-uniform distribution of levels beneath the surface; or a spectrum of midgap levels rather than two levels only.

Interference in the determination of the EL0/EL2 ratio can also result from apparent effects of strong electric fields on the electron emission. We have investigated the effects of strong fields (up to 4×10^5 V/cm) using the double pulse technique of ref. 11, and we have established that both levels exhibit a small field enhancement of electron emission, well within the range of the Poole-Frankel effect. In contrast, we observed very pronounced electric field effects, however only with diodes having large reverse bias currents. We refer to these effects as "apparent" field effects because they originate in Schottky diodes with poor characteristics rather than in the naure of EL2 and EL0. (12)

Optical Absorption

It is evident that the one midgap level (EL2) concept of melt-grown GaAs cannot be valid and that the midgap level properties of GaAs must be re-examined in view of the presence of more than one level.

Re-examination of the midgap level properties is especially urgent with respect to the infrared absorption (13) commonly utilized for the determination of the EL2 concentration in semi-insulating GaAs. In Fig. 6 we present optical absorption and photoionization capture cross section

spectra for oxygen-free GaAs containing EL2 only and for heavily oxygen-doped GaAs containing ELO and EL2 in approximately equal concentrations. It is seen that the results for both crystals are almost the same. The most plausible explanation of these results is that the optical properties of ELO and of EL2 are similar. Indeed both levels exhibit similar spectra of electron photoionization capture cross section. What is even more surprising is that both levels exhibit quite similar intracenter transitions in the region $1.05 < h\nu < 1.3$ eV manifested by the difference between the optical absorption and the photoionization cross section (shaded areas in Fig. 6). The similarities between the EL2 and the (ELO + EL2) properties could be accounted for if the ELO contribution to optical absorption is negligible in composition to that of EL2. Perhaps very precise measurements on crystals containing different ELO/EL2 concentration ratio (currently in progress) should uniquely resolve this issue. In the meanwhile, we must conclude that infrared absorption measurements in melt-grown GaAs should be treated as a measure of midgap levels rather than as a unique measure of the EL2 only.

ACKNOWLEDGMENT

We would like to acknowledge financial support form the National Aeronautics and Space Administration and the Office of Naval Research.

REFERENCES

1. M. Taniguchi and T. Ikoma, J. Appl. Phys. 54, 6448 (1983).
2. M. Taniguchi and T. Ikoma, Semi-Insulating III-V Materials, Ed. by S. Makram-Ebeid and B. Tuck, Shiva Publishing Ltd., 1982, p. 283.
3. J. Lagowski, D. G. Lin, T. Aoyama, and H. C. Gatos, Appl. Phys. Letters, 44, 336 (1984).
4. P. W. Yu and D. C. Walters, Appl. Phys. Letters 41, 863 (1982).
5. M. Kaminska, J. Lagowski, J. Parsey, K. Wada, and H. C. Gatos, Inst. Phys. Conf. Ser. 63, 197 (1981).
6. C. N. Cochran, L. M. Foster, J. Electrochem. Soc. 109, 149 (1962); J. F. Woods, N. G. Ainsle, J. Appl. Phys. 34, 1469 (1963).
7. G. M. Martin, G. Jacob, J. P. Hallais, F. Grainger, J. A. Roberts, B. Clegg, P. Blodd, and G. Poiblaud, J. Phys. C15, 1841 (1982).
8. G. M. Martin, A. Mittonneau, and A. Mircea, Electorn. Lett. 13, 191 (1977).
9. M. Jaros, Adv. Phys. 29, 409 (1980).
10. D. J. Wolford, S. Modesti, and B. G. Streetman, Inst. Phys. Conf. Ser. 65, 501 (1983).
11. S. Makram-Ebeid, Appl. Phys. Letters 37, 464 (1980); S. Makram-Ebeid and M. Lannoo, Phys. Rev. B, 25, 6406 (1982).
12. J. Lagowski, D. G. Lin, H. C. Gatos, J. M. Parsey, Jr., and M; Kaminska, submitted to Appl. Phys. Letters; (1984).
13. G. M. Martin, Appl. Phys. Letters 39, 747 (1981).

FIGURE CAPTIONS

Fig. 1. Capacitance transient corresponding to electron emission (a) from only one level EL2; (b) from two levels EL2 and ELO simultaneously present.

Fig. 2. Emission rate thermal activation plot for EL2 and for the oxygen-related level ELO.

Fig. 3. DLTS spectrum (rate window $25.6s^{-1}$) of heavily oxygen doped GaAs deconvoluted using experimentally determined emission rates of EL2 and ELO vs. temperature. (Compare with ref. 1)

Fig. 4. DLTS peak temperature vs. deep level concentration ratio. (see text)

Fig. 5. DLTS spectra and capacitance transient: (1) for long duration; and (2) for short duration filling pulses (see text).

Fig. 6. Absorption coefficient α; and photoionization cross section σ_i (determined from capacitance transient) for oxygen doped GaAs containing ELO and EL2 and for oxygen free GaAs containing only EL2.

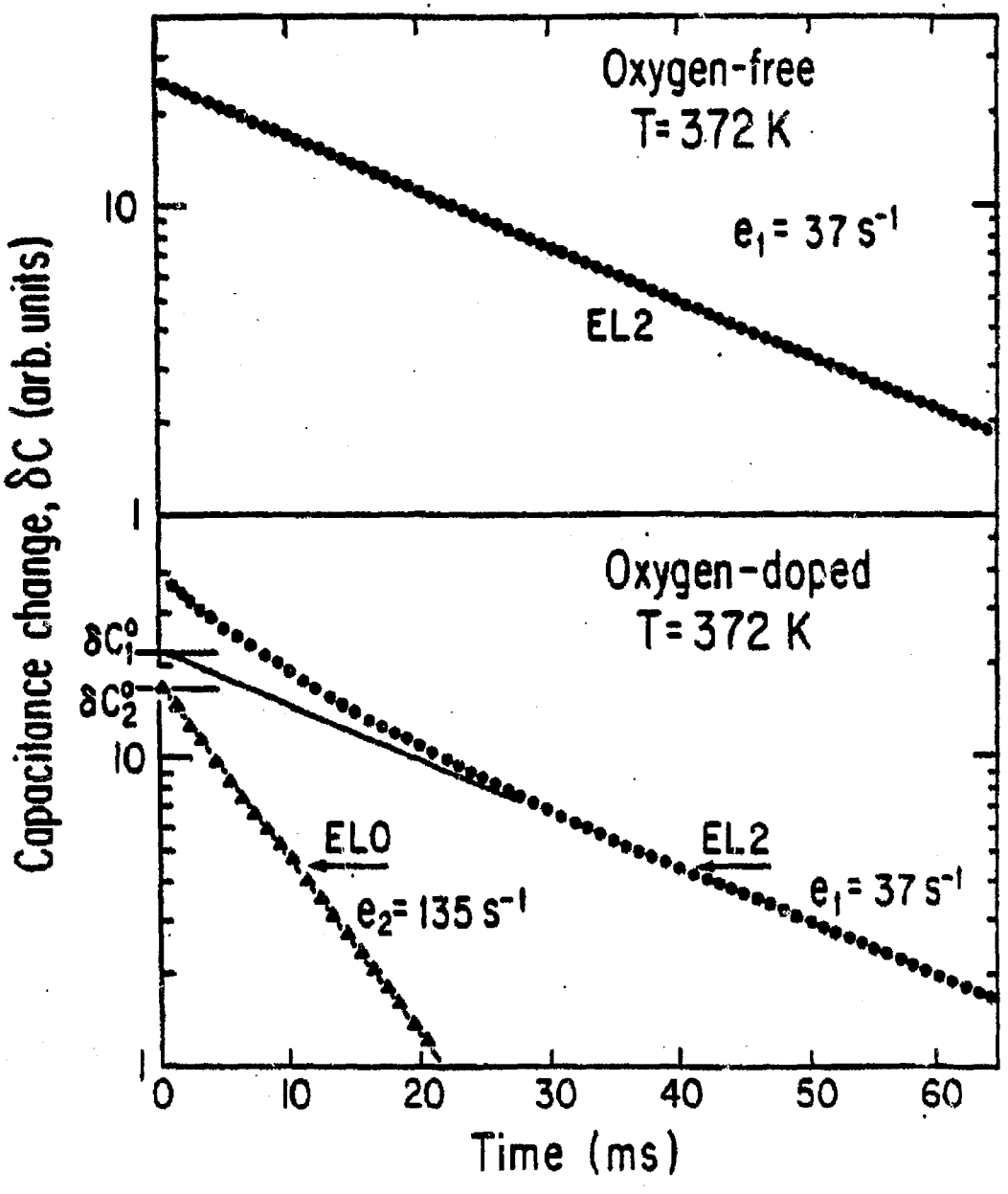

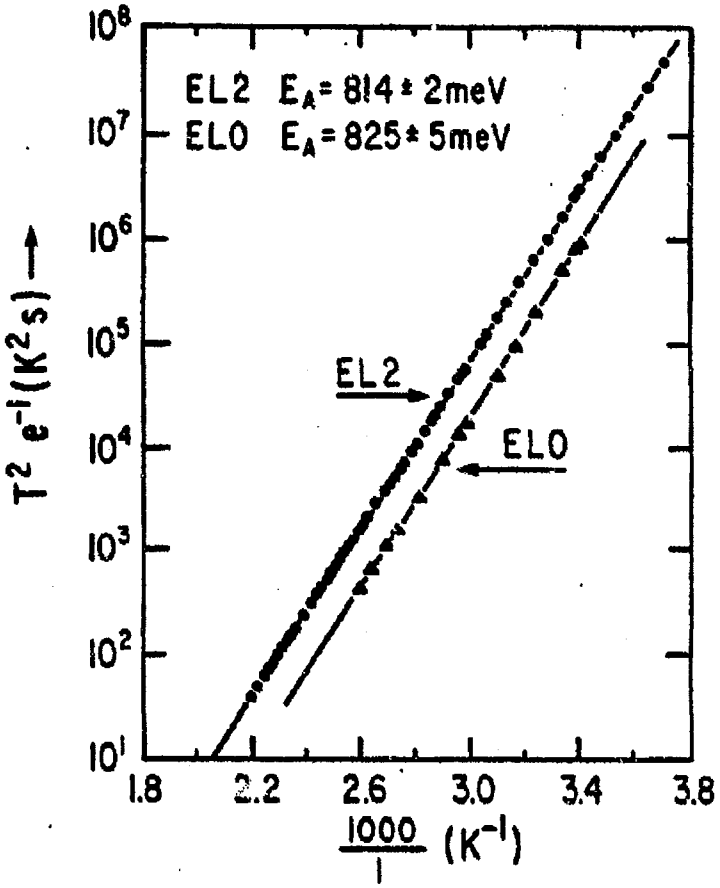

Fig 2.

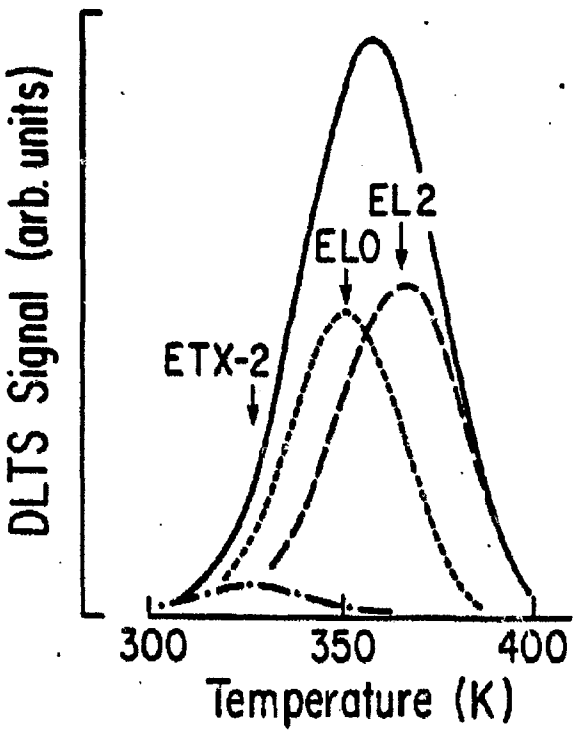

Fig 5.

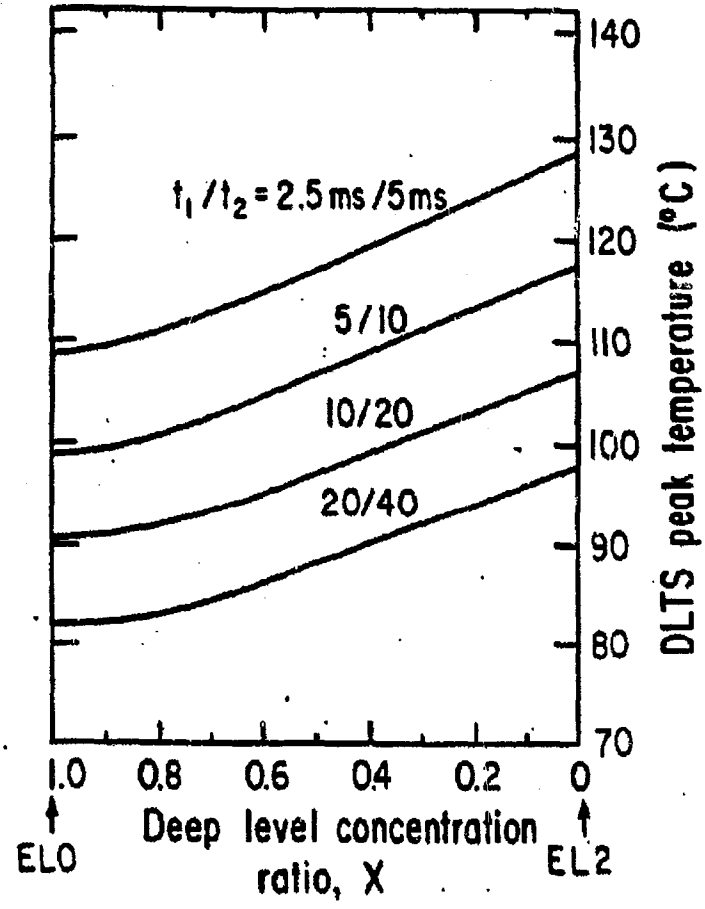

Fig. 4.

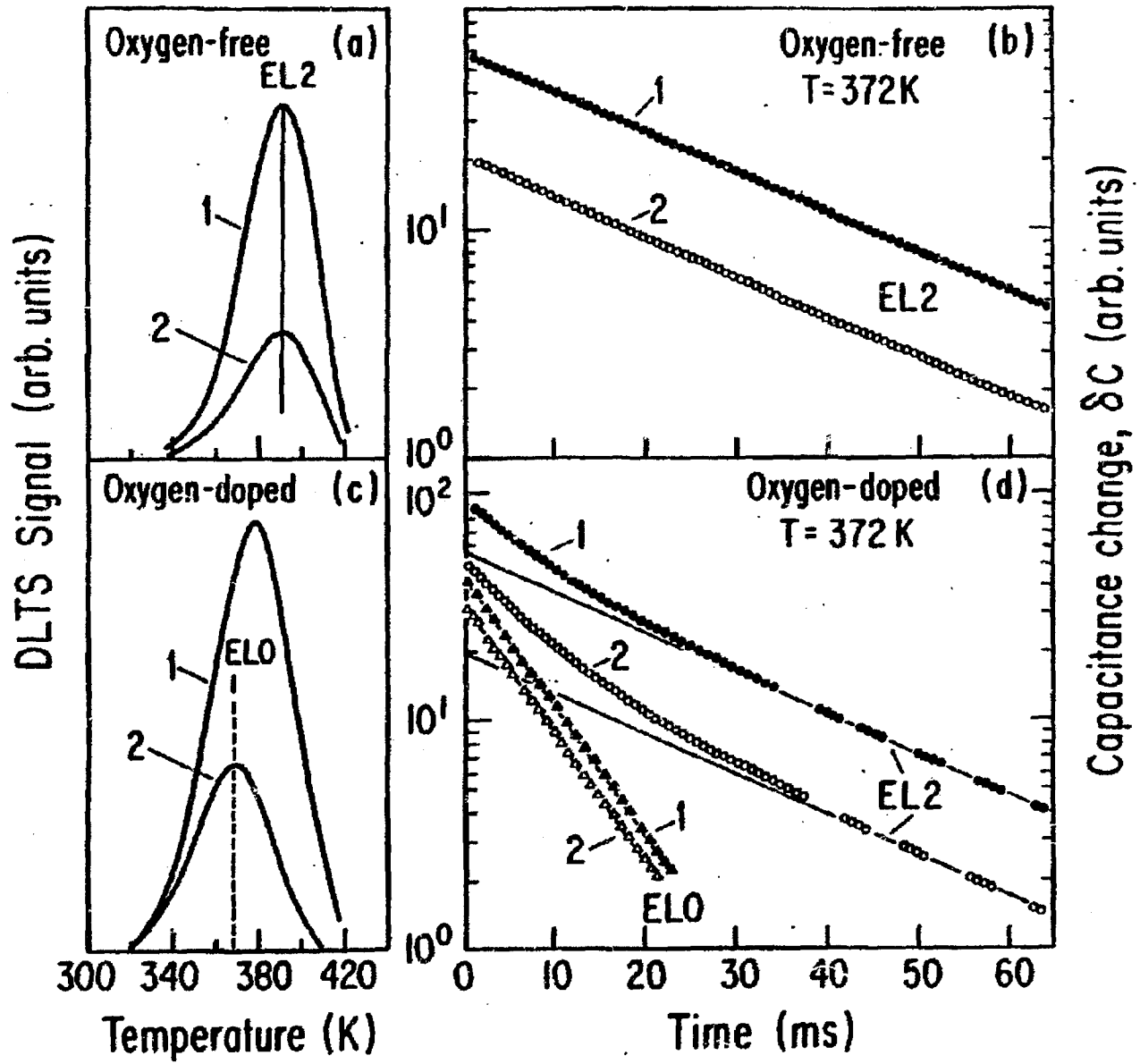

Fig 5.

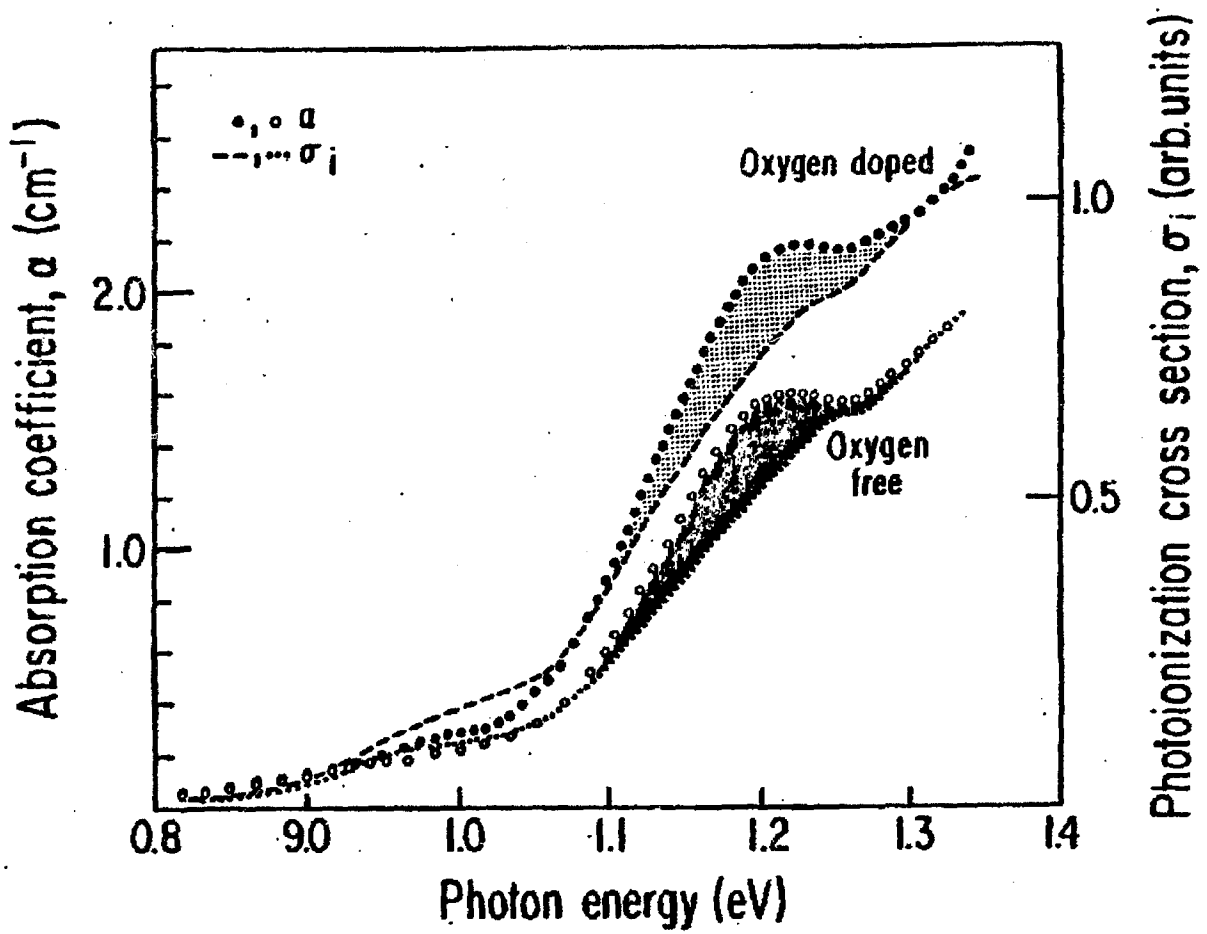

Fig 6.

submitted to Applied Physics Letters

REAL AND APPARENT EFFECTS OF STRONG ELECTRIC FIELDS ON THE ELECTRON EMISSION FROM MIDGAP LEVELS EL2 AND ELO IN GaAs

J. Lagowski, D. G. Lin and H. C. Gatos
Massachusetts Institute of Technology
Cambridge, Massachusetts 02139

J. M. Parsey, Jr.
A. T. & T. Bell Laboratories
Murray Hill, New Jersey 07974

M. Kaminska
Institute of Experimental Physics
University of Warsaw
Warsaw, Poland

Abstract

The effects of strong electric fields, up to 4 x 10^5 V/cm, on the electron emission from the GaAs dominant midgap levels EL2 and ELO were investigated by employing differential capacitance transients on GaAs-Au Schottky diodes. It was found that, in diodes with normal reverse bias characteristics, both levels exhibited a small field enhancement of electron emission, well within the range of the Poole-Frenkel effect. In contrast, very pronounced "apparent" electric field effects were observed in diodes with large reverse bias current. Thus, the conflicting reported results on the magnitude of the field enhancement of the electron emission from EL2 must be attributed to the characteristics of the Schottky diodes employed rather than to those of EL2.

Midgap levels in GaAs have received a great deal of attention as compensating centers responsible for the high resistivity material for IC applications.[1] The complex electrical and optical midgap-level properties of GaAs have been generally associated with only one deep donor referred to as EL2.[2] However, most recent discoveries[3,4] of midgap levels other than EL2, and especially of the oxygen-related level ELO,[4] have shown that the simplistic one midgap level (EL2) concept of melt-grown GaAs is generally invalid. Furthermore, the electric field ionization of EL2 has been a controversial issue because of highly conflicting experimental results. Thus, a dramatic field enhancement of the electron emission (up to 7 orders of magnitude) has been reported.[5,6] In fact, a new model of tunnel emission enhanced by coupling with phonons was proposed to account for these results.[7] On the other hand, in other studies no pronounced effect of electric fields on the electron emission from EL2 has been found.[8,9]

In view of the importance of field ionization in the determination of the deep level characteristics by means of junction-based measurements, the present study was undertaken to investigate the effect of strong electric fields on the electron emission of midgap levels particularly in the light of the newly identified ELO. The same approach was employed as that in the identification of ELO, i.e., detailed capacitance transient measurements in conjunction with measurements on reference crystals especially grown to contain only EL2.[4]

GaAs crystals were grown utilizing a horizontal Bridgman-type apparatus especially designed for precise control of the growth parameters.[10] Crystals containing EL2 and ELO at similar concentrations were grown by adding oxygen in the growth ampule (at a pressure of about 100 Torr at room temperature) or by adding equivalent amounts of Ga_2O_3.[4] These "oxygen-doped" crystals were

semiconducting $n \lesssim 2 \times 10^{16} cm^{-3}$, due to the presence of sulfur impurity. Crystals containing only EL2 (and a shallower trap EL3 at concentrations 5 to 10 times smaller than that of EL2) were grown without oxygen doping. They were n-type, Si-doped, with $n = 0.5$ to $1.5 \times 10^{17} cm^{-3}$ at 300 K (doping at higher levels leads to the rapid decrease of the EL2 concentration)[11]. Schottky diodes were prepared by evaporating Au on the As(111) surfaces after they were chemically polished (using borax), etched in HCl and rinsed in deionized water. Diodes with minimum reverse bias current were obtained when the samples were transferred immediately after cleaning to the evaporator with a base pressure below 10^{-6} Torr.

The features of our transient capacitance apparatus included: (a) precise temperature control and monitoring with an absolute accuracy and reproducibility exceeding 0.1°C; (b) direct determination of the capacitance relaxation, C(t), by recording with a signal averaging technique; the various measurements could be electronically stored and directly compared.

The effect of electric fields on the emission rate was studied using differential capacitance measurements (the same as in refs. 6 and 7.) In this approach two capacitance transients $C_1(t)$ and $C_2(t)$ are monitored following the application of filling pulses of a magnitude V_p and $V_p+\Delta V_p$, respectively. For small values of ΔV_p, (we have used $\Delta V_p = 0.1$ volt), the differential transient $\Delta C(t) \stackrel{Def}{\equiv} C_2(t)-C_1(t)$ corresponds to traps in a narrow zone of the depletion region with a well defined electric field value, determined by V_p and the net concentration of ionized impurities $N_D^+-N_A^- = n$.

Typical differential capacitance transients obtained with GaAs containing only EL2 are shown in Fig. 1 (a) and (b). It is seen that at 383 K there is a small field enhancement of the electron emission (by a factor of about 1.5, manifested as a faster $\Delta C/\Delta C_o$ decay). This small emission enhancement conflicts with the results of refs. 6 and 7, however it agrees very well with

obtained with a new technique[9] designed to minimize effects of reverse current and dopant inhomogeneities on deep level emission.) recently reported results. At 293 K the effect becomes more pronounced. The transients do conform to an experimental decay, $\Delta C/\Delta C_o = \exp(-e_n t)$; it should be pointed out that the low field values of the emission rate, e_n, are consistent with the recently revised values for EL2.[4]

The observed behavior is consistent with the Poole-Frenkel effect whereby the enhancement of emission from localized levels is caused by an effective lowering of the potential barrier surrounding the trapped charge.[12] The relative increase of the emission rate in an electric field, $\mathcal{E}$, (associated with the decrease of the barrier by $\delta E(\mathcal{E})$ is $e(\mathcal{E})/e(0) \sim e^{\delta E/kT}$. It is seen that the effect becomes less pronounced with increasing temperature, consistent with the results of Fig. 1. For a Coulombic barrier in GaAs $\delta E = 2.25 \times 10^{-4}(\mathcal{E})^{1/2}$ where δE is in eV and $\mathcal{E}$ is in V/cm. This change in the barrier in the field of 4×10^5 V/cm would lead to a 200-fold emission rate enhancement at 293 K and about 70-fold at 383 K. Experimental values are 4 and 1.5 at 293 K and 383 K, respectively. This much lower magnitude of emission enhancement is not surprising, since the deep midgap level is expected to be far more localized than the Coulombic centers.

In some instances much larger field emission enhancements were observed than those in Fig. 1 (a) and (b). These apparent enhancements were found to be invariably associated with GaAs-Au diodes exhibiting relatively large reverse bias current. Typical results are shown in Fig. 1 (c) and (d). These results were obtained on the identical GaAs sample as those of Fig. 1 (a) and (b). Thus, after the results of Fig. 1 (a) and (b) were obtained from the GaAs-Au diode with characteristics shown in Fig. 2 (diode A), the Au layer was removed and the GaAs As(111) surface was cleaned as outlined above. However, before the new Au film was evaporated the cleaned surface was exposed to the room ambient for a few hours. The resulting diode characteristics are shown in

Fig. 2 (diode B). As seen in Fig. 1, the field enhancement of emission rate for diode B is 30 and 50 at 383 and 293 K, respectively, i.e., much greater than for diode A.

It should be emphasized that both diodes exhibited the same C-V characteristics; the same ionized impurity concentration and the same concentration of deep levels. Also, for both diodes impurities and deep levels were uniformly distributed within the depletion layer. Thus, the large leakage current in diode B must be attributed to inadvertent surface effects stemming from oxide layers and/or surface contaminants.

Thus, reverse bias current of a GaAs-Au diode can be responsible for high field electron emission enhancement apparently via impact ionization.[13] The role of the reverse bias current becomes perfectly clear by comparing two transients in Fig. 1 (d) designated as V_{B1} and V_{B2}; they were taken at the same low electric field, 1.8×10^5 V/cm, but under two different reverse bias conditions indicated in Fig. 2: $V_{B1} = -9.5$ V, $J_1 = 5 \times 10^{-4}$ A/cm^2 and $V_{B2} = -4$ V, $J_2 = 3 \times 10^{-5}$ A/cm^2. Of these two transients only the one obtained at the low current density yields an emission rate which is equal to the low field value for EL2. For the higher current density the emission rate is shorter by almost a factor of two. This result shows that the effects of the reverse bias current can be appreciable even under low electric fields, apparently because impact ionization enhances emission from the levels in the entire depletion region; this behavior is in contrast to the real electric field effects (Poole-Frenkeleffect or electron tunneling) which are primarily associated with levels located in the high field zone of the depletion layer.

The study of the electron emission from the oxygen-related level EL0 (in the presence of EL2) was carried out using again differential capacitance transients, but in conjunction with reference measurements on oxygen-free samples

containing only EL2. The presence of both levels led to two-component exponential transients $\Delta C = \delta C_1^o e^{-te_1} + \delta C_2^o e^{-te_2}$, where e_1 and e_2 are the emission rates of EL2 and EL0, respectively; the slow component was the same as emission from EL2 as measured in oxygen-free crystals.[14] By subtracting the EL2 component we were able to obtain the transient corresponding to EL0. This procedure could be carried out reliably only for low reverse bias current diodes, provided, of course, the EL2 contribution was well defined from reference measurements. We found that emission from EL0 is essentially unaffected by electric fields. Up to fields of $\sim 3 \times 10^5$ V/cm the emission rates were the same as the low-field ones given in ref. (4).

For diodes with large reverse bias currents, the separation of the transients is a very complex task. Nevertheless, we observed for EL0 significant electron emission enhancements by reverse bias currents which were qualitatively similar to those observed for EL2.

Our results on the electron emission from the two midgap levels are shown in Fig. 3. They were obtained with diodes exhibiting low reverse currents and thus they must be considered as representing the upper limit of the real effects of electric fields. These results are in agreement with those reported in refs. 8 and 9. In Fig. 3 we present also results from refs. (6,7), which show unusually large enhancement of the total emission rate. It was attributed entirely to field-induced tunnelling from EL2, enhanced by phonons. But in view of the present findings, the unusually high emission rates cannot be attributed to the behavior of EL2 and EL0 in electric fields. They must be considered only apparent field effects and should be attributed to other factors such as impact ionization or the involvement of midgap levels other

than EL2 or EL0. The very good agreement of present results with those of ref. 9 is consistent with our assignment of the apparent field effects to a large reverse current.

In summary, we have identified the real effects of electric fields on the electron emission rate from the two major midgap levels EL0 and EL2. In fields up to 4×10^5 V/cm electron emission changes did not exceed a factor of 4, which is well within the range of the Poole-Frenkel effects.

ACKNOWLEDGMENT

The authors are grateful to the National Science Foundation and the National Aeronautics and Space Administration for financial support.

REFERENCES

1. E. J. Johnson, J. A. Kafalas and R. W. Davis, J. Appl. Phys. 54, 201 (1983).
2. See for example G. M. Morton, G. Jacob, J. P. Hallais, F. Grainger, J. A. Roberts, B. Clegg, P. Blodd and G. Poiblaud, J. Phys. C. 15, 1841 (1982).
3. M. Taniguchi and T. Ikoma, J. Appl. Phys. 54, 6448 (1983).
4. J. Lagowski, D. G. Lin, T. Aoyama and H. C. Gatos, Appl. Phys. Lett. 44, 336 (1984).
5. A. Mircea and A. Mitonneau, Journal de Physique Lettres (F) 40, L31 (1979).
6. S. Makram-Ebeid in Defects in Semiconductors, ed. by J. Narayan and T. Y. Tan (North-Holland, New York, 1981) vol. 2 p. 495 Appl. Phys. Letters 37, 464 (1980)
7. S. Makram-Ebeid and M. Lannoo, Phys. Rev. Letters 48, 1281 (1982): Phys. Rev. B, 25, 6406 (1982).
8. G. Vincent, A. Chantre and D. Bois; J. Appl. Phys. 50, 5484 (1979).
9. G. P. Li and K. L. Wang; Appl. Phys. Lett. 42. 840 (1983).
10. J. M. Parsey, Y. Nanishi, J. Lagowski and H. C. Gatos, J. Electrochem. Soc. 129, 388 (1982).
11. J. Lagowski, H. C. Gatos, J. M. Parsey, K. Wada, M. Kaminska and W. Walukiewicz, Appl. Phys. Lett. 40, 342 (1982).
12. J. L. Hartke, J. Appl. Phys. 39, 4871 (1968).
13. The importance of reverse bias current was discussed in ref. 6 in conjunction with emission anomalies seen in a low field region ($\lesssim 2.5 \times 10^5$ V/cm). Differences in reverse current were also suggested as possible explanation for unrealistically large emission rate differences reported in ref. 5 for diodes made on different crystallographic surfaces.

14. Energies of EL0 and EL2 are very similar. However, the emission rate of EL0 is about four times larger than that of EL2 due to the larger value of the electron capture cross section. Detailed emission rates vs. temperature values are given in Ref. 4 for both levels.

FIGURE CAPTIONS

Fig. 1. Differential capacitance transients of EL2 for GaAs-Au Schottky diode with normal reverse bias current (a and b) and for diode with large reverse bias current (c and d); see text.

Fig. 2. I-V characteristics of GaAs-Au Schottky diode with normal reverse bias current (diode "A") and with large reverse current (diode "B"); see text.

Fig. 3. Emission rate of the midgap levels EL2 and EL0 vs. electric field. o,● - present results obtained with diodes of normal reverse bias current; Δ - corresponds to experimental results of Ref. 6 and solid line corresponds to theoretical electron tunneling model of Ref. 7. The enhancement of the emission rate in Ref. 6 and 7 represents the apparent effects of electric field related to the diode characteristics.

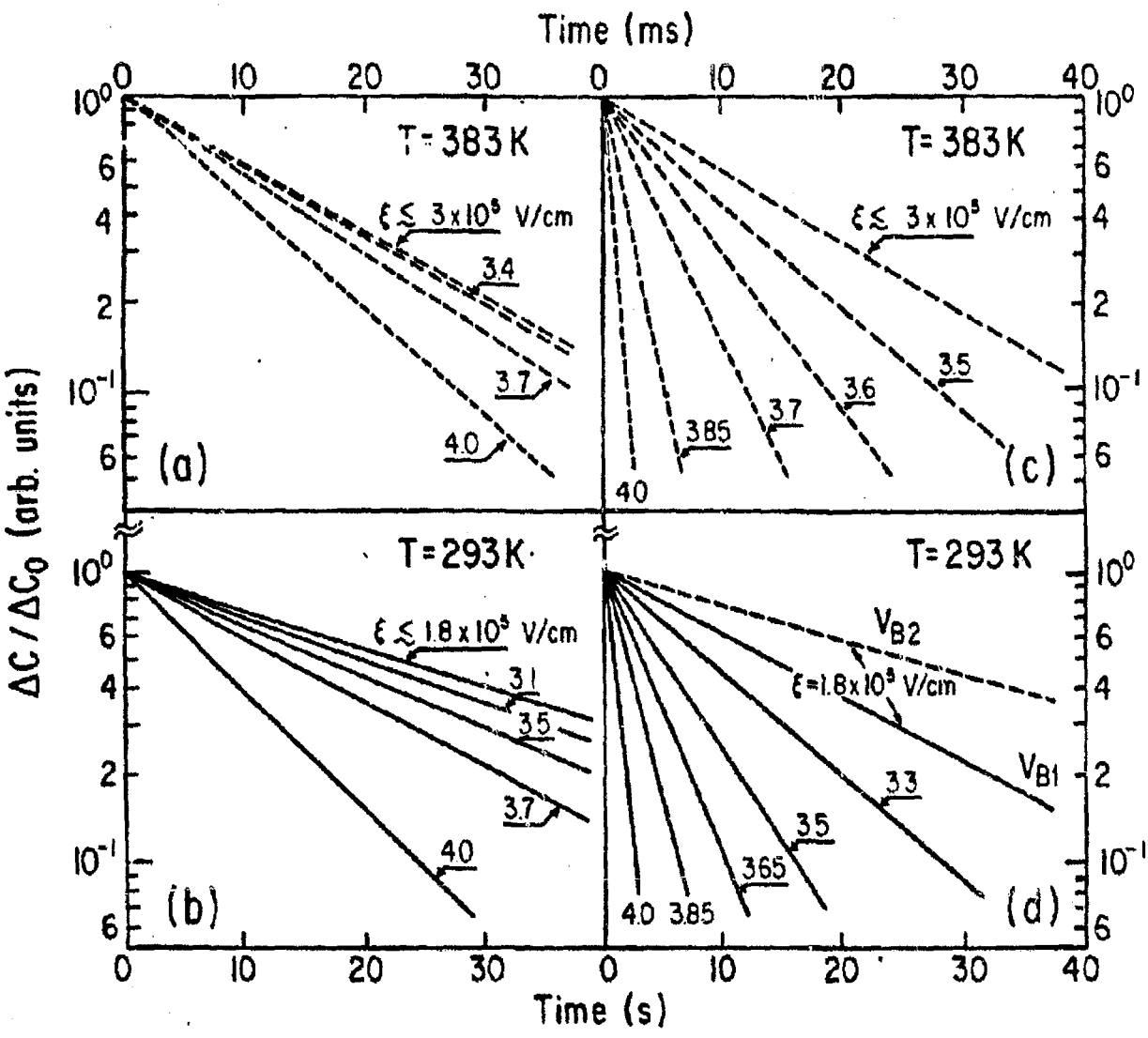

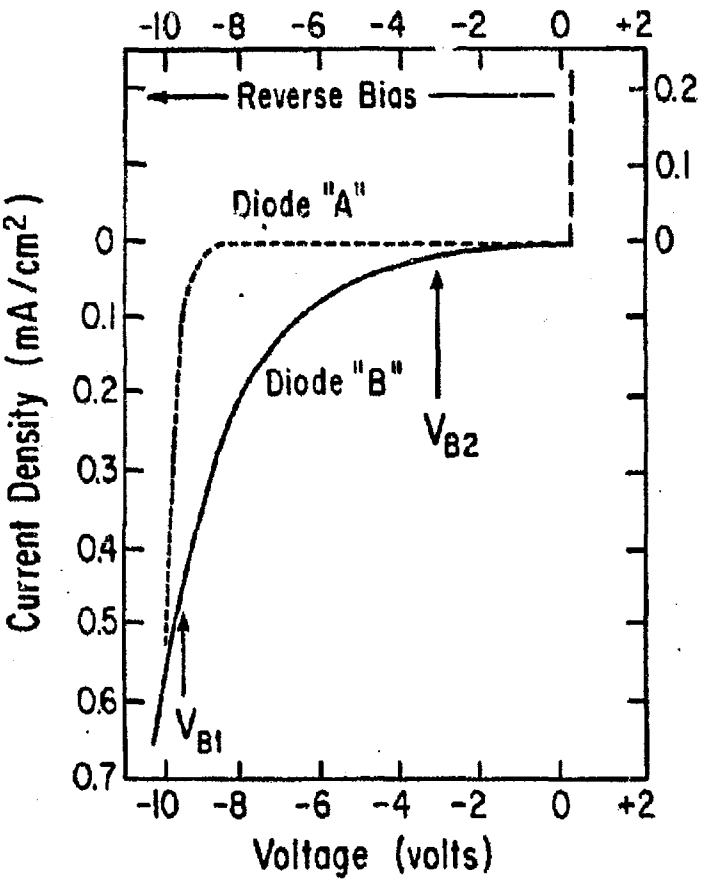
-10 -8 -6 -4 -2 0 +2
Reverse Bias
0.2
0.1
0
Diode "A"
Diode "B"
V_{B2}
V_{B1}
Current Density (mA/cm²)
0
0.1
0.2
0.3
0.4
0.5
0.6
0.7
-10 -8 -6 -4 -2 0 +2
Voltage (volts)

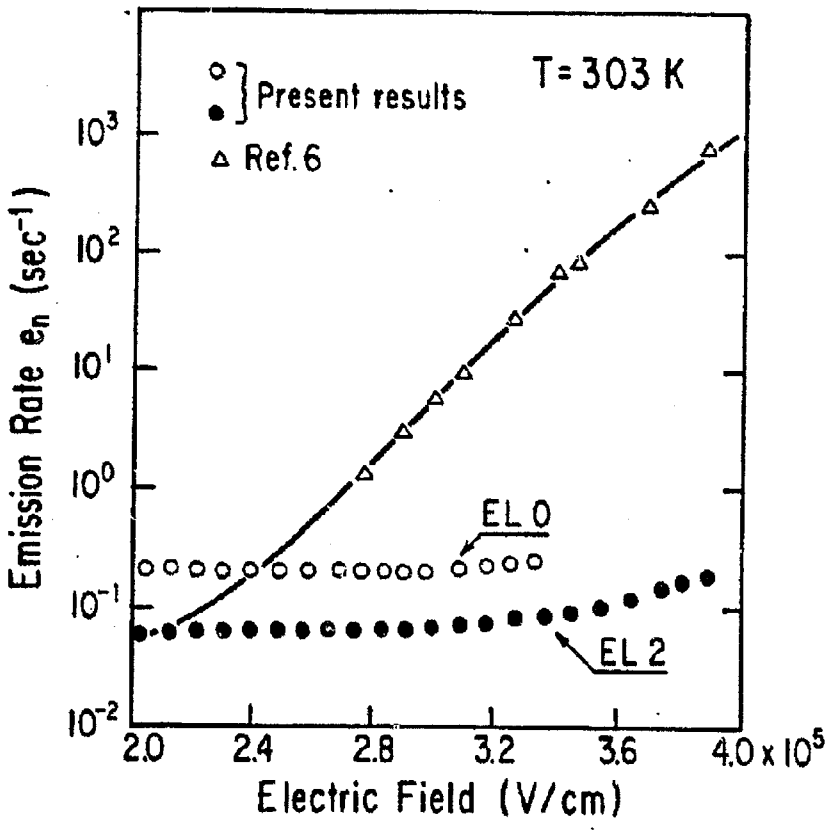
T=303 K
Present results
Ref. 6
EL 0
EL 2
Emission Rate e_n (sec^{-1})
10^3
10^2
10^1
10^0
10^{-1}
10^{-2}
2.0
2.4
2.8
3.2
3.6
4.0×10^5
Electric Field (V/cm)

submitted to
Applied Physics Letters

FERMI ENERGY CONTROL OF VACANCY COALESCENCE AND DISLOCATION DENSITY IN MELT-GROWN GaAs

J. Lagowski, H. C. Gatos, T. Aoyama[(a)] and D. G. Lin
Massachusetts Institute of Technology
Cambridge, Massachusetts 02139

Abstract

We have discovered a striking effect of the Fermi energy on the dislocation density in melt-grown GaAs. Thus, a shift of the Fermi energy from 0.1 eV above to 0.2 eV below its intrinsic value (at high temperature, i.e., near 1100 K) increases the dislocation density by as much as five orders of magnitude. The Fermi energy shift was brought about by n- and p-type doping at a level of about $10^{17}cm^{-3}$ (under conditions of optimum partial pressure of As, i.e., under optimum melt stoichiometry). This effect must be associated with the fact that the Fermi energy controls the charge state of vacancies, (i.e., the occupancy of the associated electronic states) which in turn must control their tendency to coalesce and thus the dislocation density. It appears most likely that gallium vacancies are the critical species.

It has been a common trend to treat dislocations in melt-grown crystals, and particularly in crystals grown by the Czochralski liquid encapsulated (LEC) technique, within a framework of critical stress models.[1-5] Such models assume that dislocations are generated in the solidified material when thermal stress exceeds certain critical values. The decrease of dislocation densities by electrically active impurities[3-6] (at levels $>10^{18}cm^{-3}$) and by isoelectronic impurities[3,5-7] (at levels $>10^{19}cm^{-3}$) has been treated phenomenologically as impurity hardening effects which lead to the increase of the value of the critical stress. The effects of melt composition on dislocation density in GaAs were originally reported in the mid 60's.[8] More recently we have shown that stoichiometry plays a key role in the generation of dislocations under minimized thermal stress.[9,10] By varying the arsenic source temperature, T_{As}, (i.e., arsenic partial pressure or melt stoichiometry) we found that the dislocation density exhibits a pronounced minimum at an optimum $T_{As} = 617 \pm 1°C$. We have further found that growth under "off stoichiometry" conditions leads to high dislocation densities which exceed those found in crystals grown under pronounced thermal stress.[10]

In the present communication we present experimental results which shed a new light on the dislocation formation in GaAs grown under low thermal stress; we show that in moderately doped crystals the dislocation density is controlled by the Fermi energy.

Single crystals of GaAs with a cross-sectional area up to 2 cm^2 were grown using a horizontal Bridgman apparatus especially designed for the precise control of growth parameters.[9] The growth was carried out in a high purity fused quartz boat (especially treated to prevent the melt from wetting the boat) or in a pyrolytic boron nitride boat. The arsenic source temperature, T_{As}, was varied in discrete steps of 1° to 2°C, at 1- to 2-hour intervals

corresponding to 1 to 2 cm of growth. Lightly doped ($5 \times 10^{16} cm^{-3}$), Si-doped, and Zn-doped melts were employed. The carrier concentration was determined from Hall effect and conductivity measurements. Dislocations were revealed using molten KOH etching.

In an earlier study we have established an optimum arsenic source temperature, 617 ± 1°C, which leads to a minimum dislocation density in n-type crystals.[10] The present experiments confirm these results and further show that the same behavior is also characteristic in lightly doped p-type GaAs crystals. Thus, in Fig. 1 we show the dependence of the dislocation density on the arsenic temperature, T_{As}, for p-type and n-type GaAs crystals with a free carrier concentration of about $10^{16} cm^{-3}$. A minimum dislocation density of about $10^{3} cm^{-2}$ is obtained at an optimum temperature 617 ± 1°C. Deviations from this temperature lead to an increase of the dislocation density by as much as two orders of magnitude, i.e., to dislocation densities which are comparable to (or even higher than) those found in GaAs crystals grown under large thermal stresses.

By increasing the doping level (but still maintaining it below the impurity hardening regime) we found that the effects of p-type doping are entirely different from those of n-type doping. These effects of conductivity type and carrier concentration on the dislocation density in GaAs grown under optimum T_{As} are quantitatively summarized in Fig. 2. It is seen that the transition from n-type to p-type material enhances the dislocation density by as much as five orders of magnitude.

The key to understanding the formation of dislocation in GaAs grown under (minimized) thermal stress lies in the finite existence region of GaAs, i.e., in deviations from stoichiometry at or very near the melting point. Thus, the type and concentration of vacancies in a solidifying crystal is controlled by

the melt composition (i.e., the arsenic source temperature). During the post-solidification cooling vacancies concentrations exceed saturation in the crystal, and vacancies can coalesce to form defect complexes and dislocations. The formation of dislocations from the coalescence of vacancies requires the participation of vacancies from both the Ga and As sublattices; hence a minimum in dislocation density observed under optimum melt stoichiometry (Fig. 1) is due to a minimum value of the product of the gallium vacancy and arsenic vacancy concentrations. In general, the formation of dislocations can be initiated by only one type of vacancy, such as V_{Ga}, since the corresponding defect, V_{As}, can be created upon migration of V_{Ga}.

It is well known, however, that vacancies in GaAs lead to localized electronic levels.[11] The occupancy of the levels, i.e., the charge state of the vacancies, is controlled by the Fermi energy. Obviously, the charge state of vacancies must determine their concentration, migration, and ability to coalesce.

Transition from p- to n-type GaAs caused by intentional doping shifts the Fermi energy upwards in the energy gap increasing the concentration of negatively charged, acceptor-type vacancies, and decreasing the concentration of ionized deep donor levels. According to ref. 12, critical post-solidification defect interactions in GaAs take place at a temperature of about 1100 K. Thus, in Fig. 2 we indicate the Fermi energy values of 1100 K corresponding to the concentration of free carriers measured at 300 K.[13] The plateau of the dislocation density coincides with constant Fermi energy. On the n-type region the dislocation density decreases when the added donor concentration becomes comparable to (or higher than) the intrinsic carrier concentration at 1100 K, while on the p-type region the dislocation density increases when the

acceptor concentration becomes comparable to the intrinsic carrer concentration at 1100 K. This relationship is consistent with the critical role of V_{Ga}, which in GaAs leads to an acceptor level close to the middle of the energy gap.[11] The downward shift of the Fermi energy caused by th. n- to p-type transition increases the fraction of neutral V_{Ga} which can readily migrate and coalesce to form dislocations. In the n-type region the fraction of charged V_{Ga} is increased, and thus their coalescence and consequently, dislocation formation is impeded.

The thermal stress-induced dislocations are generated at temperatures of about 1300-1400 K which are much closer to the melting point than 1100 K where nonstoichiometry dislocations are formed. Thus, the effects of Fermi energy on the propagation and multiplication of stress-induced dislocations would require a high concentration of electrically active dopant, exceeding $10^{18} cm^{-3}$. This concentration range overlaps with that considered in "impurity hardening" phenomena.

In summary, we have shown that the Fermi energy controls the dislocation density in GaAs (under minimized thermal stresses) since it controls the charge state of the vacancies, and thus the extent of their coalescence. These phenomena must characterize compound semiconductors in general.

ACKNOWLEDGEMENT

The authors are grateful to the National Aeronautics and Space Administration and the Air Force Office of Scientific Research for financial support.

REFEREES

(a) Permanent address: Hitachi Research Laboratory, Hitachi, Ltd., 4026 Kuji-cho, Hitachi, Ibaraki 319-12, Japan.

1. A.S. Jordan, R. Caruso and A.R. Von Neida, The Bell System Technical Technical Journal 59, 593 (1980).

2. M.G. Mil'vidskii and E.P. Bochkarev, J. Crystal Growth 44, 61 (1978).

3. M.G. Mil'vidskii, V.B. Osvensky and S.S. Shifrin, J. Crystal Growth 52, 396 (1981).

4. M. Duseaux and G. Jacob, Appl. Phys. Lett. 40, 790 (1982).

5. M. Duseaux, C. Schiller, J.P. Cornier, J.P. Chevalier and J. Hallais, J. de Physique 44, C4-397 (1983).

6. G. Jacob, Semi-Insulating III-V Materials, edited by S. Makram-Ebeid and B. Tuck (Shiva, London, 1982) p. 2.

7. G. Jacob, M. Duseaux, J.P. Farges, M.M.B. Van Den Boom and P.J. Roksnoer, J. Crystal Growth 61, 417 (1983).

8. J.C. Brice and G.D. King, Nature 209, 1346 (1966); J. Brice, J. Crystal Growth 7, 9 (1970).

9. J.M. Parsey, Jr., Y. Nanishi, J. Lagowski and H.C. Gatos, J. Electrochem. Soc. 128, 936 (1981); 129, 388 (1982).

10. J.M. Parsey, Jr., J. Lagowski and H.C. Gatos, Proc. III-V Opto-Electronics Epitaxy and Device Related Processes, edited by V.C. Keramidas and S. Mahajan, The Electrochemical Society, Inc., (Pennington N.J., 1983) p. 61.

11. M. Jaros, Advances in Physics 3, 409 (1980).

12. J. Lagowski, H.C. Gatos, J.M. Parsey, K. Wada, M. Kaminska and W. Walukiewicz, Appl. Phys. Lett. 40, 342 (1982).

13. Fermi energy values were calculated using GaAs parameters compiled by J.S. Blakemore, J. Appl. Phys. 53, R123 (1982).

FIGURE CAPTIONS

Figure 1. Dislocation density vs. arsenic source temperature (melt stoichiometry) for lightly doped n- and p-type GaAs.

Figure 2. Dislocation density vs. 300 K free carrier concentration for crystals grown from optimum melt stoichiometry and under optimal thermal stresses.[9] Upper portion shows the corresponding values of the Fermi energy at 1100 K.

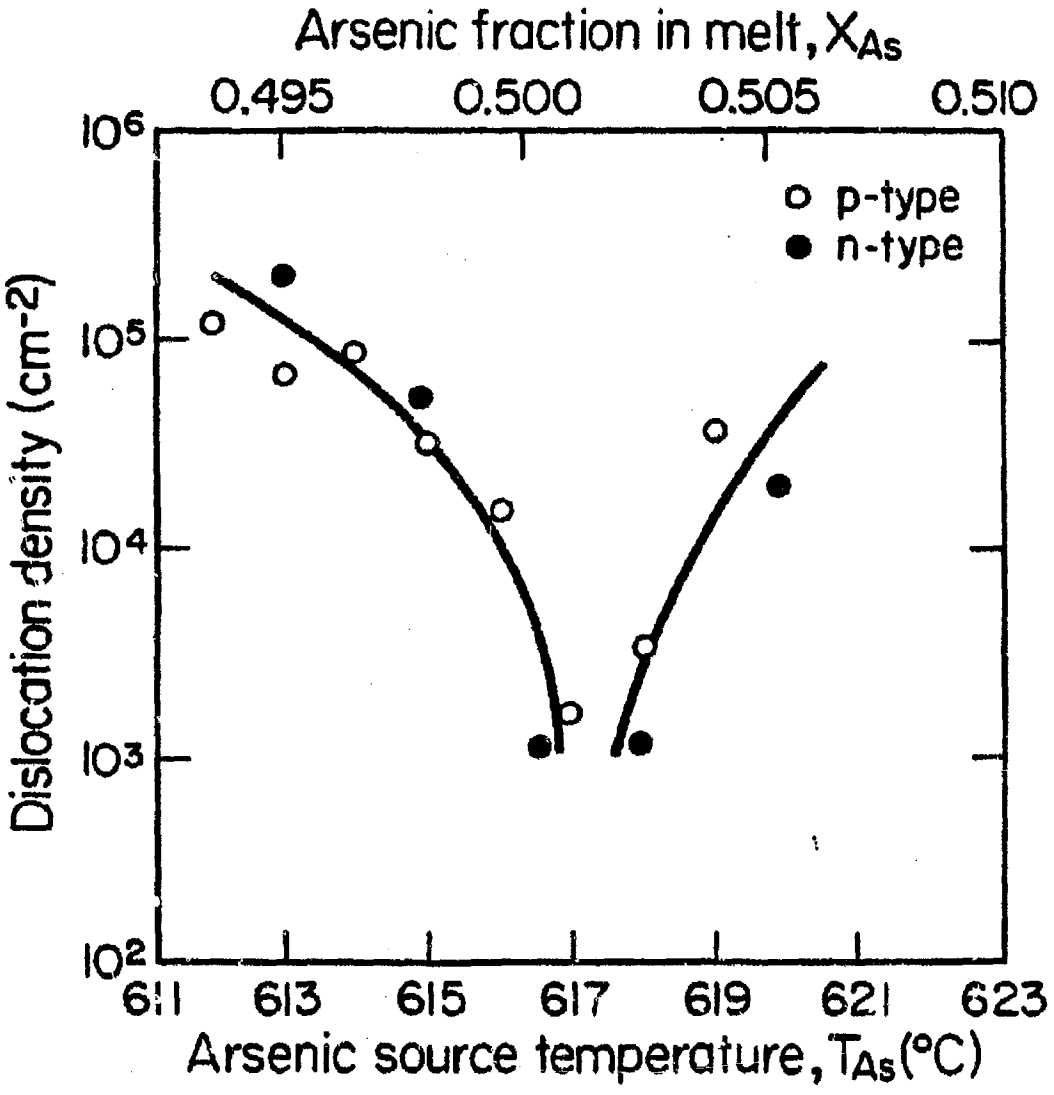

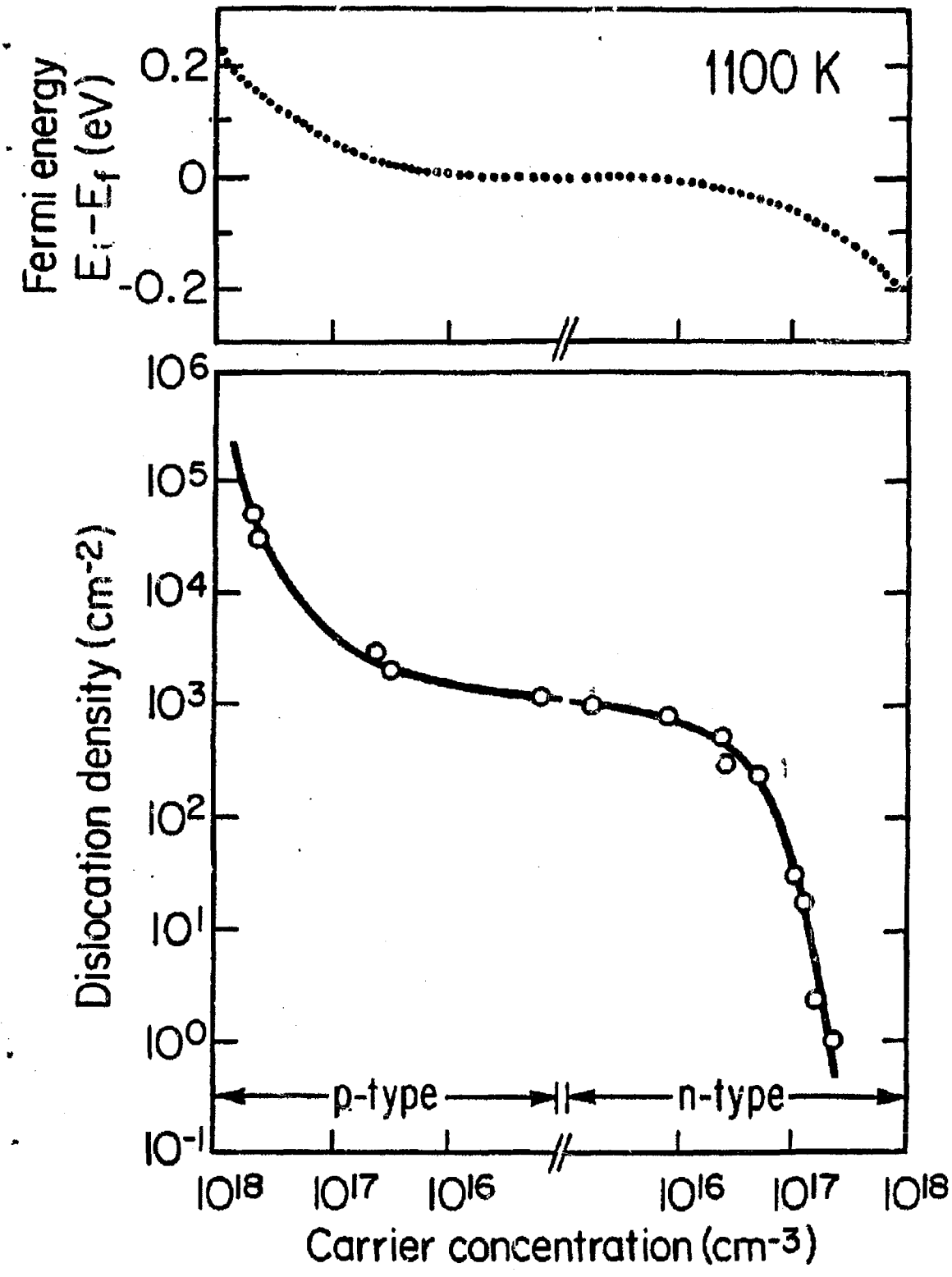
1100 K
Fermi energy
$E_i - E_f$ (eV)
0.2
0
-0.2
10^6
10^5
10^4
10^3
10^2
10^1
10^0
10^{-1}
Dislocation density (cm^{-2})
p-type
n-type
10^{18}
10^{17}
10^{16}
10^{16}
10^{17}
10^{18}
Carrier concentration (cm^{-3})

submitted to Physical Review B1

ELECTRON MOBILITY IN MODULATION DOPED HETEROSTRUCTURES

W. Walukiewicz[a)], H. E. Ruda[b)], J. Lagowski and H. C. Gatos
Massachusetts Institute of Technology
Cambridge, Massachusetts 02139

Abstract

A model for electron mobility in a two-dimensional electron gas confined in a triangular well was developed. All major scattering processes, i.e., deformation potential and piezoelectric acoustic, polar optical, ionized impurity and alloy disorder were included as well as intra- and inter-subband scattering. The model is applied to two types of modulation doped heterostructures, namely GaAs-GaAlAs and $In_{0.53}Ga_{0.47}As$-$Al_{0.52}In_{0.48}As$. In the former case phonons and remote ionized impurities ultimately limit the mobility, whereas in the latter, alloy disorder is a predominant scattering process at low temperatures. The calculated mobilities are in very good agreement with recently reported experimental characteristics for both GaAs-GaAlAs and $In_{0.53}Ga_{0.47}As$-$Al_{0.52}In_{0.48}As$ modulation doped heterostructures.

I. Introduction

The advent of modulation (or selectively) doped heterostructures (MDH) has prompted a wave of studies, both theoretical and experimental, on the two-dimensional electron gas (2DEG). As MDH with exceedingly high electron mobilities have been obtained, a new challenge associated with the understanding of the transport properties of the 2DEG has emerged.

The concept of separating electrons from their parent donors in semiconducting systems was originally proposed by Esaki and Tsu.[1] However, it was not until Molecular Beam Epitaxy (MBE) technology was sufficiently developed that such structures were grown.[2] It soon became apparent that these types of structures are the key to a new generation of high speed semiconductor devices.[3-7]

Many of the studies concerned with electron mobility treated the confining potential as a square well; this treatment is only applicable to Multiple Quantum Well Structures.[8-11] However, the highest electron mobilities have been observed in Single Quantum Well Structures, where a triangular potential well is a better suited approximation. The framework for the treatment of two-dimensional electron transport in a triangular well was originally developed for silicon inversion layers.[12-14] This approach was adapted to the treatment of scattering by ionized impurities, by alloy disorder, and by surface roughness in GaAs-GaAlAs MDH.[15] The treatment, however, was limited to intra-subband scattering, and therefore it was not applicable to higher gas densities. Effect of doping of GaAlAs on the electron mobility in GaAs-GaAlAs heterostructures has been also considered.[16] Since in MDH ionized impurity scattering is substantially reduced, even at low temperatures electron phonon interaction constitutes an important mechanism limiting electron mobility. The problem of electron phonon scattering has been addressed in general terms, and the

difficulties a proper description of optical phonon scattering would entail, especially at higher temperatures, were pointed out.[17,18] Electron mobilities have been also calculated for GaAs-GaAlAs MDH taking phonon scattering into consideration,[19] however, the calculated values are much lower than those reported recently.[20,21] A simplified approach to 2DEG mobility calculations in a triangular well has been carried out by adopting formulas valid for a square well potential and using an effective width taken as the average separation of the electrons from the interface.[22] In addition to these simplifications alloy disorder scattering was not taken into account.

An important feature of an electron gas confined in a 2d potential well is the quantization of the electron energy in the potential well leading to a splitting of the three-dimensional conduction band into two-dimensional subbands. The importance of inter-subband scattering has been implicated in numerous experimental investigations.[5,6,21,23] To date, however, apart from treatment of the phonon scattering,[17,18] the mobility calculations of 2DEG in MDH have been carried out considering only intra-subband scattering.[22,15]

In this paper we have formulated a model to calculate electron mobilities in 2DEG confined in a triangular well, taking into consideration all major scattering mechanisms, and considering both intra- and inter-subband scattering.[24,25] This paper has been structured as follows: In Section II we discuss essential features of the MDH used for the confinement of the electron gas. Also, the energetic structure of 2DEG in a triangular well is described. The relaxation times for all the considered scattering processes including intra- as well as inter-subband transitions are obtained in Section III. Results of this section are then applied in Section IV to calculate characteristics of the electron mobility for MDH based on various conducting systems. The results are compared with published experimental data. Summary and conclusions are given in Section V.

II. Electronic Structure of Single Quantum Well

We consider the single quantum well at the interface of two semiconductors of different electron affinities and band gaps. As shown schematically in Fig. 1, the larger affinity semiconductor (S1 at $z \gtrsim 0$) is nominally undoped, while the lower affinity semiconductor (S2 at $z < 0$) is selectively doped, i.e., it contains the undoped region $-d < z < 0$ (commonly referred to as the "spacer") and the region $z \lesssim -d$ highly doped with shallow donors. As a result of the electron affinity difference, electrons from the donors in S2 are transferred to S1, and accumulate in the vicinity of the interface; this results in a strong electric field perpendicular to the interface. This field leads to a quantization of the energy band structure: the subband energies and their separation depend on the electric field. In general, the electric field varies with the distance from the interface, and an accurate description of wavefunctions and eigenvalues would require elaborate numerical calculations. However, it has been found that the single quantum well of the MDH can be effectively approximated by a finite triangular well. In this approach the eigenvalues and wavefunctions for the ground and first excited subbands can be expressed in a simple manner, using one independent parameter related to the electric field within the well. For the ground subband (0) and excited subband (1), the wavefunctions are:[14,18]

$$\psi_o(\vec{r},z) = \phi_{k_x k_y}(r)\chi_o(z) = \phi_{k_x,k_y}\frac{z\exp(-\frac{b_o z}{2})}{(b_o^3/2)^{1/2}} \qquad (1a)$$

$$\psi_1(\vec{r},z) = \phi_{k_x,k_y}(\vec{r})\chi_1(z) = \phi_{k_x,k_y}A(\frac{2}{b_o^3})^{1/2}z(1-Bz)\exp(-\frac{b_1 z}{2}) \qquad (1b)$$

where $\phi_{k_x,k_y}(\vec{r})$ is the two-dimensional plane wave
$A = [3b_1^5 b_o^3/4(b_o^2 - b_o b_1 + b_1^2)]^{1/2}$ and $B = (b_o + b_1)/6$.

The parameters b_o and b_1 were evaluated by comparing the roots of the wavefunctions and their first derivatives for (0) and (1) subbands, given by eqs. (1a) and (1b) with roots of corresponding wavefunctions derived from the Airy-function solutions for a triangular well. For a given effective mass of the electron, m^*, there is a relationship between b_o and b_1. Thus, for GaAs it is found that $b_1 \approx 0.754 b_o$, which in turn gives the following relationships: $A \simeq 0.47(b_o)^3$, $B \approx 0.292 b_o$. Therefore, the forms of the wavefunctions (1a) and (1b) are determined by one parameter, b_o. On the other hand, the parameter b_o is determined by the electric field within the well, or equivalently, by the electron gas density, $b_o \propto (N_s)^{0.36}$. (2)

The energies of the (0) and (1) subbands are

$$E_{0,1}(k) = E_{0,1} + \frac{\hbar^2 k^2}{2m^*} \qquad (3)$$

where $\vec{k} = (k_x, k_y)$ is a two-dimensional wavevector and $E_{0,1}$ are the energy band minima of the ground (0) and excited (1) subbands, respectively. The total number of electrons in the well per unit area, i.e., the electron gas density, N_s, is given by the equation,

$$N_s = \frac{m^*}{\pi\hbar^2} \sum_{i=o}^{j\max} [\theta(E_F - E_i)(E_F - E_i)] \qquad (4)$$

where $\theta(E) = \begin{cases} 0 \text{ for } E < o \\ 1 \text{ for } E \geq o \end{cases}$

The equation (4) is used to determine the Fermi wavevector for the electrons in the ground subband.

In our approach the energy separation $\Delta_{10} = E_1 - E_o$ depends on the electric field, or equivalently on the parameter, b_o; For example, for the case of GaAs

$$\Delta_{10} = 1.23 \times 10^{-11} (b_o)^{1.93} \text{meV}. \qquad (5a)$$

where b_o is in cm^{-1}. Thus, the critical gas density N_s^{crit} at which the Fermi energy E_F reaches the first excited subband is given by,

$$\Delta_{10} = E_F^{crit} = \frac{\pi\hbar^2}{m^*} N_s^{crit} \qquad (5b)$$

since b_o can be expressed in terms of N_s in the present model (see eq. (2)), one has to include only two parameters, N_s and N_s^{crit}, to completely define the system.

In equilibrium the transfer electrons from the doped region to the well[15] of the MDH shown in Fig. 1 is governed by the following equation:

$$E_o + E_F = V_o - E_b - \frac{4\pi e^2 (N_s + N_{depl})^2}{2\epsilon_s N_i^r} - \frac{4\pi e^2}{\epsilon_s}(N_s + N_{depl})d \qquad (6)$$

where V_o is the conduction band energy offset, E_b is the donor binding energy in the doped part of semiconductor S2, ϵ_s is the static dielectric constant, N_{depl} is the areal concentration of ionized donors in depleted regions of (S1). The above equation was used to calculate the concentration of ionized remote impurities, N_i^r, as a function of electron gas density, N_s, and undoped spacer width, d.

III. Scattering Mechanisms

There are certain features which distinguish electron transport in two- and three-dimensions. For example, in the case of ionized impurities, there are two distinctly different types of scattering in the two-dimensional case: Electrons can be scattered by remote impurities located within the doped region of the S2 semiconductor as well as by residual background impurities in the S1 semiconductor. Also, there is the possibility of scattering by interface charges, located at the heterojunction interface.

The dominant scattering mechanisms for bulk III-V compounds are now well established.[26] In our calculations of electron mobility in the 2DEG we included all these mechanisms, and in addition included scattering processes unique to the 2DEG structures, as alluded to above. We consider a range of electron gas densities which justifies the use of degenerate electron statistics at temperatures below 60 K. Therefore, the inverse of the total relaxation time $1/\tau_{tot}$ can be calculated from the sum of the scattering rates for the

individual processes:

$$1/\tau_{tot} = \sum_i 1/\tau_i \qquad (7)$$

At higher temperatures, relation (7) may not be valid due to the limited applicability of degenerate statistics, and also of the relaxation time approximation for the polar optical phonon scattering. However, for temperatures higher than 60 K the scattering in 2DEG is dominated by polar scattering. Accordingly, we have calculated this scattering separately using general Fermi-Dirac statistics in a three-dimensional approximation. In our calculations of electron transport, we consider the two lowest subbands (0) and (1). In general, to calculate electron transport in such systems, one must treat the two subbands as coupled through intersubband (0↔1) scattering. For low electron gas densities, subband (1) is empty, and the conductivity within this subband does not contribute to the total conductivity. The major effect of subband (1) is through the density of the final states available for the scattering of electrons; it increases abruptly when the Fermi energy exceeds the energy separation between two subbands, Δ_{10}. Intersubband scattering would result in an abrupt decrease of the electron mobility for electron concentrations exceeding N_s^{crit}. However, since the actual density of states function is broadened, one expects a gradual increase of inter-subband scattering for N_s close to N_s^{crit}. We included these effects by considering the broadening to be described by a simple Lorentzian function with energy independent broadening parameter Γ. The relaxation time for inter-subband scattering is then modified in the following way:

$$\left(\frac{1}{\tau_i(E)}\right)_{broad} = \left(\frac{1}{\tau_i(E)}\right)_{unbroad.} \frac{1}{\pi}\left[\frac{\pi}{2} + \tan^{-1}\left(\frac{E-E_1}{\Gamma}\right)\right]. \qquad (8)$$

(4)

Phonon scattering

It has been shown[26] that phonon scattering plays an important role in limiting the electron mobility in III-V semiconducting compounds. The most important phonon scattering processes are: (i) deformation potential acoustic, (ii) piezoelectric acoustic, and (iii) polar optical scattering. To calculate the matrix elements for the appropriate scattering process, a quasi three-dimensional approximation was adopted, in which the perturbing potential has a spherical 3d type symmetry. Using the two-dimensional wavefunctions of equation (1), the square of the matrix elements for phonon scattering are:

$$|I_o|^2 = |\langle \psi_o(\vec{R}) | e^{i\vec{Q}\vec{R}} | \psi_o(R) \rangle|^2 = \frac{b_o^6}{(b_o^2+q_z^2)^3} \delta(\vec{k}-\vec{k}'-\vec{q}) \qquad (9)$$

where

$\vec{Q} = (\vec{q}, q_z)$ and $\vec{R} = (\vec{r}, z)$ for intra-subband scattering, and

$$|I_1|^2 = |\langle \psi_1(\vec{R}) | e^{i\vec{Q}\vec{R}} | \psi_o(\vec{R}) \rangle|^2 = \frac{4A^2 q_z^2}{(\alpha^2+q_z^2)^4} \delta(\vec{k} - \vec{k}' - \vec{q}) \qquad (10)$$

where $\alpha = 3B = (b_o+b_1)/2$ for inter-subband scattering. The relaxation time for deformation potential scattering is given by

$$\frac{1}{\tau_i^{0,1}} = \frac{R_{av}}{2\pi\hbar} \int_o^{2\pi} d\theta \int dq_z \int q dq C_i (1-\cos\theta) \quad |I_{o,1}|^2 \delta[E_o(\vec{k}) - E_{0,1}(\vec{k}+\vec{q})] \qquad (11)$$

where i refers to either deformation potential or piezoelectric scattering, with $C_i = C_{ac} = \frac{D^2 k_B T}{2C_\ell}$ for the deformation potential scattering and $C_i = C_{pe} \frac{e^2 k_B T P^2}{\epsilon_s (q^2+q_z^2)}$ for piezoelectric scattering. θ is the angle between $\vec{k}$ and $\vec{k}+\vec{q}$, D is the deformation potential constant, P is the piezoelectric coefficient, C_ℓ is the longitudinal elastic constant, R_{av} is defined by the equation,

$$R_{av} = (2N_p + 1) \frac{\hbar u_\ell k_F}{2k_B T} \qquad (12)$$

where $N_p = \left(\frac{1}{\exp\left(\frac{\hbar u_\ell k_F}{k_B T}\right) - 1}\right)$

The factor R_{av} approximately accounts for the phonon occupation number at very low temperatures, where the phonon energy $\hbar u_\ell k_F$ is comparable to $k_B T$. We have approximated the average wavevector of phonons participating in the scattering process by the value of the electron wavevector at the Fermi energy. To a good approximation R_{av} equals unity at temperatures exceeding 5 K. At very low temperatures $N_p \to 0$, and therefore, as seen from equation (12), the relaxation rates for phonons saturate.

Standard integration of the equation (11) gives the following results for the relaxation times.

$$\frac{1}{\tau^o_{ac}} = \frac{3m^* D^2 k_B T b_o}{16\hbar^3 C_\ell} R_{av} \qquad (13)$$

and $1/\tau^1_{ac} = b_{eff}/\tau^o_{ac} b_o$,

$$b_{eff} = \frac{2}{3}\frac{A^2}{\alpha^5} \qquad (14)$$

For the piezoelectric scattering,

$$\frac{1}{\tau^o_{pe}} = \frac{e^2 k_B T P^2 m^*}{2\pi \epsilon_s \hbar^3 k^2} I(k, b_o) \qquad (15)$$

where $I(k,b_o) = \frac{3\pi(4k^2 - b_o^2) - 4kb_o(5b_o^2 - 8k^2)}{16b_o^5(4k^2 - b_o^2)^2}$ -

$$-\frac{3}{16(4k^2-b_o^2)^2}\begin{cases}\dfrac{1}{\sqrt{4k^2-b_o^2}}\log\left(\dfrac{2k-\sqrt{4k^2-b_o^2}}{2k+\sqrt{4k^2-b_o^2}}\right) & : 2k > b_o \\ \dfrac{2}{\sqrt{b_o^2-4k^2}}\text{Arcos}\left(\dfrac{4k^2}{b_o^2}\right) & : 2k \le b_o\end{cases}$$

and

$$\frac{1}{\tau_{pe}^{1}} = \frac{2A^2e^2k_BTP^2m^*}{\varepsilon_s\hbar^3k}\int_{-\infty}^{\infty}\frac{q_z\,dq_z}{(k^2+q_z^2)(\alpha^2+q_z^2)^4} \qquad (16)$$

The relaxation time for inter-subband scattering was obtained in an approximate manner. Since the wavevectors of electrons in the excited subband are much smaller than those in the ground subband, we have assumed that the wavevector change can be approximated by $|\vec{k}_o-\vec{k}_1| \approx |\vec{k}_o| = k_F$. This is a good approximation for the electron density N_s, which is not much larger than N_s^{crit}.

Both of the aforementioned scattering processes are elastic, and therefore the relaxation time approximation could be used. However, polar optical scattering in GaAs is highly inelastic, due to the large optical phonon energy, $\hbar\omega_o$ = 36 meV. Therefore, a proper treatment of this mechanism in a two-dimensional formalism, would necessitate the inclusion of all the excited subbands which are separated from the Fermi energy by less than the optical phonon energy. The scattering rate is thus the sum of many inter- and intra-subband scattering processes over a wide energy range. This will result in a smearing out of the features which are characteristic of confinement of electrons in a two-dimensional system[18] including the electron density distribution within the well. Therefore, it can be argued that the three-dimensional approach to polar optical phonon scattering is justifiable also for 2DEG. Accordingly, the optical phonon contribution was calculated using a variational method developed for bulk semiconductors.[27]

Alloy-Disorder Scattering

For MDH involving ternary compounds, the additional scattering due to alloy disorder potential should be included. Two distinct types of heterostructures may be invisaged in which the 2DEG is confined either within the alloy, or within the compound semiconductor. In the latter case, alloy disorder scattering affects only the electrons which have penetrated into the alloy. In the former case, practically all of the electrons are subject to alloy disorder scattering. As both deformation potential acoustic and alloy disorder scattering result from short-range potentials, there is a formal similarity between the relaxation times in both cases. Thus, for intra-subband scattering the relaxation time can be written as[28,29]

$$\frac{1}{\tau^{0,1}_{alloy}} = \frac{m^* x(1-x)\Omega \langle V \rangle^2}{\hbar^3} I^{0,1}_{alloy} \qquad (17)$$

where x is the mole fraction composition of the ternary alloy, $\langle V \rangle$ is the alloy disorder scattering parameter, Ω is the unit cell volume. For electrons within the alloy,

$$I^0_{alloy} = \int_0^\infty |\chi_o(z)|^4 dz = \frac{3}{16} b_o \qquad (18)$$

$$I^1_{alloy} = \int_0^\infty |\chi_o(z)|^2 |\chi_1(z)|^2 dz = \frac{3}{16} b_{eff} \qquad (19)$$

with b_{eff} given by eq. (14). However, for the 2DEG within the compound semiconductor,

$$I^o_{alloy} = \int_{-\infty}^0 |\chi'_o(z)|^4 dz \qquad (20)$$

and

$$I^1_{alloy} = \int_{-\infty}^0 |\chi'_o(z)|^2 |\chi'_1(z)|^2 dz \qquad (21)$$

where

$\chi'_{0,1}(z) = M_{0,1} \exp(\sqrt{2m^*V_o/\hbar^2}\, z)$ for $z < 0$ is the part of the wavefunction for both ground (0) and first excited subband (1), which describes penetration of the electron gas into the alloy. For large parameter V_o, M_0 and M_1 can be approximately determined from the balance of the forces acting on electrons at the interface. Using the approach of ref. 15, one obtains,

$$|M_o|^2 \approx \frac{4\pi e^2}{\epsilon_s V_o} \left(\frac{1}{2} N_s + N_{depl} \right) \tag{22}$$

and

$$|M_1|^2 \approx \frac{4\pi e^2}{\epsilon_s V_o} \left[g N_s + N_{depl} \right] \tag{23}$$

where $g = \left\{ 1 - \frac{4A^2}{b_o(\alpha+b_o)^3} \left[\frac{6}{(\alpha+b_o)^2} + \frac{3}{(\alpha+b_o)b_o} + \frac{1}{b_o^2} \right.\right.$

$$\left.\left. - \frac{\alpha}{\alpha+b_o} \left(\frac{10}{(\alpha+b_o)^2} + \frac{4}{(\alpha+b_o)b_o} + \frac{1}{b_o^2} \right) \right] \right\}$$

In our calculations the screening of acoustic phonon and alloy disorder scattering by free carriers was neglected. This effect certainly should be included for all long-range interactions such as electron-piezoelectric acoustic phonon interaction. However, it is not obvious whether the short-range potentials, such as alloy disorder and deformation potential acoustic should be screened by free carriers. Most of the analyses of transport in three-dimensional electron gas have neglected this type of short-range potential screening.

Ionized Impurity Scattering

The scattering of electrons confined in a triangular well by a screened ionized impurity potential was originally considered for silicon inversion

layers.[12] The relaxation time for this scattering process can be written in the following general form.[15]

$$\frac{1}{\tau^{0,1}_{ion}} = \frac{2\pi e^2}{\hbar} \int_{-\infty}^{\infty} dz N_i(z) \int_0^{2\pi} d\theta \int \frac{dq}{q} \frac{(1-\cos\theta)}{\varepsilon^2(q)}$$

$$\delta\{E_0(\vec{k}) - E_{0,1}(\vec{k}+\vec{q})\} |F^{0,1}(q,z)|^2 \qquad (24)$$

where

$$F^{0,1}(q,z) = \int dz' \chi_0^*(z') \chi_{0,1}(z') \exp(-q|z-z'|), \qquad (25)$$

$$\varepsilon(q) = \varepsilon_s\left(1 + \frac{q_s}{q}\right), \qquad (26)$$

and q_s is the screening parameter defined in the appendix.

As an approximation for the dielectric function for inter-subband scattering the dielectric function for ground subband was used. This approximation is expected to be good, as long as the occupation of the excited subband is small. The function $N_i(z)$ represents the impurity distribution in the heterostructure and is shown in Fig. 1a. The integration over z can be divided into four integrals, corresponding to remote scattering from the doped region of the S2 semiconductor, ($z<-d$) the undoped spacer ($-d<z<0$), from interface charges at $z=0$ and from background residual impurities in the undoped semiconductor ($z>0$). The expressions for relaxation times due to all of these scattering processes are given in the Appendix.

As discussed in the previous section, eq. (6) gives the relationship between the 2DEG density in the well and the concentration of remote ionized impurities. Thus, the only unknown parameters are the densities of residual ionized impurities in the spacer, N_i^s, residual impurities in the well, N_i^b, and the charge localized at the interface, N_i^{int}. It should be noted, however,

that the contribution of ionized impurities located within the spacer is negligible for densities lower than about $3 \times 10^{15} cm^{-3}$.

Another scattering mechanism which has been found to be important for silicon inversion layers is the surface (or interface) roughness scattering.[15] In the case of MDH, part of this scattering process is included in the alloy disorder scattering. Furthermore, interfaces extremely flat (on an atomic scale) are obtainable by the state-of-the-art MBE, and thus, this scattering mechanism was excluded from the present calculations.

IV. Mobility Charscteristics of Modulation Doped Heterostructures

Lattice matching represents one of the most severe limitations on achieving high quality MDH. To date, three semiconducting alloy systems have been shown to be suitable for MDH, namely, GaAs-(Ga,Al)As, $In_{0.53}Ga_{0.47}As$ - InP[30] and $In_{0.53}Ga_{0.47}As$-$In_{0.48}Al_{0.52}As$.[31,32] In the first case, the 2DEG is primarily confined in the GaAs, whereas in the latter two cases the electrons are located within the $In_{0.53}Ga_{0.47}As$. In Table I, all the parameters used to calculate the electron mobility are listed. The values of the effective masses given are somewhat higher than for the bulk material; this is commonly attributed to the non-parabolicity of the conduction band.[15] There is a large margin of uncertainty regarding the values of the alloy disorder parameters. However, several studies on GaAlAs have estimated this parameter to lie in the range of 0.8-1.0 eV.[35,36] In the case of (Ga,In)As MDH, since alloy disorder scattering dominates low temperature scattering, we were able to determine this parameter by fitting the available experimental data[31] with our theoretical model.

The highest electron mobilities reported for MDH were obtained for the (Ga,Al)As-GaAs system[20,21] at low temperatures. In fact, most of the work on single quantum well-MDH has been reported for this system.

Temperature Dependence of Mobility

A basic mobility characteristic of MDH, which reveals the importance of the different mechanisms, is temperature dependence of the electron mobility. In Figs. 2 and 3 the calculated electron mobilities in the range 1-300 K are given for (GaAl)As GaAs together with experimental data of refs. 21 and 20, respectively. The component mobilities are also presented. At high temperatures, polar optical phonon scattering is the dominent scattering mechanism; on the other hand, at low temperatures electron mobility is limited by deformation potential acoustic and piezoelectric acoustic phonon scattering, together with alloy-disorder scattering and ionized impurity scattering. The equilibrium concentration of remote ionized impurities in the doped region of the semiconductor S2 is related to the interface electron density N_s and the spacer width, d, by equation (6). Therefore, remote ionized impurity scattering is always present in MDH. Thus, an "inherent limit" determined by alloy disorder, phonon and remote ionized impurity scattering, exists for a given MDH. In Fig. 2, the inherent mobility limit saturates at low temperatures at about $1.5 \times 10^6 cm^2/Vs$; the experimental data points of ref. 21 lie very close to this limit, indicating that the other scattering mechanisms are not significant in this case. Slightly lower values of experimental mobility at low temperatures may be attributed to temperature-independent scattering processes. In fact, an excellent agreement is obtained when a small contribution from background ionized impurity scattering at a concentration of $9 \times 10^{13} cm^{-3}$ (which is very close to the ionized impurity concentration one expects for "undoped" GaAs) is included. This result is a clear indication that additional scattering mechanisms such as surface roughness and/or interface charge scattering are not appreciable in this case. Alloy disorder is also insignificant for such low electron densities.

As seen in Fig. 1, these mechanisms only contribute at very low temperatures, resulting in a slight lowering of the absolute limit defined purely by phonons.

In Fig. 3 experimental results of ref. 20 for MDH with spacer width of 230 Å are given, together with the results of the theoretical calculations. The solid points correspond to experimental data taken in the dark. These experimental mobilities are much lower than the inherent limit. To account for this discrepancy additional contributions are required from scattering by background impurity, interface charges and/or surface roughness scattering. The higher mobility values (open circles in Fig. 3) correspond to data measured under illumination. As a result of the persistent photoconductivity effect, illumination increases the 2DEG density in the well from $2.2 \times 10^{11} cm^{-2}$ to about $3.8 \times 10^{11} cm^{-2}$. Taking this into account, we have calculated the total electron mobility both in the dark and under illumination, assuming additional contributions from background ionized impurities at the same level of $1 \times 10^{15} cm^{-3}$. Good agreement with experiment is seen in Fig. 3 at both electron densities. As discussed in ref. 15, the surface roughness scattering rate rapidly increases (corresponding mobility decreases) with increasing N_s; therefore, the observed mobility increase upon increase of N_s could not have been explained if surface roughness scattering was important.

The saturation of the phonon-limited electron mobility at very low temperatures results from the temperature dependence of the phonon occupation (see eq. (12)) and leads to a saturation of the absolute electron mobility at $\sim 9 \times 10^6 cm^2/Vs$ for $N_s = 3.8 \times 10^{11}$ and at $1.8 \times 10^7 cm^2/Vs$ for $N_s = 2.2 \times 10^{11}$.

Electron Density Dependence of Mobility

The 2DEG density may be continuously varied in MDH by external means: for example, illumination or gate voltage. Corresponding mobility changes are very pronounced, and they are of practical and fundamental importance. In Fig. 4, the calculated values of component mobilities of individual scattering processes are given as functions of N_s. There are two reasons why these processes exhibit N_s dependences; first, direct dependence on k vector, and secondly dependence on the parameter b_o. For example, acoustic deformation potential scattering mobility decreases with N_s, solely due to the dependence of b_o on N_s, derived using considerations of section II. Alloy disorder scattering exhibits the strongest N_s dependence, which originates from the enhanced penetration of the 2DEG into the alloy with increasing N_s (see eqs. (22) and (23).

The alloy disorder mobilty values in Fig. 4 are more than one order of magnitude greater than mobility calculated by Ando,[15] for the same MDH and using the same alloy disorder potential. The reason for such a large discrepancy is not known at present; however, it certainly cannot be attributed to our approximate description of the penetration of the electron gas into the GaAlAs. It should be emphasized that the present model is in agreement with calculations reported in ref. 28. Using our formulae, we have calculated alloy disorder mobility limited by scattering within the barrier of InP-In(Ga)As, i.e., for the conditions similar to those outlined in footnote 9 of ref. 28. Adopting the same set of parameters we obtain $\mu_{alloy} \approx 1.06 \times 10^8 cm^2/Vs$ as compared with the value $9.5 \times 10^7 cm^2/Vs$ of ref. 28.

The increase of the experimental mobility seen in Fig. 4 with increasing N_s may be attributed to the presence of background and remote ionized impurities. The mobility due to these scattering mechanisms increases strongly with N_s.

Accordingly, as seen in Fig. 4, for the MDH with the spacer width d = 150 Å the ionized impurity electron mobility can be expressed in the form $\mu \sim N_s^{\gamma}$ with γ = 1.4 and 1.2 for remote and background impurity scattering, respectively.

At higher N_s, values ($>7 \times 10^{11} cm^2$), effects of inter-subband scattering are important. They result in a lowering of the electron mobility compared with simple intra-subband scattering, as seen in the insert of Fig. 4. The most pronounced drop in the electron mobility is obtained for alloy disorder scattering; this may be attributed to the large overlap of the parts of the electron wavefunctions for ground (0) and (1) states, which describe penetration of the 2DEG into the GaAlAs. On the other hand, inter-subband scattering for remote ionized impurities at finite spacer widths is negligible, owing to the exponential factor $\exp(-2|\vec{k}_o - \vec{k}_1|d)$ (see eq. (A2) of the Appendix). The combination of all the aforementioned scattering processes can provide an excellent explanation of the experimental date of ref. 21, both at 5 K and at 77 K. In the latter case optical phonons were included, with $\mu_{opt} \simeq 6.5 \times 10^5 cm^2/Vs$.

Spacer Width Dependence of Mobility

The basic concept of MDH is to separate the 2DEG from parent ionized donors, thereby limiting ionized impurity scattering from these remote centers. This consideration would dictate maximizing the spacer width, d, to maximize the mobility. However, according to eq. (6) an increase of d leads to a decrease in the 2DEG density in the well, which has a deleterious effect on the electron mobility.

Importance of high N_s is highlighted in device applications of MDH, where one is more concerned with maximizing the channel conductivity ($\sigma_{ch} = eN_s\mu_e$) rather than just the mobility values. Fig. 5 gives the calculated component electron mobilities evaluated at maximum conductivities as a function of d.

The inherent mobility limit increases rapidly with increasing spacer width, reaching mobilities of about 2 x $10^6 cm^2/Vs$ at large spacer widths (>350 Å). The introduction of 1 x $10^{15} cm^{-3}$ background ionized impurities significantly alters this dependence, resulting in a peak mobility at $d \approx 160$ Å. Higher background impurity concentrations shift the peak mobility to successively lower d values. The background concentration as a function of d at which the electron mobility attains its maximum value is given in Fig. 6; for MDH exhibiting high mobility the maximum shifts to very large spacer widths. This behavior can qualitatively explain the reported mobility dependences on spacer width given in the literature; it has been found that in very high mobility MDH the mobility increases continuously with d,[20,21] whereas it has a distinct maxima for lower mobility MDH.[37]

In Fig. 7 the maximum inherent conductivity σ_{inh}^{max} (maximized with respect to N_s at a given d), is plotted versus spacer width. Also, the N_s and N_i^r values required to maximum σ_{inh} are given in this figure. The ionized impurity scattering is very sensitive to the distribution of ionized impurities and is therefore altered by smearing out the doping profile resulting from diffusion of impurities into the space, or even the well. This would have an especially profound effect at small spacer widths. However, it should be negligible for MDH with larger spacers exhibiting higher electron mobilities.

In(Ga)As-Based MDH

MDH based on $In_{0.53}Ga_{0.47}As$, and lattice matched to either InP[30] or $Al_{0.52}In_{0.48}As$[31] have recently attracted a lot of interest. In these structures, the 2DEG is confined within the ternary compound In(Ga)As rather than on a binary system (GaAs) discussed above; therefore, it has been soon realized[28,29] that alloy disorder scattering should play a much more prominent role. We have applied our model to the $In_{0.53}Ga_{0.47}As$-$Al_{0.52}In_{0.48}As$ MDH.

Fig. 8 gives the total electron mobility, calculated as a function of temperature using the parameters listed in Table I, and compared with the experimental data of ref. 31. As stated in ref. 31, for $N_s > 4.5 \times 10^{11} cm^{-2}$, the first excited band is already occupied, and thus inter-subband scattering should be included. We have calculated the electron mobility including both intra- and inter-subband scattering processes. It should be noted that our results for the intra-subband alloy disorder scattering are in very good agreement with calculations of ref. 28 where only the ground subband was considered. Inclusion of the inter-subband scattering results in about 29% lower alloy disorder mobility. Background impurity scattering was calculated using the limits for the background ionized impurity concentration given in ref. 31 (N_I^b = 0.5 to 1 x $10^{16} cm^{-3}$). By fitting the calculated mobilities to the experimental values at low temperatures, we were able to determine the alloy disorder scattering parameter in this system. This determination is believed to be very accurate, as alloy scattering is the primary scattering mechanism limiting the electron mobility. Within this range of background impurity concentration, we have determined this parameter to be in the range 0.55 - 0.63 eV, which compares favorably with the bulk value of 0.60 eV as determined in ref. 38.

In the case of InGaAs-GaAlAs MDH, one may expect a different electron mobility dependence on N_s compared to GaAs-GaAlAs MDH. This originates from the opposite dependence of the electron mobility on N_s for alloy disorder scattering as contrasted with ionized impurity scattering. N_s dependence can therefore provide information about the relative contribution of alloy disorder scattering to the total mobility.

Summary and Conclusions

In conclusion, we have presented a model for electron mobility calculations which is directly applicable to single quantum well modulation-doped heterostructures. In this model a triangular well approximation for the confinement potential was used. All the major scattering processes were included, considering both intra- and inter-susbband transitions. Therefore, all the basic mobility characteristics of the 2DEG could be explained. We successfully described electron mobility over a broad range of temperatures (1-300 K) and electron densities (10^{11}-10^{12} cm^{-2}). These calculations provided limits on the electron mobilities that are attainable in various semiconducting systems. In GaAs-$Ga_{1-x}Al_xAs$ heterostructures the inherent mobility limit increases with decreasing temperatures, reaching at very low temperatures a limit of about 2×10^6 for $x = 0.3$ and at large spacer widths. On the other hand, for $In_{0.53}Ga_{0.47}As$-based heterostructures, alloy disorder scattering limits the mobility to a level ($\sim 10^5$ cm^2/Vs) at temperatures below 60 K. An accurate determination of alloy disorder scattering potential parameter, $\langle V \rangle$ for InGaAs mixed crystals was therefore made. For both semiconducting systems considered, at temperatures above 60 K, optical phonons begin to limit the mobility. Furthermore, we have analyzed the effect of spacer width in optimizing channel electron conductivity. Our results show that for the highest quality heterostructures maximum channel conductivity is only achieved at very large spacer widths, whereas for heterostructures exhibiting mobilities well below the inherent limit, an optimum spacer width is predicted.

ACKNOWLEDGEMENT

The authors are grateful to the National Aeronautics and Space Administration for financial support.

TABLE I. Parameters employed in present publication.

MDH	GaAlAs-GaAs	$In_{0.53}Ga_{0.47}As$-$Al_{0.52}In_{0.48}As$
Parameter		
Electron effective mass, m*	$0.076m_o$ [a]	$0.05\ m_o$ [f]
Deformation potential D(ev)	7 [b]	7 [b]
Elastic constant, c_ℓ (dyn/cm^2)	13.97×10^{11} [b]	13.09×10^{11} [b]
Piezoelectric constant, P	0.064 [c]	0.034 [b]
Static dielectric constant, ε_o	12.9 [b]	13.8 [b]
High freqency dielectric constant, ε_∞	10.9 [b]	10.3 [b]
Optical phonon energy, $\hbar\omega_o$ (meV)	36 [b]	39.3 [b]
Alloy disorder parameter, $\langle V \rangle$(eV)	1 [d]	0.63 - 0.55
Conduction band energy offset, V_o, (eV)	0.3 [e]	0.53 [g]

[a] Ref. 33
[b] Ref. 26
[c] Ref. 34
[d] Ref. 35
[e] Ref. 15
[f] Ref. 31
[g] Ref. 30

REFERENCES

(a) Permanent address: Institute of Physics, Polish Academy of Sciences, Warsaw, Poland.

(b) Present address: University of Toronto, Downsview, Ontario, Canada.

1. L. Esaki and R. Tsu, IBM Res., International Rep. RC 2418, March 26 (1969).
2. R. Dingle, H.L. Störmer, A.C. Gossard and W. Wiegmann, Appl. Phys. Lett. 33, 665 (1978).
3. S. Hiyamizu, T. Mimura, T. Fuji, K. Nanbu and H. Hashimoto, Jap. J. Appl. Phys. 20, L245 (1981).
4. T.J. Drummond, H. Markoç and A.Y. Cho, J. Appl. Phys. 52, 1380 (1981).
5. D.C. Tsui, A.C. Gossard, G. Kaminsky and W. Wiegmann, Appl. Phys. Lett. 39, 712 (1981).
6. H.L. Störmer, A.C. Gossard, W. Wiegmann and K. Baldwin, Appl. Phys. Lett. 39, 912 (1981)
7. K.Y. Cheng, A.Y. Cho, T.J. Drummond and H. Markoç, Appl. Phys. Lett. 40, 147 (1982).
8. S. Mori and T. Ando, Surface Sci. 98, 101 (1980).
9. K. Hess, Appl. Phys. Lett. 35, 484 (1979).
10. B.K. Ridley, J. Phys. C: Solid State 15, 5899 (1982).
11. J. Lee, H.N. Spector and V.K. Arora, Appl. Phys. Lett. 42, 363 (1983).
12. F. Stern and W. Howard, Phys. Rev. 163, 816 (1967)
13. F.F. Fang and W.E. Howard, Phys. Rev. Lett. 16, 797 (1966).
14. T. Ando, A.B. Fowler and F. Stern, Rev. Mod. Phys. 54, 437 (1982).
15. T. Ando, J. Phys. Soc. Jap. 51, 3900 (1982).

16. F. Stern, Appl. Phys. Lett. 43, 974 (1983).

17. P.J. Price. Ann. of Phys. 133, 217 (1981).

18. P.J. Price, Surf. Sci. 113, 199 (1982).

19. P.K. Basu and B.R. Nag, Phys. Rev. B22, 4849 (1980).

20. J.V. DiLorenzo, R. Dingle, M. Feuer, A.C. Gossard, R. Hendel, J.C.M. Hwang, A. Kastalsky, V.G. Keramides, R.A. Kelhl and P. O'Connor, IEDM Tech Dig. 25, 578 (1982).

21. S. Hiyamizu, J. Saito, K. Nanbu and T. Ishikawa, Jap. Jour. Appl. Phys. 22, L609 (1983).

22. K. Lee, M.S. Shur, T.J. Drummond and H. Markoç, J. Appl. Phys. 54, 6432 (1983).

23. H.L. Störmer, A.C. Gossard and W. Wiegmann, Solid State Comm. 41, 707 (1982).

24. The inter-subband scattering for Si inversion layers was considered by S. Mori and T. Ando, Phys. Rev. B19, 6433 (1979).

25. W. Walukiewicz, H.E. Ruda, J. Lagowski and H.C. Gatos, Phys. Rev. B15, to be published.

26. See, for example, D.L. Rode in Semiconductors and Semimetals, edited by R.K. Willardson and A.C. Beer (Academic, New York, 1975) vol. 10, chap. 1.

27. W. Walukiewicz, J. Lagowski, L. Jastrzebski, M. Lichtensteiger and H.C. Gatos, J. Appl. Phys. 50, 889 (1979).

28. G. Bastard, Appl. Phys. Lett. 43, 591 (1983).

29. P.K. Basu and B.R. Nag, Appl. Phys. Lett. 43, 689 (1983).

30. Y. Guldner, J.P. Vieren, P. Voisin, M. Voos, M. Razeghi and M.A. Poisson, Appl. Phys. Lett. 40, 877 (1982).

31. A. Kastalsky, R. Dingle, K.Y. Cheng and A.Y. Cho, Appl. Phys. Lett. 41, 274 (1982).

32. K.Y. Cheng, A.Y. Cho, T.J. Drummond and H. Markoç, Appl. Phys. Lett. 40, 147 (1982).

33. H.L. Störmer, A. Dingle, A.C. Gossard, W. Wiegmann and M.D. Sturge, Sol. State Comm. 29, 705 (1979).

34. J.S. Blakemore, J. Appl. Phys. 53, R 123 (1982).

35. D.J. Chadi and M.L. Cohen, Phys. Stat. Sol. (b) 68, 405 (1975).

36. K. Masu, E. Tokumitsu, M. Konagai and K. Takahashi, J. Appl. Phys. 54, 5788 (1983).

37. T.J. Drummond, H. Markoç and A.Y. Cho, J. Appl. Phys. 52, 1380 (1981).

38. J.R. Hayes, A.R.Adams and P.D. Greene, in GaInAsP Alloy Semiconductors, edited by T.P. Pearsall, (Wiley, New York, 1982).

APPENDIX

The integration in eq. (24) for the ionized impurity scattering rate can be divided into four integrals, corresponding to regions of different ionized impurity concentration: (1) remote ionized impurity scattering from the heavily doped region, $z < -d$, with $N_i(z) = N_i^r$; (2) remote ionized impurity scattering from the ions located within the spacer $-d < z < o$ with $N_i(z) = N_i^s$. Scattering rates from the ions in both of the above-mentioned regions can be expressed in the form

$$\frac{1}{\tau_{r,s}} = C_o \frac{b_o^6}{k^2} \int_0^{2k} \frac{[N_i^s + (N_i^r - N_i^s)e^{-2qd}]qdq}{P_o(q,b_o)\sqrt{4k^2-q^2}} \qquad (A1)$$

for intra-subband scattering and

$$\frac{1}{\tau_{r,s}} = C_1 P_1(k_F,\alpha)[N_i^s + (N_i^r - N_i^s)e^{-2k_F d}] \qquad (A2)$$

for inter-subband scattering where $C_o = \frac{128\pi m^* e^4}{\hbar^3 \epsilon_s^2}$, $C_1 = \frac{2\pi^2 m^* e^4}{\hbar^3 \epsilon_s^2}$,

$\alpha = (b_o+b_1)/2$, $P_o(q,b_o) = [8q(q+b_o)^3 + q_s(8b_o^3 + 9b_o^2 q + 3b_o q^2)]^2$,

$P_1(k,\alpha) = \frac{A^2(\alpha + 2k)^2}{(k+q_s)^2(k+\alpha)^6 k}$ and $q_s = \frac{2e^2 m^*}{\epsilon_s \hbar^2} \frac{E_F}{k_B T}\left(\left[1+\exp\left(-\frac{E_F}{k_B T}\right)\right]\ln\left[1+\exp\left(\frac{E_F}{k_B T}\right)\right]\right)^{-1}$

is the inverse screening length.[14] As seen from eq. (A2), the inter-subband scattering rate due to remote ionized impurity scattering depends on the exponential factor $\exp(-2k_F d)$ which becomes very small at large spacer width, d. Scattering from charges located at the interface with $N_i(z) = N_i^{int}\delta(z)$ gives an inverse relaxation time of the form,

$$\frac{1}{\tau_{int}^o} = 2C_o \frac{b_o^6 N_i^{int}}{k^2} \int_0^{2k} \frac{q^2 dq}{P_o(q,b_o)\sqrt{4k^2-q^2}} \qquad (A3)$$

for intra-subband scattering and

$$\frac{1}{\tau_{int}} = 2C_1 P_1(k_F,\alpha) k_F N_i^{int} \qquad (A4)$$

for inter-subband scattering. Although the concentration of residual background ionized impurities is typically very small, their proximity to the 2DEG results in very effective electron scattering. The scattering rates for intra- and inter-subband scattering are, respectively

$$\frac{1}{\tau_b^o} = \frac{4C_o N_i^b}{b_o k^2} \int_{0.5-x_k}^{0.5} \frac{F(x)(1-2x)}{\sqrt{x_k^2-(0.5-x)^2}}\, dx \qquad (A5)$$

where

$$F(x) = \frac{[69 - 336x + 630x^2 - 580x^3 + 264x^4 - 48x^5]}{[32(1-2x)(1-x)^3 + \beta(10 - 15x + 6x^2)]^2}$$

$$x_k = \frac{k}{b_o} \quad \text{and} \quad \beta = \frac{q_s}{b_o}$$

and

$$\frac{1}{\tau_b^1} = C_1 \frac{8A^2 N_i^b}{(k_F+q_s)^2} \{\frac{C(k_F)^2}{2k_F} - 2C(k_F)R(k_F) + T(k_F)\} \qquad (A6)$$

where $C(k) = 1 - \frac{3B}{\alpha-k}$

$$R(k) = \frac{a_o}{\alpha-k} + \frac{a_1}{(\alpha+k)^2} + \frac{2a_2}{(\alpha+k)^3} + \frac{6a_3}{(\alpha+k)}$$

$$T(k) = \frac{a_o}{2\alpha} + \frac{a_o a_1}{2\alpha^2} + \frac{a_1^2 + 2a_o a_2}{4\alpha^3} + \frac{3[a_o a_3 + a_1 a_2]}{4\alpha^4} + \frac{3[a_2^2 + 2a_1 a_3]}{4\alpha^5} +$$

$$\frac{10a_2 a_3}{\alpha^6} + \frac{45a_3^2}{8\alpha^7},$$

$$a_o = \frac{3B}{\alpha-k} + 1 - \frac{(\alpha-k)^3}{(\alpha+k)^3} + \frac{3B(\alpha-k)^3}{(\alpha+k)^4}$$

$$a_1 = (\alpha-k)\left[1 - \frac{(\alpha-k)^2}{(\alpha+k)^2} - \frac{3B}{\alpha-k} + \frac{3B(\alpha-k)^2}{(\alpha+k)^3}\right]$$

$$a_2 = \frac{(\alpha-k)^2}{2}\left[1 - \frac{\alpha-k}{\alpha+k} - \frac{3B}{\alpha-k} + \frac{3B(\alpha-k)}{(\alpha+k)^2}\right]$$

FIGURE CAPTIONS

Fig. 1. Schematic representation of (a) the doping profile, and (b) the energy configuration for a single quantum well modulation doped heterostructure; see text.

Fig. 2. Temperature dependence of the electron mobility in GaAs-GaAlAs heterostructures. Points are experimental data of ref. 21 for a carrier density of $3 \times 10^{11} cm^{-2}$. The curves are calculated mobilities for this carrier density and a remote ionized impurity concentration of $8.6 \times 10^{16} cm^{-3}$.

Fig. 3. Temperature dependence of the electron mobility in GaAs-GaAlAs heterostructure. The experimental data of ref. 20 were obtained in the dark - ● and under illumination - o with $N_s = 2.2 \times 10^{11} cm^{-2}$ and $3.8 \times 10^{11} cm^{-2}$ respectively. The component mobilities given in the figure were calculated with $N_s = 2.2 \times 10^{11} cm^{-2}$.

Fig. 4. Electron mobility at 5 K and 77 K versus interface carrier density. Solid and open circles correspond to the experimental data of ref. 21 measured in the dark and under illumination, respectively. Theoretical mobilities were calculated using remote and background ionized impurity concentrations of $8.8 \times 10^{16} cm^{-3}$ and $1 \times 10^{15} cm^{-3}$, respectively. The critical concentration is $8 \times 10^{11} cm^{-3}$ corresponding to $N_{dep} = 5 \times 10^{10} cm^{-2}$. The insert shows the effect of inter-subband scattering. The upper curves correspond to the intra-subband mobility, while the lower curves include the effect of the inter-subband scattering with the broadening parameter $\Gamma = 0.5$.

Fig. 5. Electron mobility values at maximum conductivity ($eN_s\mu_e$) versus spacer width for GaAs-$Ga_{0.7}Al_{0.3}As$ at 5 K. The "total" curve corresponds to a background impurity concentration $N_i^b = 1 \times 10^{15} cm^{-3}$.

Fig. 6. Background ionized impurity concentration and mobility for GaAs-$Ga_{0.7}Al_{0.3}As$ as a function of spacer width at which mobility attains its maximum value.

Fig. 7. Maximum inherent channel conductivity (maximized with respect to the charge density) as a function of the spacer width. The corresponding charge density and remote ionized impurity concentration are also given in the figure.

Fig. 8. Electron mobility is $In_{0.53}Ga_{0.47}As$-$Al_{0.52}In_{0.48}As$ with 80 Å spacer width. Experimental data points are from ref. 31. The theoretical mobility was calculated for N_s taken from ref. 31 with $N_s^{crit} = 4.5 \times 10^{11} cm^{-2}$ and $N_{dep} = 0$. The upper and lower background ionized impurity limited mobilities correspond to $N_i^b = 0.5 \times 10^{16}$ and $1 \times 10^{16} cm^{16}$, respectively. Alloy disorder scattering potential was used as a fitting parameter.

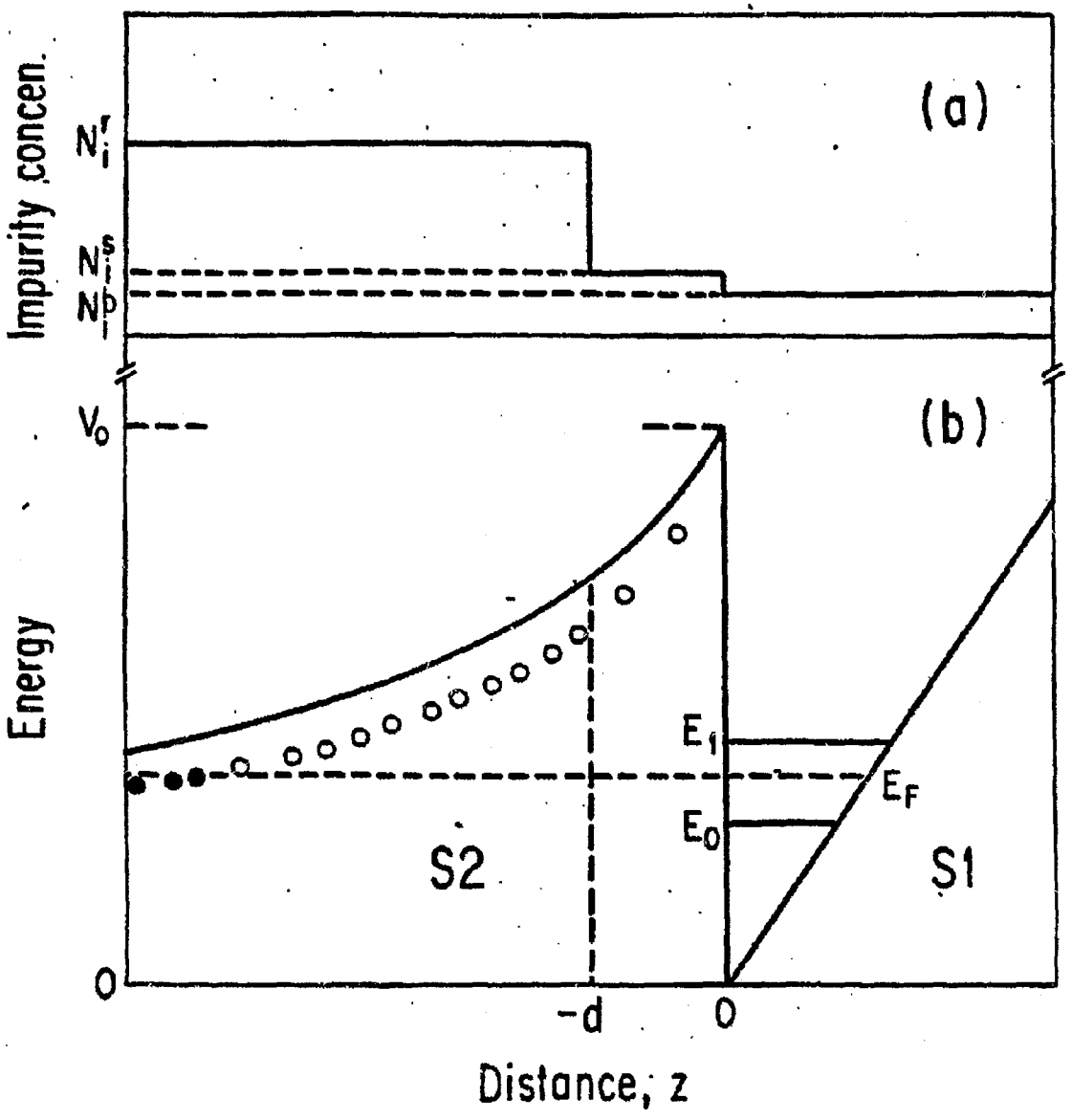
Impurity concen.
N_i^r
N_i^s
N_i^p
(a)
V_0
(b)
Energy
E_1
E_F
E_0
S2
S1
0
-d
0
Distance; z

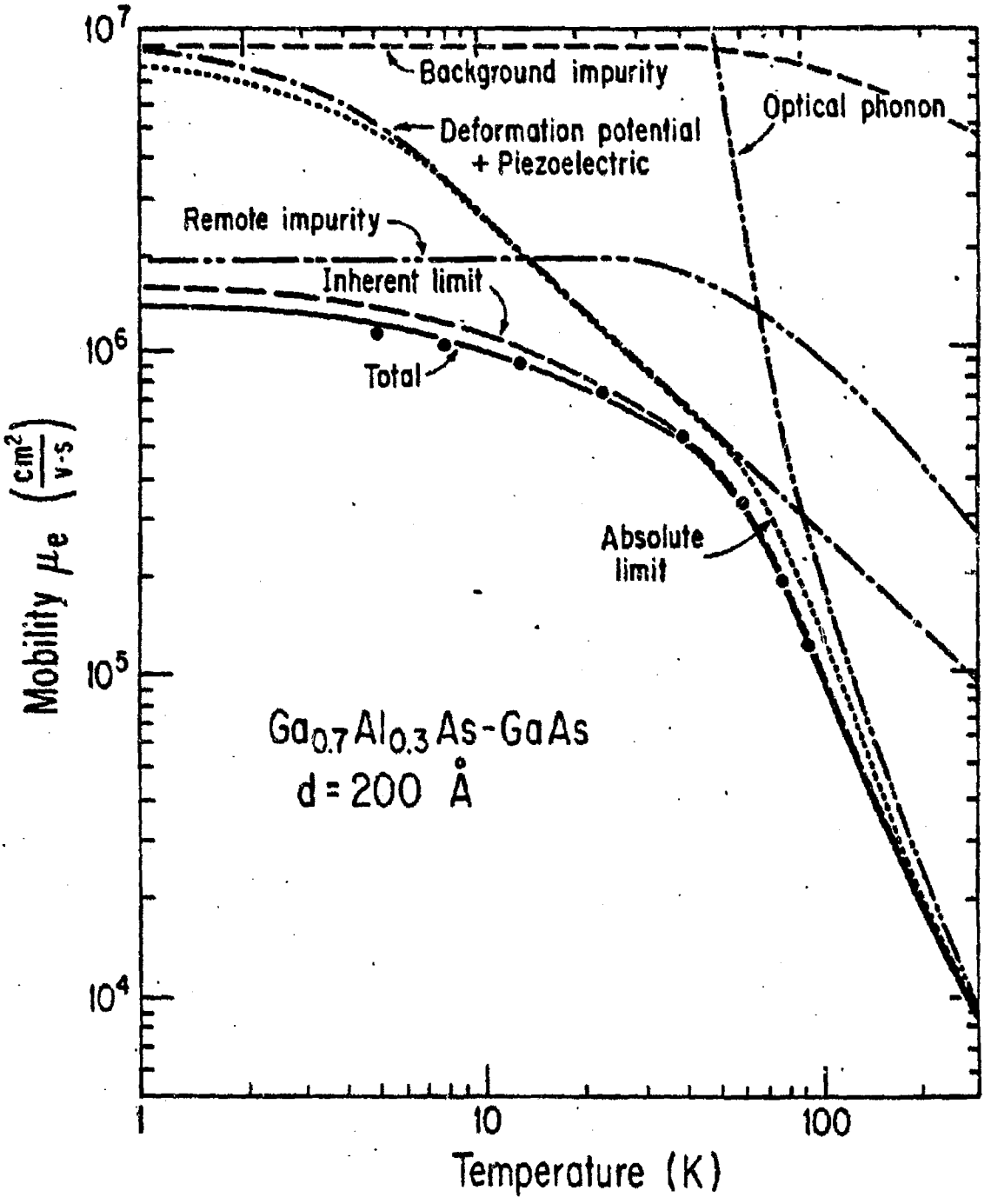

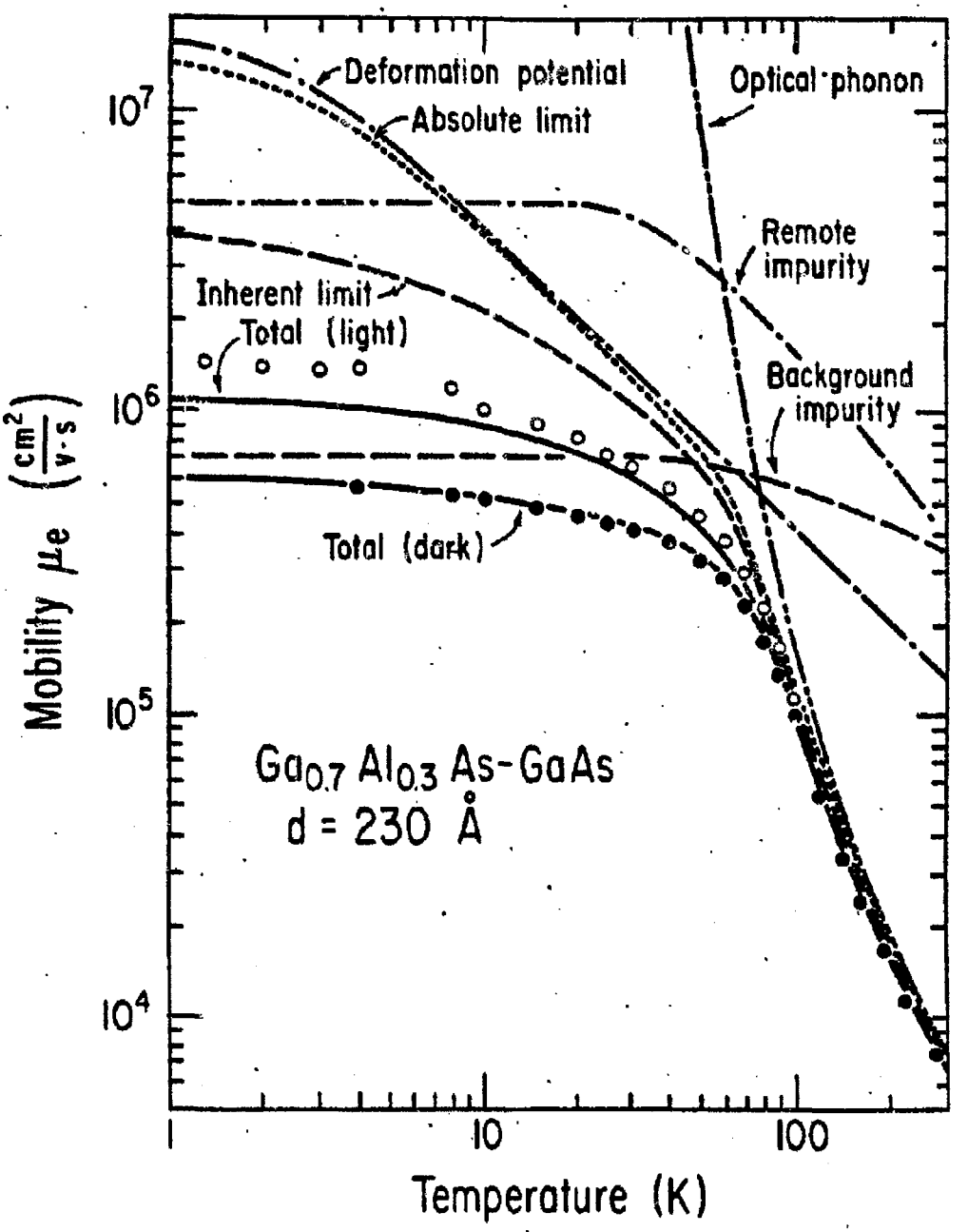

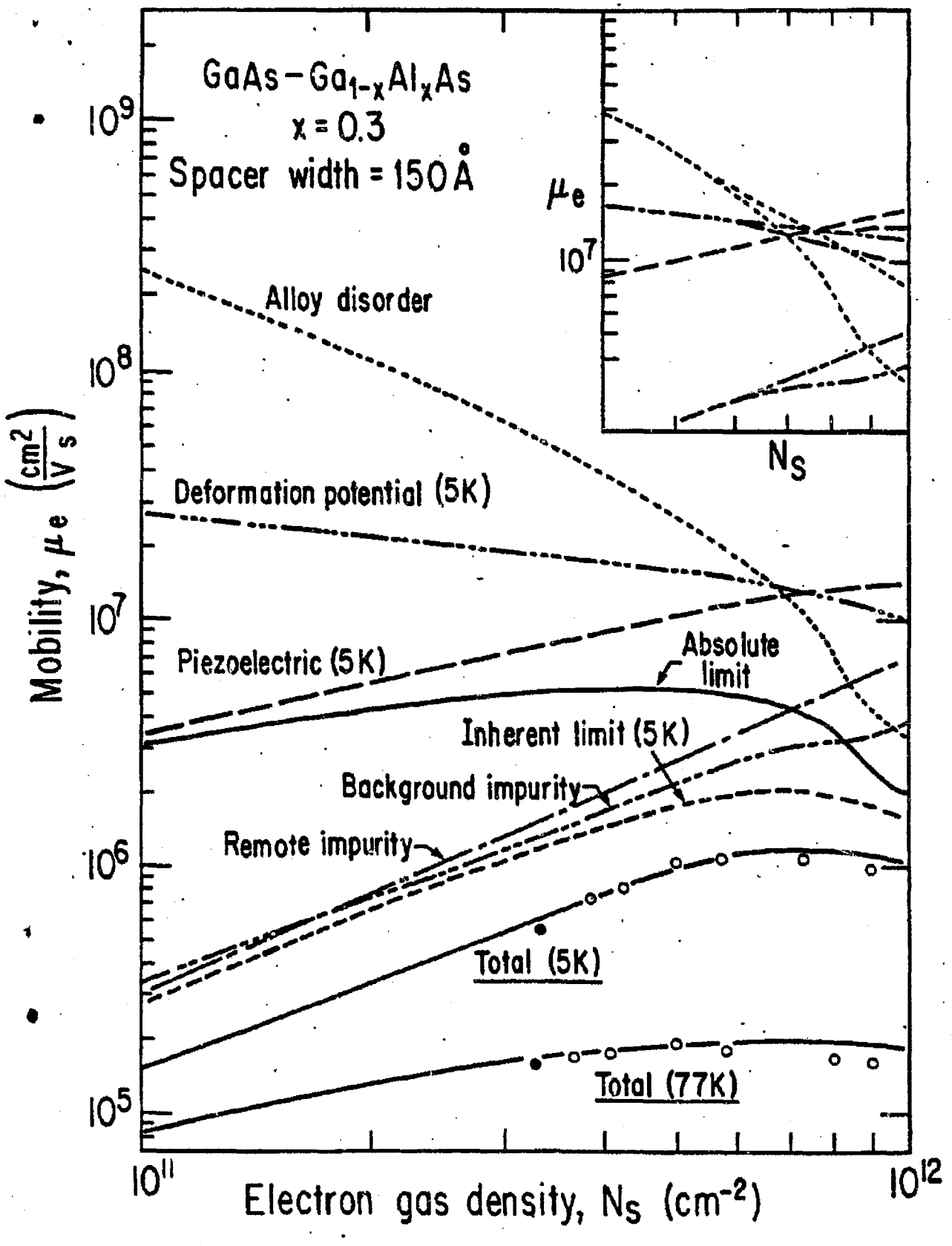

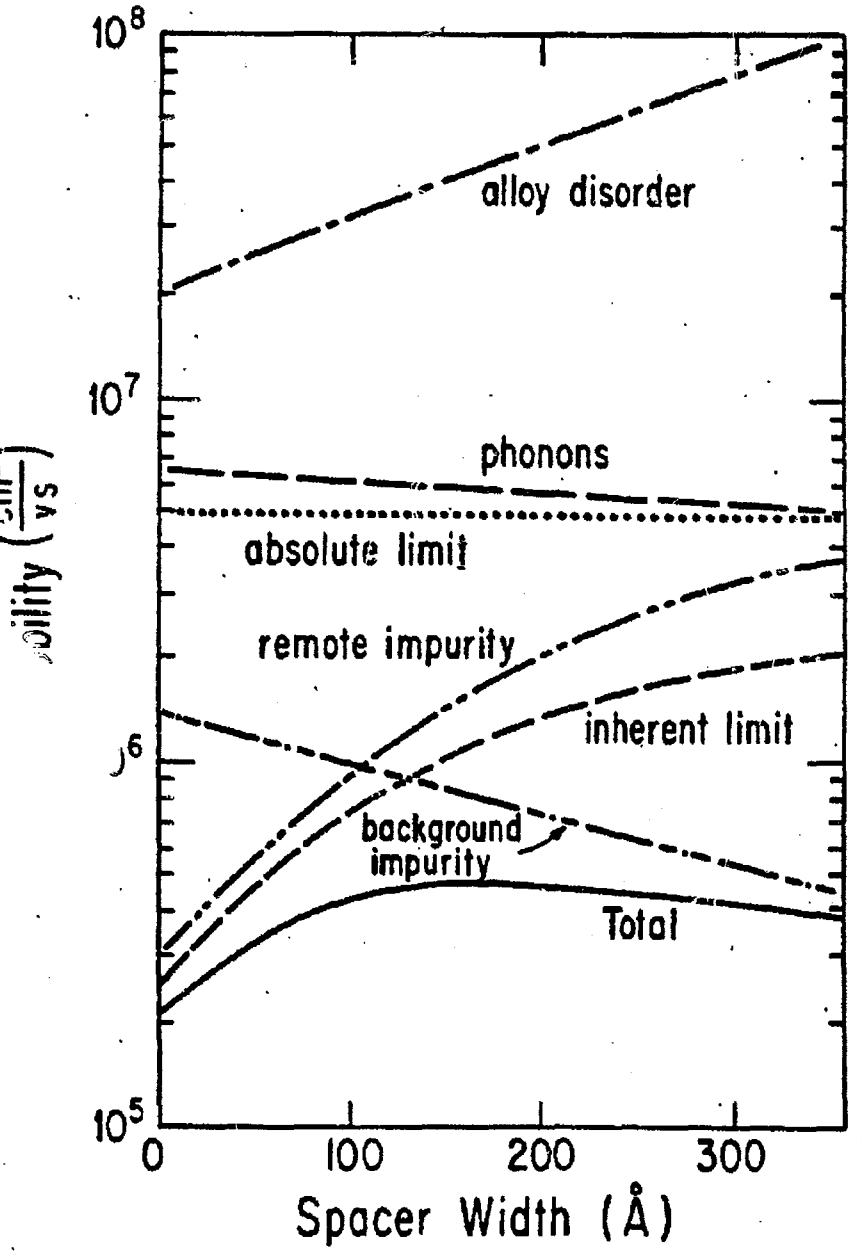
10^8
10^7
10^6
10^5
alloy disorder
phonons
absolute limit
remote impurity
inherent limit
background impurity
Total
0
100
200
300
Spacer Width (Å)
$\left(\frac{cm^2}{Vs}\right)$

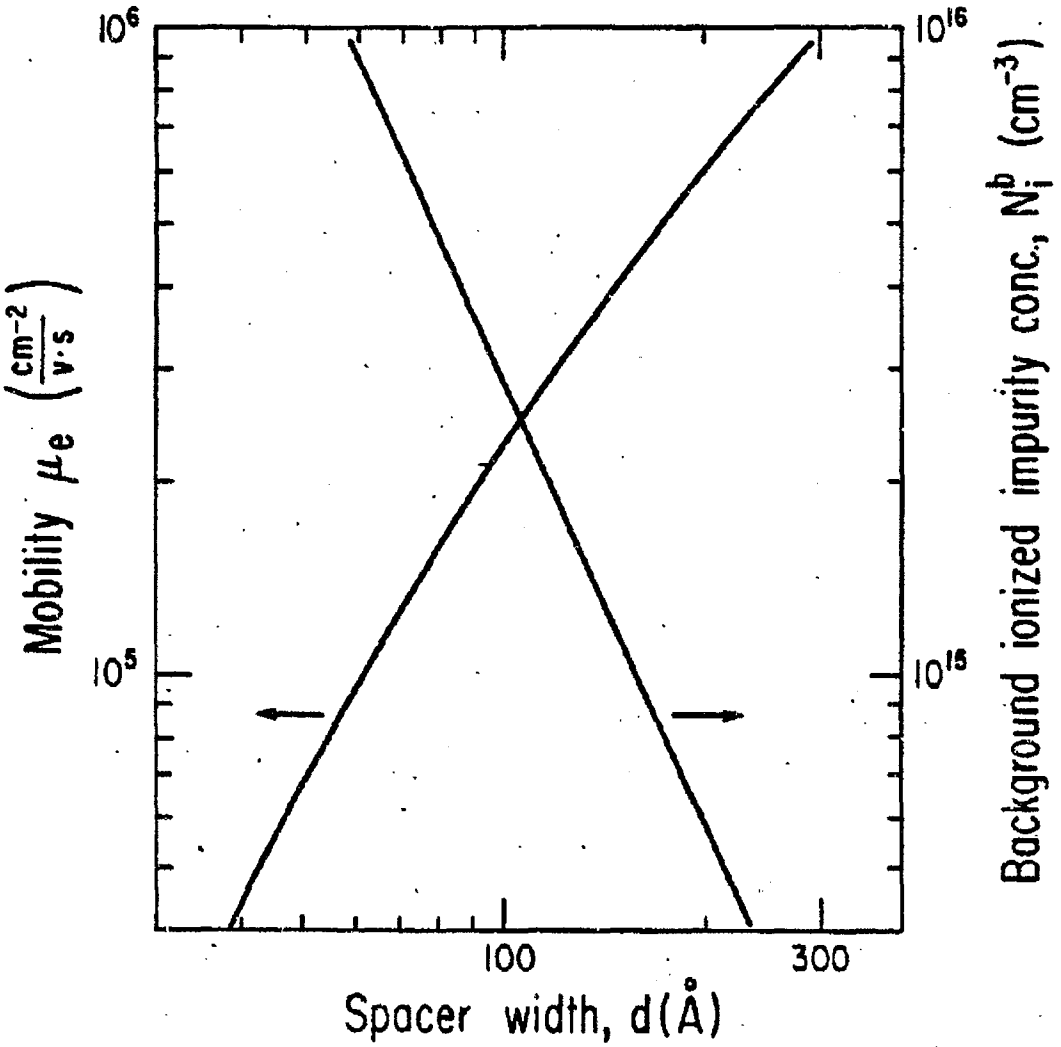

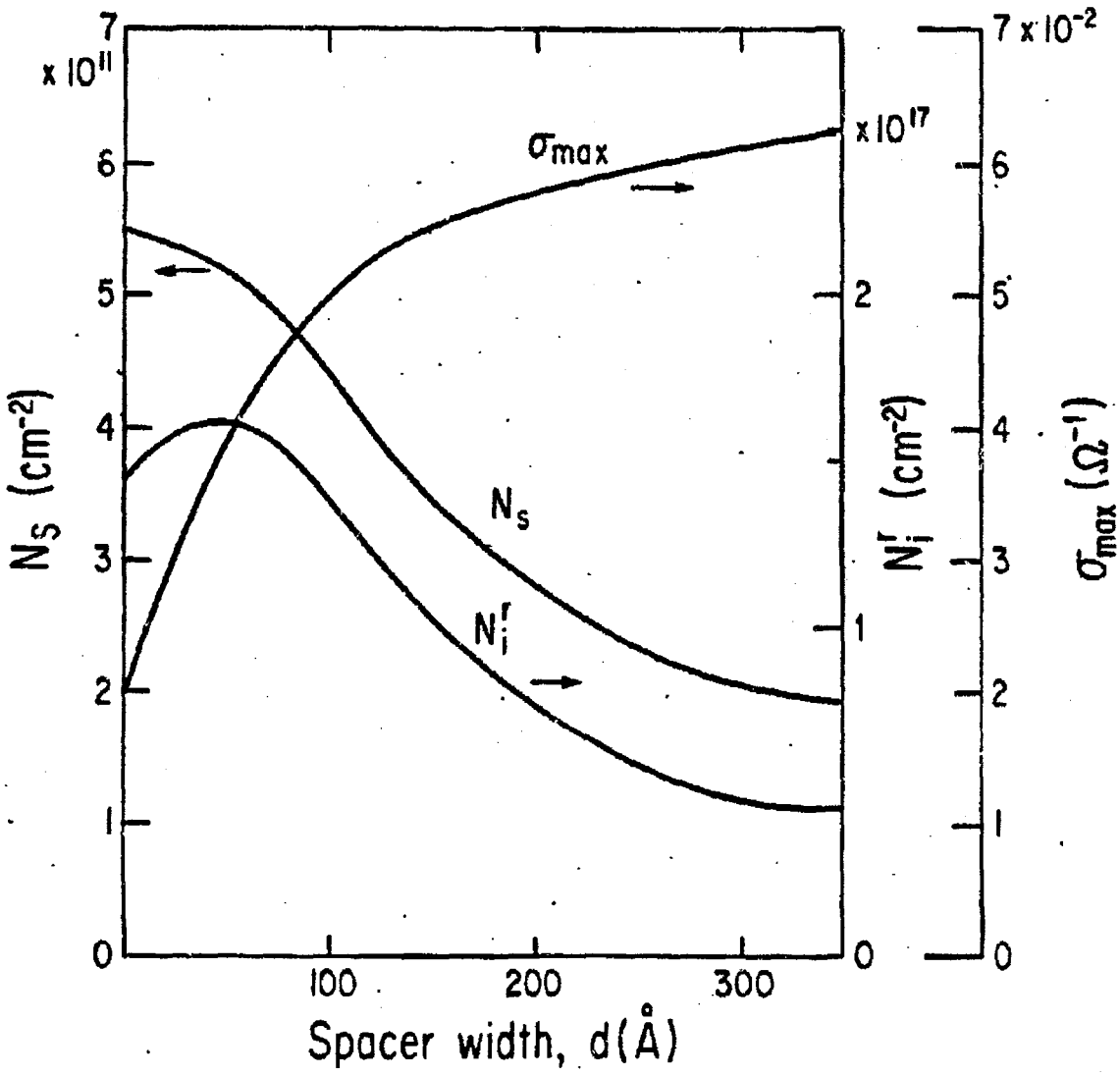

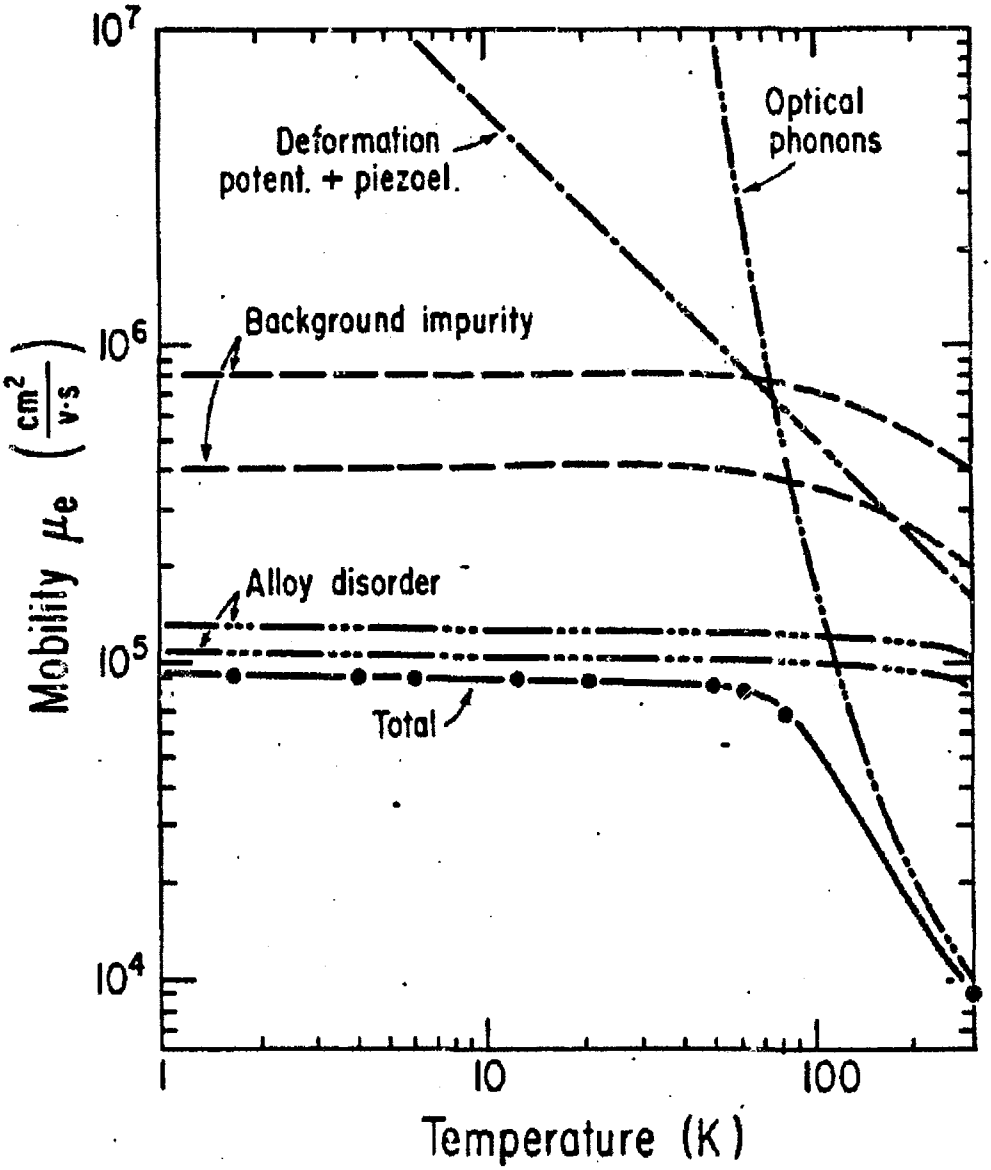

submitted to The Journal of the
Electrochemical Society

PARTIALLY-CONFINED CONFIGURATION FOR CRYSTAL GROWTH FROM THE MELT IN ZERO GRAVITY ENVIRONMENT

J. Lagowski and H.C. Gatos
Massachusetts Institute of Technology
Cambridge, Massachusetts 02139

Abstract

A novel partially-confined configuration is proposed for the growth of semiconductor crystals from the melt. A triangular prism is employed to contain the growth melt. Due to surface tension, the melt will contact the prism along three parallel lines. This partial confinement will force the melt to acquire an elongated cylindrical shape needed for directional solidification. The three empty spaces between the cylindrical melt and the edges of the prism will accommodate the expansion of the solidifying semiconductor, and in the case of semiconductor compounds with a volatile constituent, will permit the presence of the desired vapor phase in contact with the melt for controlling the melt stoichiometry.

Background Remarks

The advantages of zero gravity conditions in solidification in general and semiconductor growth in particular, stem primarily from the suppression (or virtual elimination) of thermal convection and solutal convection in the melt.(1) As demonstrated in early experiments, elimination of thermal convection caused impurity segregation to proceed under ideal diffusion control conditions and led to a uniform dopant distibution and enhanced homogeneity of the crystals.(2,3)

The potential advantages of space in growing compound semiconductors and

especially GaAs have recently been magnified by the discovery of the profound role of the melt stoichiometry and stoichiometry fluctuations.(4) Thus, during the last three years it has been established that stoichiometry is the single most important growth parameter which controls all of the key properties of melt-grown GaAs, namely, compensation,(5) mobility, excess carrier lifetime, deep levels,(5,6) dislocation density(7) and response to thermal processing(8) in a macro- and micro-scale. Elimination of solutal and thermal convection should eliminate stoichiometry fluctuations to make it possible to achieve growth of GaAs with enhanced control of the electronic and structural properties.

An additional advantage of space environment is that melt containers may be eliminated so that contamination of the melt can be avoided. However, unconfined melts acquire a spherical shape which is not suitable for directional single crystal growth. Furthermore, melts with volatile constituents cannot be processed in an unconfined configuration.

For these reasons in crystal growth experiments from the melt confined configurations have been employed, and in particular cylindrical containers.(9) Regarding the growth of semiconductor crystals, due to volume expansion upon solidification, confinement of the melt presents the serious problem of the solidifying crystal pressing against the confining walls leading to crystal defect formation. A second major problem arises when a vapor phase in contact with the melt is necessary during crystal growth, as for example, in the case of GaAs where the pressure of arsenic effectively controls the melt stoichiometry.

To overcome these problems "soft confinements" have been considered whereby a suitable soft material is positioned between the melt and the

container. To our knowledge, no such soft materials have been formally reported.

In the present communication we report a novel approach to crystal growth from the melt in the absence of gravity which overcomes the above major problems associated with the growth of single crystals in space.

The New Approach

We propose that a triangular prism used to confine growth in space provides an excellent solution to the problems outlined above. As seen in Fig. 1, the melt in a triangular prism acquires a cylindrical shape in space. Thus, the empty spaces between the cylindrical melt and the edges of the prism provide the necessary room to accommodate expansion during solidification. Furthermore, they constitute three channels through which a vapor phase of controlled pressure can be in contact with the melt during the growth process. In Fig. 1, GaAs crystal growth is considered in a Bridgman-type configuration. An arsenic source is used to provide the arsenic vapor pressure desired to control the melt composition during growth by means of an arsenic source temperature. This aspect is of fundamental importance for the reasons pointed out above.

The container can be shaped to achieve necking in the initiation of growth and thus minimize the propagation of dislocations into the crystal; it can be made of quartz, boron nitride, or any other material suitable for the particular system under consideration. We intend to employ the presently described configuration for the growth of GaAs single crystals.

In summary, a novel partially confined configuration is presented for solidification in general and semiconductor crystal growth in particular, under zero gravity conditions. It is our expectation that the proposed configuration will encourage the design of new materials processing experiments to be carried out in space.

ACKNOWLEDGEMENT

The authors are grateful to the National Aeronautics and Space Administration for financial support.

REFERENCES

1. H.C. Gatos in "Space for Mankind's Benefit," edited by J. von Puttkamer and T.J. McCullough, NASA SP-313, Washington, D.C., 1972.
2. H.C. Gatos, in "Materials Processing in Reduced Gravity Environment of Space," edited by G. Rindone, Elsevier Publishing Co., Inc., 1982, p. 355.
3. A.F. Witt, H.C. Gatos, M. Lichtensteiger, M.C. Lavine and C.J. Herman, J. Electrochem. Soc. 125 (1975) 276; A.F. Witt, H.C. Gatos, M. Lichtensteiger and C.J. Herman, Ibid., 125 (1978) 1832.
4. H.C. Gatos and J. Lagowski, "Proceedings III-V Optoelectronics Epitaxy and Device Related Processes," edited by V.G. Keramidas and S. Mahajan, The Electrochemical Society, Inc., Pennington, N.J., 1983, p. 1.
5. D.E. Holmes, R.T. Chen, K.R. Elliott and C.G. Kirkpatrick, Appl. Phys. Lett. 40 (1982) 46.
6. J. Lagowski, H.C. Gatos, J. Parsey, K. Wada, M. Kaminska and W. Walukiewicz, Appl. Phys. Lett. 40 (1982) 342.
7. J. Parsey, J. Lagowski and H.C. Gatos, "Proceedings III-V Optoelectronics Epitaxy and Device Related Processes," edited by V.G. Keramidas and S. Mahajan, The Electrochemical Society, Inc., Pennington, N.J., 1983, p. 61.
8. H.M. Hobgood, L.B. Ta, A. Rahatgi, G.W. Eldridge and R.N. Thomas, in "Semi-Insulating III-V Materials," edited by S. Makram-Ebeid and B. Tuck, Shiva Publishing, Ltd., Nantwich, England, 1982.
9. "Skylab Science Experiments," edited by G.W. Morgenthaler and G.E. Simonson, Science and Technology Series, vol. 38, an American Astronautical Society Publication, 1975.

10. Apollo-Soyuz Test Program, Summary Science Report, NASA-412, Vol. I, 1977.

FIGURE CAPTION

Figure 1. Schematic representation of a partially-confined configuration for the growth of GaAs crystals from the melt in space.

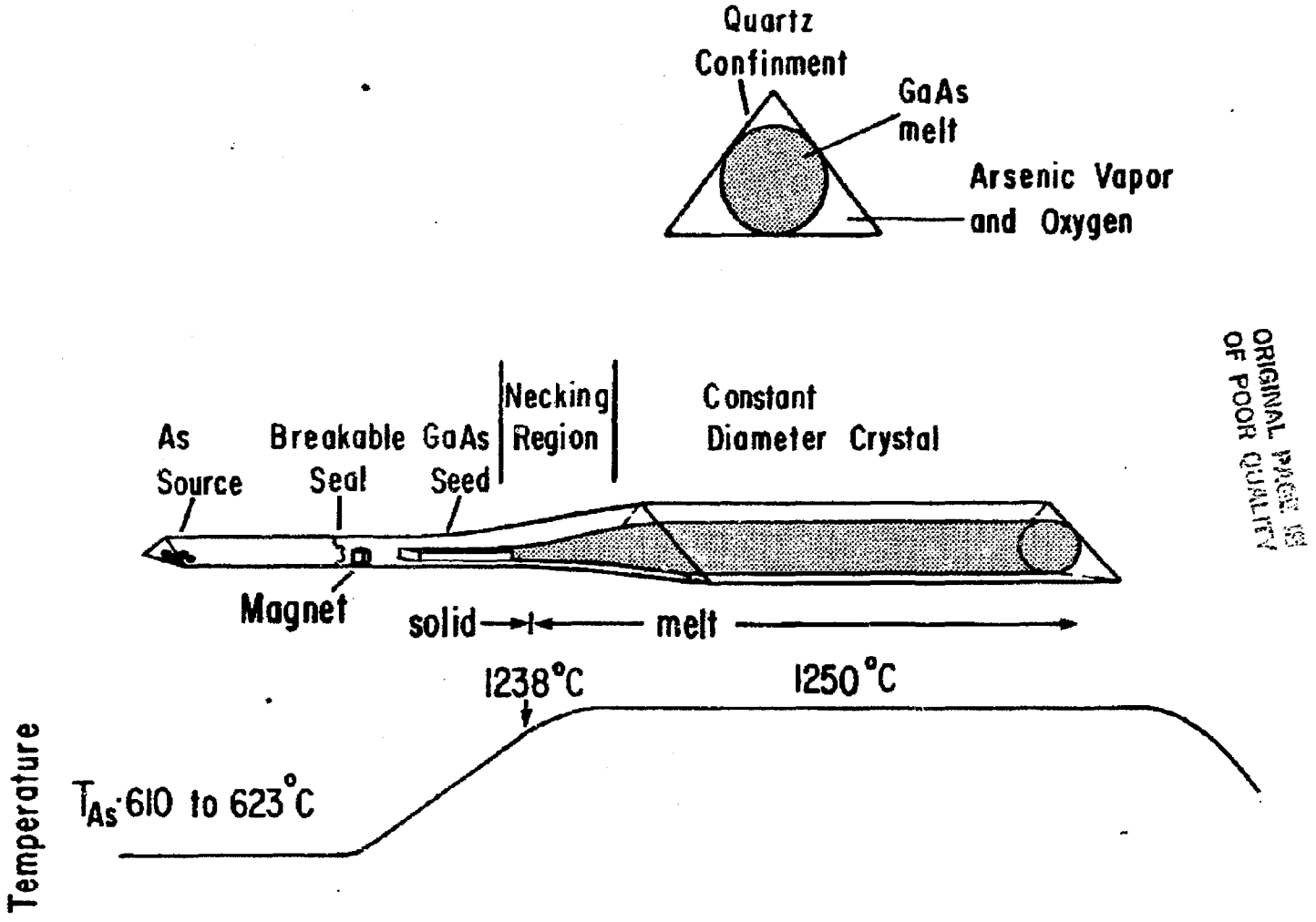

Figure 1.

Reproduced by NTIS

U.S. DEPARTMENT OF COMMERCE
Technology Administration
National Technical Information Service
Springfield, VA 22161 (703) 605-6000